

Sheffield Hallam University

Computer aided fatigue design.

YAZDANPANAHA, Amir.

Available from the Sheffield Hallam University Research Archive (SHURA) at:

<http://shura.shu.ac.uk/20587/>

A Sheffield Hallam University thesis

This thesis is protected by copyright which belongs to the author.

The content must not be changed in any way or sold commercially in any format or medium without the formal permission of the author.

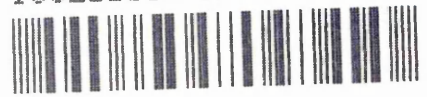
When referring to this work, full bibliographic details including the author, title, awarding institution and date of the thesis must be given.

Please visit <http://shura.shu.ac.uk/20587/> and <http://shura.shu.ac.uk/information.html> for further details about copyright and re-use permissions.

POLYTECHNIC LIBRARY
POUND STREET
SHEFFIELD S1 1WB

TELEPEN

100263112 2



Sheffield City Polytechnic Library

REFERENCE ONLY

Fines are charged at 50p per hour

27 JUN 2002 4:33

26 FEB 2004
8-50

15/1/96 20.41

5.29 pm

26 NOV 2001
9pm

ProQuest Number: 10701234

All rights reserved

INFORMATION TO ALL USERS

The quality of this reproduction is dependent upon the quality of the copy submitted.

In the unlikely event that the author did not send a complete manuscript and there are missing pages, these will be noted. Also, if material had to be removed, a note will indicate the deletion.



ProQuest 10701234

Published by ProQuest LLC (2017). Copyright of the Dissertation is held by the Author.

All rights reserved.

This work is protected against unauthorized copying under Title 17, United States Code
Microform Edition © ProQuest LLC.

ProQuest LLC.
789 East Eisenhower Parkway
P.O. Box 1346
Ann Arbor, MI 48106 – 1346

COMPUTER AIDED FATIGUE DESIGN

by

AMIR YAZDANPANA B.Sc, M.Tech

A thesis submitted in partial fulfilment of the requirements
of the COUNCIL FOR NATIONAL ACADEMIC AWARDS for the degree of
DOCTOR OF PHILOSOPHY

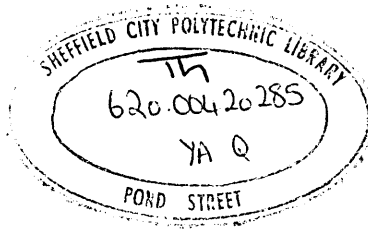
Sponsoring Establishment:

Sheffield City Polytechnic,
Sheffield, S1 1WB.

Collaborating Establishment:

nCode International Limited,
230 Woodbourn Road,
Sheffield, S9 30Q.

May 1990



TO MY WIFE AND FRIEND,

CHRISTINE,

THANK YOU FOR YOUR PATIENCE AND UNDERSTANDING.

ACKNOWLEDGEMENTS

The author wishes to express his gratitude to Mr D E Eaton, Mr G Cockerham, Dr K Morton, and Dr L Lack for their helpful supervision during the course of this project. Thanks are also expressed to Dr S R Bradbury and other research assistants for their constructive suggestions and comments.

The technical assistance offered by Mr R Teasdale and his staff was much appreciated and in particular the author wishes to thank Messrs J Stanley, K Wright, D Allen, R Sidebottom and R Wilkinson for their valued contribution at various stages of this work. Finally, my gratitude to members of staff at nCode International Limited for technical assistance offered.

DECLARATION

The author declares that no part of this work has been submitted in support of another degree or qualification to this or any other establishment. The author further declares that he has not been a registered candidate or enrolled student for another award of CNAA or other academic or professional institution during the course of the research programme

A Yazdanpanah

NOMENCLATURE

A	=	Area
b	=	Fatigue strength exponent
c	=	Fatigue ductility exponent
b	=	Fatigue strength in bending
C _t	= t =	Fatigue strength in twisting
E	=	Modulus of elasticity
f	=	Functional relationship
F	=	Force
G	=	Modulus of rigidity
K _t	=	Theoretical elastic concentration factor
K _σ	=	True Stress Concentration factor
K _ε	=	True Strain Concentration factor
K'	=	Cyclic Strength coefficient
N _f	=	Cycles to failure
n'	=	Cyclic strain hardening
ΔS	=	Nominal Stress range
σ _{yt}	=	Yield strength
σ _{eq}	=	equivalent stress
Δσ	=	Stress at notch root
σ _f '	=	Fatigue strength coefficient
ε ₁ , ε ₂ , ε ₃	=	Principal Strains
Δe	=	Nominal strain
ε _a = $\frac{\Delta \epsilon}{2}$	=	Axial strain amplitude
ε _e	=	Elastic strain
ε _p	=	Plastic strain
ε _T	=	Total strain
ε _f '	=	Fatigue ductility coefficient

- ϵ_n = Tensile strain normal to the plane of maximum shear.
- λ = Biaxial strain ratio, $\frac{\Delta\gamma}{\Delta\epsilon}$
- ν = Poisson's ratio
- $\frac{\Delta\sigma}{2}$ = Axial stress amplitude
- $\sigma_1, \sigma_2, \sigma_3$ = Principle stresses
- $\frac{\gamma}{2}$ = Maximum shear strain
- τ_a = Shear stress amplitude on plane of maximum range of shear stress
- σ_τ = Normal Stress amplitude on plane of maximum range of shear stress
- ρ = Density
- W_s = The elastic strain energy per unit due volume to the nominal remote stress
- W_σ = The strain energy per unit volume due to local stress and strain at the notch root.

ABSTRACT

COMPUTER AIDED FATIGUE DESIGN

A Yazdanpanah B.Sc, M.Tech

Today's competitive market requires engineers to produce reliable light weight products at low cost. This can be achieved by more effective use of computer aided engineering tools during early stages of the design process.

A research programme has been undertaken to investigate the data requirements of integrating commercially available software packages (finite element analysis and fatigue life evaluation) to evaluate the integrity and durability of engineering components at the conceptual design stage.

A real engineering component, in the form of a steering arm, supplied by a European truck manufacturer was used as a basis for the investigation. This is a typical vehicle component, in which, under service loading conditions, a multiaxial state of stress occurs.

A geometric model of the component was created using the Prime "MEDUSA" software suite. The model was used to locate the boundary co-ordinates necessary for the development of a PAFEC Finite Element model. By imposing the conditions experienced during the service, the critical areas of the component were identified by analysing the F.E. model and a detailed description of the elastic stress/strain fields were also established. These were incorporated in an energy density approach and Neuber's uniaxial analysis to predict total local elastic/plastic strains at these critical locations. These were compared with strain gauge measurements. The calculated results were used to plot a number of load/local strain calibration curves for the development of a load history, suitable for experimental fatigue life assessment.

Fatigue crack initiation tests were performed on the steering arm using a computer controlled DARTEC multiaxial fatigue testing machine. Fatigue life assessment based on full service loading was carried out using a software package based on the critical location approach. A comparison of computerised, experimental and actual test circuit fatigue lives has been made.

The work enabled a specification to be produced for the integration of the two items of software. This integrated software was developed by third parties and used to produce a computerised life map of the steering arm.

CONTENTS	PAGE
ACKNOWLEDGEMENTS	ii
DECLARATION	iii
NOMENCLATURE	iv
ABSTRACT	vi
CONTENTS	vii
INDEX TO FIGURES	xi
CHAPTER 1 - INTRODUCTION	
1.1 The Engineering Design Process	1
1.1.1 Background	1
1.1.2 Design Philosophy	2
1.1.3 Marketing Stage	4
1.1.4 Product Specification	4
1.1.5 Conceptual Design	5
1.1.6 Detailed Design	6
1.1.7 Application Of Computers In The Design Process	7
1.2 Computer Aided Engineering	9
1.3 Historical Perspective of Fatigue	11
1.4 Scope Of The Present Work	15
1.5 Principal Objectives Of Research Programmes	17
CHAPTER 2 - FATIGUE LIFE EVALUATION TECHNIQUES	
2.1 Introduction	23
2.2 Neuber's Rule	24
2.3 The Cyclic Stress/Strain Curve	27
2.4 Methods Of determining The Cyclic Stress/Strain Curve	30
2.4.1 Multiple Step Tests	30
2.4.2 Incremental Step Tests	30
2.5 Analysis Of Strain-Life Curve	31
2.6 Extracting Hysteresis Loops (Cycle Counting)	34

CONTENTS (contd.)	PAGE
2.7 Energy Density Approach For Elastic/Plastic Stress/Strain Calculation At the Notch Root	36
2.8 Multiaxial Fatigue	38
2.8.1 Principle of Static Yield Criteria to Fatigue	41
2.9 Critical Location Approach	44
CHAPTER 3 - STEERING ARM DESCRIPTION	
3.1 Introduction	59
3.2 Steering Arm	60
3.2.1 Function Of A Steering Arm System	61
3.3 Chemical And Mechanical Properties	61
3.4 Micro-Structure Examination	62
3.5 Manufacturing Processes	64
3.6 Test Track Trails	65
3.7 Durability Assessment	66
3.8 Discussion	68
CHAPTER 4 - COMPUTER BASED ANALYSIS OF STEERING ARM	
4.1 Introduction	93
4.2 Software Summary	94
4.2.1 MEDUSA	95
4.2.2 PAFEC	96
4.2.3 PIGS	97
4.2.4 FAMbuild	98
4.3 Two and Three Dimensional Geometric Modelling	98
4.4 Finite Element Analysis	101
4.4.1 Component Geometry and Material Properties	101
4.4.2 Development Of The Finite Element Model	102
4.5 Results and Discussion	105
4.6 Conclusions	110

CHAPTER 5 - STATIC STRAIN MEASUREMENT OF THE STEERING ARM

5.1	Introduction	126
5.2	Test Equipment	126
5.3	Experimental Rigs	129
5.4	Strain Measurements	130
5.4.1	Strain Gauge Specification	130
5.4.2	Static Loading Results	130
5.5	Conclusions	134

CHAPTER 6 - COMPUTER BASED FATIGUE LIFE CALCULATIONS

6.1	Aims And Objectives	143
6.2	Software Summary	145
6.3	Measured Strain-Time History	146
6.4	Material	146
6.5	Fatigue Reduction Factor	147
6.6	Fatigue Life Evaluation	147
6.6.1	FATIMAS Fatigue Life Assessment: Measured strain-time Service History	147
6.6.2	Fatigue Life Assessment: Load calibrated measured strain-time Service History	148
6.7	Conclusion	151

CHAPTER 7 - FATIGUE TESTING OF THE STEERING ARM

7.1	Introduction	167
7.2	Test Equipment	167
7.3	Fatigue Testing	167
7.3.1	Crack Detection Methods	168
7.3.2	Fatigue Crack Initiation Tests	171
7.4	Visual Examination Of The Fracture Surface	172
7.5	Fractography Investigation	173
7.6	Microstructure	174
7.7	Discussion	174

CHAPTER 8 - INTEGRATED F.E. AND FATIGUE COMPUTATIONS

8.1	New Software Structure	194
8.2	Steering Arm Fatigue Predictions	195
8.3	Discussion	197
8.4	Conclusions	198

CHAPTER 9 - DISCUSSION

9.1	Introduction	209
9.2	Computer Based Modelling and Analysis	211
9.3	Theoretical and Experimental Life Evaluation	215

CHAPTER 10 - CONCLUSIONS AND SUGGESTIONS FOR FUTURE WORK

10.1	Computer Based Analysis	218
10.2	Practical Applicability of the Technique	220
10.4	Scope for Future Work	222
	REFERENCES	224

INDEX TO FIGURES	PAGE
CHAPTER 1	
1.1 French's Model Of The Design Process	20
1.2 Archer's Model Of The Design Process	21
1.3 Pugh And Smith's Model Of The Design Process	22
CHAPTER 2	
2.1 Variation Of Stress Concentration Factor And Strain Concentration Factor As Stress Increases	47
2.2 Solving The Neuber Equation	48
2.3 Monotonic And Cyclic Stress/strain Curve	49
2.4 Stable Stress/Strain Hysteresis Loop	50
2.5 Strain Control Programmes For Obtaining An Approximate Cyclic Stress/Strain Curve From One Specimen	51
2.6 Strain-Life Curves Showing Total Elastic And Plastic Strain Components	52
2.7 Rainflow Cycle Counting	53
2.8 Example Of Rainflow Cycle Counting Method	54
2.9 A Load Versus Time History Repeatedly Applied To A Notched Component And The Resulting Notch Strain Response	55
2.10 Mohr's Circle Of Strain	56
2.11 Case A And Case B System Of Crack Extension	57
2.12 A Typical r Plot	58
CHAPTER 3	
3.1 The Steering Arm	70
3.2 Steering Arm Dimensional Details	71
3.3 The exploded View Of The Steering System	72
3.4 Unetched Micro-Structure Showing The Inclusions	76
3.5 Etched Micro-Structure Showing Bainite In A Matrix Of Martensite	77
3.6 The Spectra Of Inclusion Plot	78

3.7	Time Temperature Transformation Curve	79
3.8	Manufacturer's Test Track Surfaces	80
3.9	Recorded Stubaxle Strain-Time Service History	81
3.10	Cyclic Stress/Strain Curve (SAE 1046 V)	82
3.11	Strain/Life Curve (SAE 1046 V)	83
3.12	STW/Life Curve (SAE 1046 V)	84
3.13	Cyclic Stress/Strain Curve (41 Cr S4)	85
3.14	Strain/Life Curve (41 Cr S4)	86
3.15	STW/Life Curve (41 Cr S4)	87
3.16	Cyclic Stress/Strain Curve (41 Cr 4V)	88
3.17	Strain/Life Curve (41 Cr 4V)	89
3.18	STW/Life Curve (41 Cr 4V)	90
3.19	Stubaxle Cycle Distribution	91
3.20	Stubaxle Damage Distribution	92

CHAPTER 4

4.1	Three Dimensional Geometric Model Of The Steering Arm	111
4.2	Shaded Image Of The Steering Arm	112
4.3	Element Types	113
4.4	A Mesh Used For Three Dimensional Finite Element Analysis Of The Full Component	114
4.5	Stress Contours Of The Full Component	115
4.6	A Mesh Used For Three Dimensional Analysis Of The Critical Part Of The Component	116
4.7	Stress Contours Of The Critical Part Of The Component	117
4.8	Example Of Solving Neuber's Equation	123
4.9	Monotonic Estimated Load/Notch Root Strain Calibration Curves	124
4.10	Cyclic Estimated Load/Notch Root Strain Calibration Curves	125

CHAPTER 5

5.1	Dartec Fatigue Testing Machine Showing The Swivel Joints, Rig And Component In Position	135
5.2	Exploded View Of The Rig	136
5.3	Location Of Post-Yield Strain Gauges	137
5.4	Monotonic, Measured And Estimated Load/Notch Root Strain Calibration Curves	141
5.5	Comparison Of Monotonic, Predicted And Measured Strain	142

CHAPTER 6

6.1	Dashboard Strain-Time Service History	153
6.2	Fatigue Life Assessment	157
6.3	Hysteresis Loops	158
6.4	Cycle Distribution For Dashboard History	159
6.5	Damage Distribution For Dashboard History	160
6.6	Load Versus Life Comparison Of The FE Predicted Fatigue Lives	163
6.7	Load Versus Life Comparison Of The FATIMAS Measured History, and FE Predicted Fatigue Lives	166

CHAPTER 7

7.1	Dashboard Strain-Time Service History	178
7.2	Dashboard Load-time Service History	179
7.3	Load Versus Life Comparison Of The Experimental And FATIMAS Predicted Fatigue Lives	182
7.4	Comparison Of Experimental And FATIMAS Predicted Fatigue Lives	183
7.5	The Fracture Surface Of The Component	184
7.6	The Surface Immediately Surrounding The Initiation Point	185
7.7	Crack Propagation Region	186

7.8	The Transition Area Between Slow Crack Growth And Ductile Shear Failure	187
7.9	An Area Of Ductile Shear Failure	188
7.10	An Area Of Ductile Fracture, Showing Mixed Fracture Modes	189
7.11	An Area Of Ductile Fracture, Showing Non-Metallic Inclusions	190
7.12	Final Brittle Fracture, Showing Two Modes Of Fracture (a) Intergranular (b) Cleavage	191
7.13	Brittle Fracture, Showing Intergranular And Cleavage Fracture	192
7.14	Brittle Fracture Region, Final Catastrophic Failure	193

CHAPTER 8

8.1	An Overview Of The FALCON Structure	200
8.2.	Fatigue Life Contours For The Steering Arm (Maximum Principal Stress Method)	201
8.3	Fatigue Life Contours For The Steering Arm (Tresca Method)	202
8.4	Fatigue Life Contours For The Steering Arm (von Mises Method)	203
8.5	Fatigue Life Contours For The Steering Arm (σ_{xx} Method)	204
8.6	Comparison Of The Experimental FALCON And FATIMAS Predicted Fatigue Lives	207
8.7	The Flow Chart Showing An Overview Of The Routes Taken To Assess The FATigue Life Of The Steering Arm	208

CHAPTER 1

INTRODUCTION

1.1 The Engineering Design Process

1.1.1 Background

Design engineers in many industries today are expected to produce reliable products of light weight and low cost. This can be achieved by more effective use of computer aided engineering tools during the design process [1, 7]*. However, an understanding of the design processes is necessary before computers can be used to support them. Understanding these processes is the first and probably one of the most important steps in the development of an integrated computer aided design and durability assessment package. Such insights certainly make the designer more aware of the advantages and pitfalls of advanced and sophisticated computer software packages.

The designer must consider a whole variety of events and circumstances before attempting to use computers to enhance the process. Presently, computer systems assist in the development of geometric modelling and can be linked to finite element software for load analysis. This produces elastic stress fields and guides the designer in his endeavours and quite often fatigue life assessment is necessary using separate software or physical prototype.

* Numbers refer to references given at the end of this text.

This chapter briefly describes the different stages of the design process and identifies the areas where an integrated CAD system might be successfully used. A brief historical development of fatigue life evaluation methods is also presented for completeness.

1.1.2 Design Philosophy

It is now widely accepted that a systematic approach to problem solving is needed, if a high proportion of problems are to be solved in the best way [8].

In the past most designers' approach to problem solving has been intuitive rather than systematic. When they have exercised their art, native wit has been relied upon to produce a design and they would possibly find it difficult to explain how the design evolved [9].

The designer must implement a set of specific objectives for investigating the needs and circumstances of the design activity, and synthesising these design objectives into an optimum solution. The failure to consider all aspects of the design in a systematic way may possibly lead to a workable solution, however, the designer will have little justification of the design solution. There are many structured design strategies available to the designer the following being typical [10-12] (see figures 1.1 to 1.3):-

- i) French procedure
- ii) Archer procedure
- iii) Pugh and Smith procedure

Any systematic strategy may be selected during the design activity. The decision as to which strategy or tactic to use will depend upon the industry and the circumstances of the problem.

The following factors should be considered irrespective of approach:- market needs, specification, conceptual design, detail design, manufacture, and sales. The above phases are applicable to any area of design be it construction, industrial product, or consumer product. It must be appreciated that design processes are highly interactive and iterative [10, 13].

Two further inputs are required to enable the design processes to work, these being technology and techniques.

Technological and other relevant information are dependent upon the industry and the product area in which the designer is working. The informational inputs are the 'life blood' of design. This is an area which is continuously changing and expanding through new material development and methods of storage and retrieval.

The traditional techniques of designers are creativity, evaluation, costing, analysis, sketching, scale drawing,

perspectives, models and the like. These techniques are used to manipulate the information inputs to a suitable form which then can be integrated into the design process.

1.1.3 Marketing Stage

Marketing can be defined as directing all the activities of an organisation (men, machine, material, money and building) towards satisfying the potential need of consumer. The ultimate objective being to produce a competitive, cost effective product that fits a market or creates a market of its own [10]. To achieve this an organisation must consider the following factors:- "population, technology, consumer taste and fashion, politics, income, and competition", although changes in need reflect changes in one or more of these factors. The aim of the market research activity is to clarify the design objectives and to identify the course of actions that are capable of bringing about a fully definitive product specification.

1.1.4 Product Specification

The starting point for any design is, or should be a fully definitive product specification. This is formulated in conjunction and as a result of the information obtained in the marketing phase. This should be a clear document outlining all the design objectives and constraints related to the product attributes and performance.

1.1.5 Conceptual Design

The conceptual stage of any design should be concerned with synthesis, which Collins Dictionary defines as: "combination, composition, putting together, building up of separate elements, especially of conception or propositions or facts into a connected whole, especially a theory or system" [87]

From the above definition it is clear that creative tactics are used in the conceptual (synthesis) stage of the design process and are for the purpose of generating functional solutions to the problem stated. Most designers are involved in the creative process in their search for the optimum solution to a design problem.

Conceptual design is about identifying possible solutions to a design problem within the scope of the design specification but without necessarily any detail commitment to individual component shapes, sizes or materials. Many eminent designers believe that a systematic approach helps to generate many alternative concepts which then need to be evaluated through comparison with the requirements of the specification.

Computers can be used in a limited fashion to explore alternatives but only in circumstances where the solution has fairly tight technical boundaries. If a wide range of alternative solutions are possible and therefore need to

be explored, then computer aided draughting and design can be useful in the early stages of evaluation for techniques of geometric acceptability. Rapid determination through CAD of volumes, areas or enclosing envelopes are all helpful in eliminating unsuccessful concepts. If technical issues are not resolved it may be necessary to carry forward several concepts or at the technical evaluation stage, good concepts fail, therefore we have to start again [13].

1.1.6 Detailed Design

Upon completion of the concept design, the detail design activity begins. At this stage the commitment to the development is very high, although no hardware has yet been produced.

The conceptual and detailed design activities are highly interactive processes. The level of interaction is dependent upon the simplicity or complexity, nature and type of product which is being designed. The simplicity/complexity are directly related to the number of elements which an artefact contains, the ultimate in simplicity being only one component.

This is the last phase, in which all the essential detail drawings and analytical procedures are decided. In this phase the ultimate objective is or should be the production of a product which contains the minimum number

of components, hence minimum complexity - maximum simplicity. Additionally the reliability is built into each component through the understanding of service loads, materials and stress distributions. Finite element analysis tends to be used when component geometry is established to a large extent and provides opportunities for detail analysis and redesign.

Linking C.A.D, finite element analysis and fatigue life prediction gives an opportunity for evaluation of alternative concepts some way into the detail design phase and therefore reduces the time spent in the development and testing of prototypes.

1.1.7 Application Of Computers In The Design Process

Now that the design activities have been explored it is necessary to examine the applicability or otherwise of computer software packages at each stage of design.

During the market research phase the computers may be used to store the information on the existing product range, level of competition, etc. This information can then be analysed manually or using appropriate computer techniques.

The application of computers in the specification phase of the design activity is again limited to the compilation of information. The decision, whether or not to use computers

depends on the justification of the time and cost involved.

The application of computers in the conceptual and detail stages of the design activity is dependent upon the industry and the type of product being designed.

There exist numerous separate computer software packages (e.g. computer aided draughting, finite element analysis and fatigue life evaluation etc.) which can be employed successfully to define the shape and assess the integrity and durability of components very quickly and accurately. Therefore, computers are used successfully as part of the analytical tools of the designer.

The introduction of computers already has improved the efficiency of the design process. CAD has improved the quality of detailing and reduced the occurrence of errors. Finite Element Analysis techniques have been used successfully to assess the integrity of the components and hence reduce the static testing time. In the past these computer software packages have been used individually. The transfer and exchange of information from one application to another was often tedious if not feasible. With ever increasing use of computer solid modellers for design of engineering components the natural progression has been to generate finite element meshes automatically so that the solid modelling and analysis processes are integrated. This avoids the tedious and

error-prone manual transfer of data, hence saving both time and money [6,7].

The next logical step is or should be the integration of finite element output data with fatigue life analysis software. This enables the designer to assess the integrity and durability of the components in the design stage before any commitment to prototype manufacture and testing has been made.

1.2 Computer Aided Engineering

In many engineering situations components are subjected to variable amplitude multiaxial stresses under service loading conditions. The engineer often uses traditional theories from strength of materials to analyse and stress the load bearing components under such complex loading conditions. However, because of the limitations of the theoretical methods and techniques used, the above procedure almost always requires the manufacture and testing of prototype components. Therefore, a major proportion of engineering time is used in the building and testing of prototypes. To shorten the development cycle time and minimise the associated costs it is necessary to reduce the number of prototypes produced for testing. Consequently, the initial prototype should be close to the final product. The manufacturers have an urgent need for a reliable method to assess the fatigue life of such components at the pre-prototype design stage. Computer

aided engineering methods offer possible techniques [1, 2].

The overall aim of this project is to evaluate the engineering requirements of combining computer based geometric modelling, finite element analysis and fatigue life prediction software packages. A system of this type could allow engineers to proceed from concept to manufacture at the CAE workstation reducing the need for expensive and time consuming prototype build and test programmes.

The three areas of computer aided engineering mentioned previously are well established as separate entities. At the present time commercially available links are established between the first two processes. However, as yet no effective link exists between finite element analysis and computerised fatigue life assessment. The manual transfer and exchange of information from finite element to fatigue life assessment systems is often tedious and time consuming, if feasible. Indeed, the precise form that the finite element analysis should take to produce data relevant for fatigue life analysis is not clear. Therefore, computerised fatigue life prediction methods are primarily used during the development stage as they rely on a prototype being available to give strain or stress histories. Once these stress and strain histories are known, alternative methods of predicting fatigue life are possible i.e. critical location[3], fracture

mechanics[4], S-N curves[5]. Each method is complicated by multiaxial loading and random loading conditions. For this work the critical location approach will be used, because it is extensively used in the ground vehicle industry and also can be incorporated into a computer program.

The next step in this overall process is the integration of finite element analysis and fatigue life assessment to assess the durability of engineering components at the design stage.

If successful, this approach could significantly reduce the need for prototype testing but at the same time ensure high component reliability.

1.3 Historical Perspective of Fatigue

As early as the 1840's, many researchers were investigating the behaviour and properties of engineering materials undergoing fatigue failure. In the 1850's August Wohler [14] performed many laboratory fatigue tests under repeated stresses. He showed from stress versus life (S-N) diagrams how fatigue life decreases with higher stress amplitudes and that below a certain stress amplitude the test specimens did not fracture. Thus Wohler introduced the concept of the S-N diagram and the fatigue limit. He pointed out that for fatigue the range of stresses is more important than the maximum stress. Wohler's (S-N) curve is still widely used today as one of the methods of quantifying fatigue resistance. During the 1870's and

1890's Gerber [15] investigated the influence of the mean stress, and Goodman [16] proposed a simplified theory concerning mean stress. Another notable contributor of this period was Basquin [17] who introduced the exponential relationship between stress and fatigue.

The next important step was the work by Bairstow [18, 19] at the National Physical Laboratory. His 1909 paper contains the earliest published hysteresis loops. This work indicates the phenomenon of materials undergoing cyclic softening. He also demonstrated that "the maximum width of any loop measured parallel to the axis of extension added to the elastic extension of the specimen is the total change of length in each cycle". In the 1920's Gough [20] and associates performed studies of the fatigue limit on bending and torsion and found that the ratio of the fatigue limit in torsion to that of bending varied with material. In 1929/1930 Haigh [21] investigated the difference in the response of high tensile strength steel and mild steel to fatigue when notches are present. He used the concept of notch strain analysis and self-stresses. During the 1930's an important practical advance was achieved by the introduction of shot-peening in the automobile industry. Almen [22, 23] correctly explained the spectacular improvements by compressive stresses produced in the surface layers of peened parts and promoted the use of peening and other processes that produce beneficial self stresses.

In 1937 Neuber [24] introduced stress gradient effects at notches and the elementary block concept, which consider that the average stress over a small volume at the root of the notch is more important than the peak stress at the notch. Neuber's Rule is now an essential part of most modern computer based methods of fatigue life predictions. In the same period the development of the bonded wire resistance strain gauge by Ruge and De Forest at MIT and Simmons and Clark at the California Institute of Technology revolutionised the technique of service load measurements. In 1945 Miner [25] formulated a linear cumulative fatigue damage criterion suggested by Palmgren in 1924 [26]. This linear damage criterion is now recognised as the Palmgren Miner Law. It has been used extensively in fatigue life calculations involving random load histories.

In the 1950's Gassner [27] recognised the complex nature of service loading. To overcome the pitfalls of constant amplitude testing he suggested the variable-loading test be carried out for both ground vehicles and air craft. He proposed the use of block programming, where the service data are analysed and broken down into blocks of loading to be applied sequentially.

Major contributions to the subject of fatigue in the 1950's included the introduction of closed-loop electro-hydraulic test systems, which allowed better simulation of

load histories on specimens, components and total mechanical systems. Electron microscopy revealed new horizons to a better understanding of fatigue mechanisms. Irwin [28] introduced stress intensity factor, K_I which has been accepted as the basis of linear elastic fracture mechanics (LEFM) and of fatigue crack growth predictions. Low cycle strain- controlled fatigue behaviour became prominent with the Manson-Coffin[29, 30] relationship between plastic strain amplitude and fatigue life. These ideas are the basis for current local strain fatigue analysis.

Many multiaxial fatigue life prediction theories have been proposed by many eminent researchers. However, as yet no universally acceptable method exists. The traditional approach to multiaxial fatigue life evaluation has been based on the extension of the static yield criteria to fatigue [53, 64]. This is used to reduce the multiaxial component of stress or strain to a single equivalent parameter, which can then be analysed using the conventional techniques developed. More recently, it has become clear that single parameter description of fracture is inadequate, but two parameters are required for more accurate fatigue analysis. Among the leaders in this school of thought are Brown and Miller [42]. The theory is based on critical plane approaches, which postulate that cracks initiate and grow on certain planes and that the strain normal to those planes assist in the fatigue crack growth process.

With the development of finite element techniques by the aerospace industry in the 1950's and 60's stress analysis of complex structures was made possible. Prior to this all components had to be analysed by extremely complex and often tedious techniques. Indeed, some methods became so complex that they were impossible to solve. Empirical data and past experience were often the most useful tools at the engineer's disposal and as a consequence, large factors of safety were incorporated resulting in large and over weight components.

The availability of low cost, high performance computers and associated fatigue software packages, together with advancement in load measurement and analysis method can now significantly aid the engineer and enable the development of efficient, effective and economic products. Application of these tools to component design can also reduce the need for expensive prototype 'build and test' programmes [31].

1.4 Scope Of The Present Work

Major advances have been made during the last 150 years in the development of analytical procedures to assess structural damage resulting from repetitive loadings. However, failures due to fatigue still occur in many areas of engineering with disastrous consequences in terms of both human life and cost. It is for this reason that the

analytical procedures used during the design stage are supported with full scale prototype build and test programmes. There are two weaknesses in this approach. First of all, once the most suitable concept is selected, the detail design and analysis procedures are followed. In this phase, quite often the static load analysis is carried out and peak stresses are limited to fatigue strength of the material but are not totally representative of the service environment. Secondly, upon completion of the above procedures, prototype build and test begins. This is used to identify durability weaknesses in a given prototype. Obviously this process of build and test takes place very late in the design stage. Any limitations in the design analysis lead to repetition of the above procedures. This makes the process of design time consuming and prohibitively expensive [1, 2].

The present investigation into the integration of geometric modelling, finite element analysis and fatigue life prediction software is being carried out in association with nCode International Limited, suppliers of the FATIMAS [32] software which uses the critical location approach to estimate fatigue lives from a service strain history. Other software packages used are geometric modelling software (MEDUSA) [33] and finite element analysis software (PAFEC) [34, 35]. The above software has all the necessary capabilities to support the project. It should be pointed out that already a link exists between MEDUSA and PAFEC, ie FECS software[36] which will be used and evaluated as a minor element of the project.

Although the project concentrates on providing a link between PAFEC and FATIMAS, it is intended that any final conclusions will be applicable to other finite element and fatigue life prediction packages.

In this programme of work, the actual component used for evaluating the procedures developed was a steering arm of a 32 ton track supplied by a European manufacturer. This was evaluated for a real service load history supplied by the manufacturer, which had been recorded during the prototype testing of the vehicle driven on mixed test road surfaces at their test track. Material data was also supplied.

1.5 Principal Objectives Of Research Programmes

The principal objectives of the work programme are therefore:-

- i) To use a CAD software package to create a two and three dimensional geometric model of the steering arm, which will be used to select the boundary coordinates for development of a finite element mesh.
- ii) To use a finite element package to develop a model and to identify the critical stress points in the steering arm together with the elastic stress/strain data.

- iii) To use the local elastic stresses and strains generated in (ii), together with both the energy density approach [37] and Neuber's uniaxial equation [38], to give the total elastic/plastic strains at the critical points. Other inputs required for the analysis are the material properties, an appropriate geometric stress concentration factor, K_t , and service loading history. The analysis will include biaxial loading.

- iv) To use strain gauge measurements under static loads to monitor the total elastic/plastic strains at these critical areas in the component in order to examine the validity of the application of the analysis outlined above (iii).

- v) To use the total elastic/plastic strains obtained in (iii) to develop load/strain calibration curves for the component. These can be used to create a load history, suitable for experimental fatigue life analysis.

- vi) To experimentally monitor fatigue life measurement of the steering arm using a load controlled DARTEC computer controlled servo hydraulic multiaxial testing machine.

- vii) To use computerised fatigue life software FATIMAS to predict the fatigue life of the steering arm under service loading conditions.
- viii) To compare the experimental, computerised and actual test track fatigue lives to examine the validity of the technique proposed.
- ix) To propose the data requirements for the integration of the finite element elastic stress/strain output data file with that of fatigue life software package to produce a life map of the component.
- x) To critically evaluate the proposed procedures.

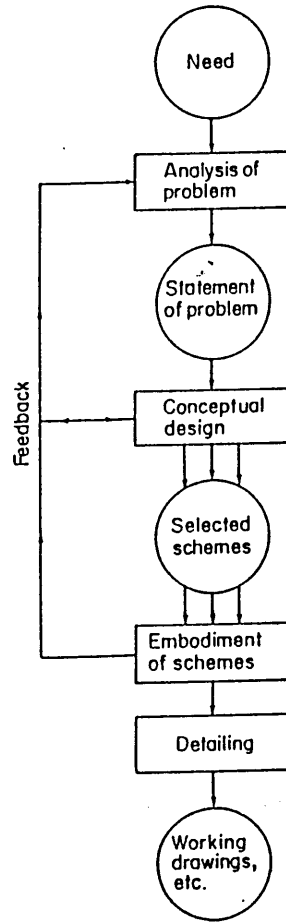


Fig. 1.1 French's model of the Design Process(II).

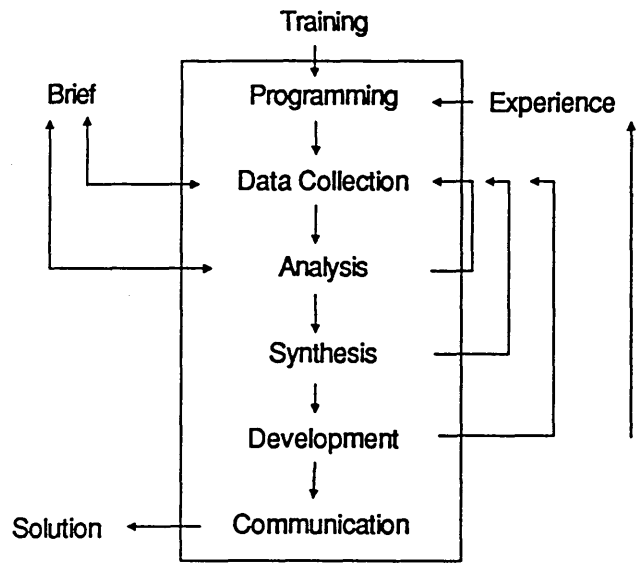


Fig. 1.2 Archer's Model of the Design Process (8).

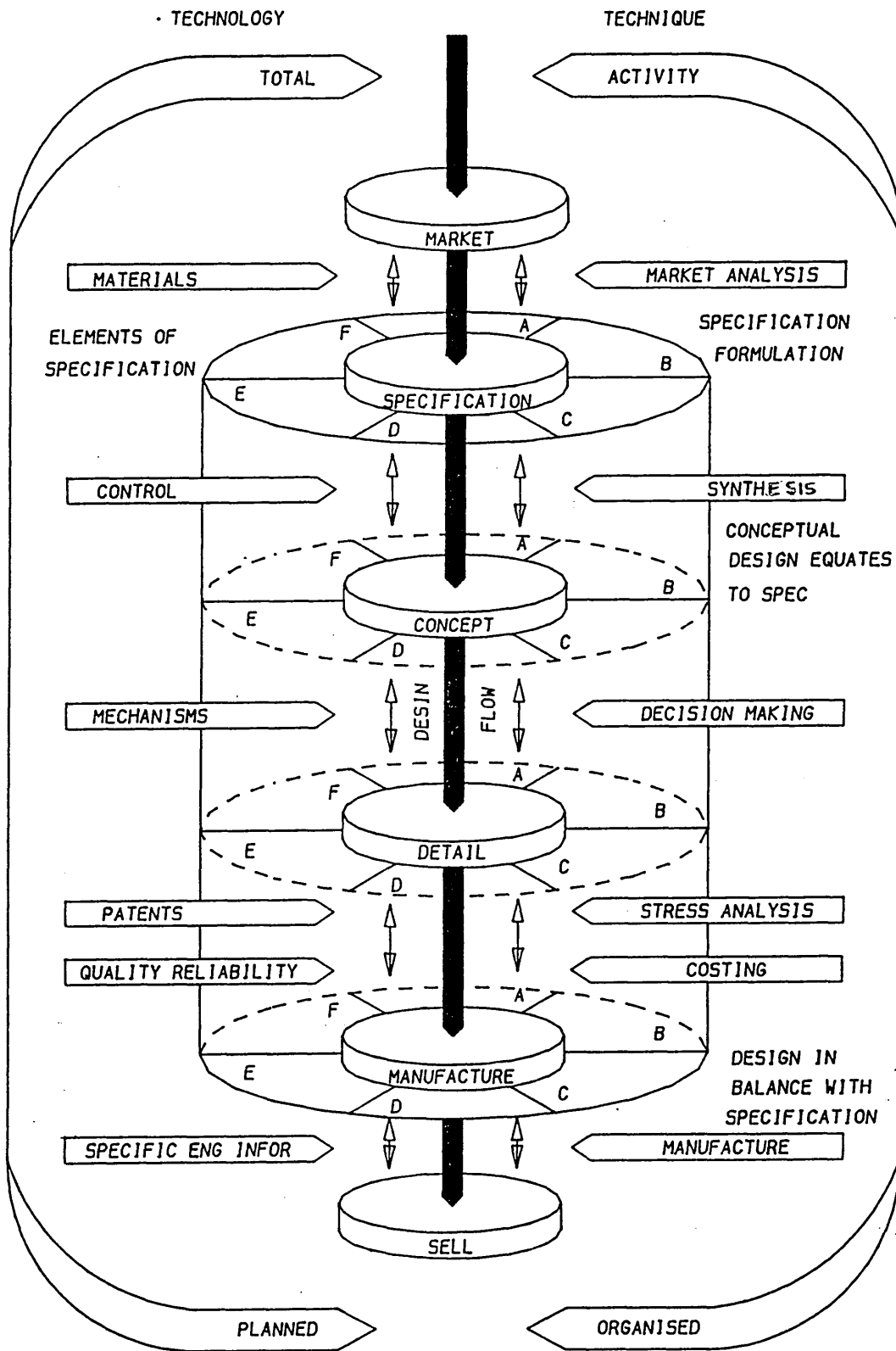


Fig. 1.3 Pugh and Smith's Model of the Design Process (12,13).

CHAPTER 2

FATIGUE LIFE EVALUATION TECHNIQUE

2.1 Introduction

It is generally accepted that fatigue analysis based upon a knowledge of strain in a component is more logical than one based upon stress, since strain is the phenomenon deemed more appropriate for modelling the plasticity which the component undergoes at the site of failure [39].

The local stress/strain method places emphasis on the local cyclic stresses and strains at the root of the notch where failure originates. Normally local values are derived from nominal values, by applying Neuber's rule [24] as determined by Topper, Wetzel, and Morrow [38, 39], and the cyclic properties of the material are used instead of the monotonic values. Multiaxiality causes complications and one approach is to reduce the complex stresses to a single equivalent parameter [53, 64].

The critical location method has been established as realistic for predicting the durability of engineering components. This approach is finding wide-spread use by many manufacturing companies [40, 41], in particular the automotive industry.

Alternative methods of multiaxial fatigue evaluation have been based on critical plane approaches as proposed by Brown and Miller [42]. These theories are based on crack initiation and growth on specific geometric planes. One advantage suggested for this theory is the opportunity for

physical interpretation of fatigue damage accumulation. However, this approach is insufficiently developed to deal with non-proportional loading or accumulation of damage under random out-of-phase biaxial histories. Furthermore, the guidelines to deal with stress concentration factors, stress gradients etc, are not available. Thus it's usefulness in the automotive field is at present very limited.

2.2 Neuber's Rule

The fatigue behaviour in a notched component can be predicted on the basis of known behaviour of a simple smooth specimen. The basis of the prediction is Neuber's rule [24], which takes into account the possibility of non-linear deformations at the root of the notch. Neuber developed a mathematical expression of the stress and strain concentration at a notch root.

$$K_t = (K_\sigma \cdot K_\epsilon)^{\frac{1}{2}} \quad - 2.1$$

Where:-

K_t = Theoretical elastic concentration factor.

K_σ = True stress concentration factor.

K_ϵ = True strain concentration factor.

Equation 2.1 is exact when the notch root remains elastic. In this case, any concentration of stress is accompanied by the same concentration of strain, which can be calculated using Hooke's law.

Thus $K_{\sigma} = K_{\epsilon}$ and from equation 2.1 $K_{\sigma} = K_t$ as shown in figure 2.1. The validity of Neuber's expression is not necessarily obvious when yielding takes place at the notch root. However, it suggests that as K_{σ} decreases, K_{ϵ} increases in non-linear deformation, so their product could be constant.

For fatigue application equation 2.1 is usually altered by replacing K_t with K_f and defining K_{σ} and K_{ϵ} as the ratio of the ranges of stress and strain which result in:-

$$K_f = \left(\frac{\Delta \sigma}{\Delta S} \cdot \frac{\Delta \epsilon}{\Delta e} \right)^{\frac{1}{2}} \quad - 2.2$$

Where:-

$\Delta \sigma$ = Stress range at notch root

ΔS = Nominal stress range

$\Delta \epsilon$ = Strain range at notch root

Δe = Nominal strain range

K_f = Fatigue concentration factor

Equation 2.2 may be transposed giving:-

$$K_f (\Delta S \cdot \Delta e)^{\frac{1}{2}} = (\Delta \sigma \cdot \Delta \epsilon)^{\frac{1}{2}} \quad - 2.3$$

All terms on the left side are determinable for each reversal from the load history and cyclic stress-strain curves, and all terms on the right side represent the local stress/strain behaviour of the material at the notch root.

If the nominal conditions away from the notch are elastic then:-

$$\Delta e = \frac{\Delta S}{E} \quad - 2.4$$

Giving:-

$$K_f \cdot \Delta S = (\Delta \sigma \cdot \Delta \epsilon \cdot E)^{\frac{1}{2}} \quad - 2.5$$

The right hand side of the above equation is a determinable constant for each half-cycle of load. The equation is of the form, $X \cdot Y = C$, which is a rectangular hyperbola [39, 43].

For simulations of the material at the notch root, the smooth specimen must be strained until the product of the stress and the strain equal the constant C , where $C = (K_f \cdot \Delta S)^2 / E$ as shown in figure 2.2.

2.3 The Cyclic Stress-Strain Curve

The cyclic stress/strain curve which provides a measure of the steady-state cyclic deformation resistance of a material can be different from the monotonic stress/strain curve. The cyclic stress/strain curve, is the locus of tips of the stable hysteresis loops from several companion tests at different completely reversed constant strain amplitudes [43]. Such a steady-state stress-amplitude strain-amplitude curve can be compared directly with the monotonic stress/strain curve. Cyclically induced changes in deformation resistance then become immediately apparent. If the cyclic stress/strain curve is above the monotonic curve the material is said to cyclically harden; if the cyclic curve is below the monotonic curve the material is said to cyclically soften [44].

Cyclic stress/strain properties are determined by testing smooth polished specimens under axial cyclic strain control. The cyclic stress/strain curve is defined as the locus of tips of stable "true stress/strain hysteresis loops" obtained from companion test specimens. A typical stable hysteresis loop with a cyclic stress/strain curve drawn through the loop tips is shown in figure 2.3.

As shown in figure 2.4 the height of the loop from tip-to-tip is defined as the stress range ($\Delta\sigma$). For completely reversed testing one half of the stress range is generally equal to the stress amplitude. While one half of the width from tip-to-tip is defined as the strain amplitude ($\Delta\epsilon_T/2$). The plastic strain amplitude is found by

subtracting the elastic strain amplitude ($\Delta \epsilon_e / 2$) from the total strain amplitude.

$$\frac{\Delta \epsilon_p}{2} = \frac{\Delta \epsilon_T}{2} - \frac{\Delta \epsilon_e}{2} \quad - \quad 2.6$$

For elastic conditions:

$$\frac{\Delta \epsilon_e}{2} = \frac{\Delta \sigma}{2E} \quad - \quad 2.7$$

Where;

E = modulus of elasticity

Then:

$$\frac{\Delta \epsilon_p}{2} = \frac{\Delta \epsilon_T}{2} - \frac{\Delta \sigma}{2E} \quad - \quad 2.8$$

The relation between cyclic stress and plastic strain can be described mathematically by a power function similar to that used for the monotonic curve [44, 45].

$$\frac{\Delta \sigma}{2} = k' \left(\frac{\Delta \epsilon_p}{2} \right)^{n'} \quad - \quad 2.9$$

where:

$$\frac{\Delta \sigma}{2} = \text{Stable Stress Amplitude}$$

$$\frac{\Delta \epsilon_p}{2} = \text{Stable plastic strain amplitude}$$

$$n' = \text{Cyclic strain hardening exponent}$$

$$k' = \text{Cyclic strength coefficient.}$$

The value of n' is found to be between 0.05 and 0.30 and usually close to 0.15 for most metals regardless of their initial condition [44, 45].

In many field test conditions it is desirable to convert measured strains to the corresponding stresses in order to estimate fatigue life. Equation 2.8 can be rewritten:-

$$\frac{\Delta \epsilon_T}{2} = \frac{\Delta \sigma}{2E} + \frac{\Delta \epsilon_p}{2} \quad - 2.10$$

Equation 2.9 may be rearranged giving:-

$$\frac{\Delta \epsilon_p}{2} = \left(\frac{\Delta \sigma}{2k'} \right)^{1/n'} \quad - 2.11$$

Substituting equation 2.11 into equation 2.10 yields an equation relating cyclic stress amplitude in terms of the previously defined properties and the modulus of elasticity.

$$\frac{\Delta \epsilon_T}{2} = \frac{\Delta \sigma}{2E} + \left(\frac{\Delta \sigma}{2k'} \right)^{1/n'} \quad - 2.12$$

2.4 Methods of Determining the Cyclic Stress/Strain Curve

2.4.1 Multiple Step Tests

In 1910 Bairstow [46] and the later Dugdale [47] showed that the hysteresis loop rapidly adjusts to a stable steady state following sudden changes in cyclic strain amplitude. This makes it possible to obtain several points on the cyclic stress/strain curve from a single specimen by cycling at different strain amplitudes. Such a program is shown in figure 2.5a. Each strain amplitude step and the corresponding stable stress amplitude provides one point on the cyclic stress/strain curve. Cycling to about 20 percent of the life at a given strain amplitude normally gives a reasonable indication of the stable behaviour. The effect of strain sequence can be important. A high-to-low strain sequence is generally preferable. To avoid mean stress effects the strain amplitude should be decreased incrementally to zero stress and strain between blocks.

2.4.2 Incremental Step Tests

A specimen may be subjected to blocks of gradually increasing and then decreasing strain amplitudes, as shown in figure 2.5b, to quickly determine the cyclic stress/strain curve. After a number of these blocks, the metal cyclically stabilises. A continuous plot of the hysteresis loops through a block results in a series of superimposed loops with a clearly defined locus of tips corresponding to the cyclic stress/strain curve [48].

2.5 Analysis of Strain-life Curve

An analysis of the stable stress/strain hysteresis loops show that the strain is made up of elastic and plastic components, so that at any given fatigue life these two components are present. At large strains or short lives, the plastic strain component is predominant, and at small strains or longer lives the elastic strain component is predominant [39, 48]. This is indicated by the straight lines and the hysteresis loop sizes in figure 2.6. The intercepts of the two straight lines at $2N = 1$ are ϵ'_f for the plastic component and σ'_f/E for elastic component. The slopes are c and b respectively. This provides the following equations for strain-life data of small smooth specimens:-

$$\frac{\Delta \epsilon_T}{2} = \frac{\Delta \epsilon_e}{2} + \frac{\Delta \epsilon_p}{2} \quad - 2.13$$

$$\frac{\Delta \epsilon_T}{2} = \frac{\sigma'_f}{E} (2N_f)^b + \epsilon'_f (2N_f)^c \quad - 2.14$$

Where:-

$$\frac{\Delta \epsilon_T}{2} = \frac{\epsilon_a}{2} \quad \text{total strain amplitude}$$

$$\frac{\Delta \epsilon_e}{2} = \quad \text{Elastic strain amplitude}$$

$$\frac{\Delta \epsilon_p}{2} = \quad \text{Plastic strain amplitude}$$

$$\epsilon'_f = \quad \text{Fatigue ductility coefficient}$$

$$\sigma'_f = \quad \text{Fatigue strength coefficient}$$

$$c = \quad \text{Fatigue ductility exponent}$$

$$b = \quad \text{Fatigue strength exponent}$$

$$2N_f = \quad \text{number of reversals to failure}$$

The above relationship does not take mean stress into account; to overcome this disadvantage two laws have been proposed.

- a) Morrow's law, which empirically reduces the fatigue strength coefficient by an amount equal to the mean stress [48, 49].

$$\frac{\Delta \epsilon_T}{2} = \left(\frac{\sigma'_f - \sigma_m}{E} \right) (2N_f)^b + \epsilon'_f (2N_f)^c - 2.15$$

b) Smith-Watson-Topper parameter [50]

$$\sigma_{\max} \cdot \epsilon_a = \frac{\sigma'_f}{E} (2N_f)^{2b} + \sigma'_f \cdot \epsilon'_f (2N_f)^{b+c} \quad - 2.16$$

Where:-

σ_{\max} = maximum stress of the reversal.

The number of cycles N_f before failure at a certain level of strain range can be calculated using the above laws. The damage caused by one reversal is assumed to be equal to $1/2N_f$. This stems from the Palmgren-Miner theory for linear cumulation damage [39, 51]. The formal statement of the linear damage concept is that the summation of all fractions of life equals one.

$$\sum n_i / N_i = 1 \quad - 2.17$$

Where n_i is the total number of cycles applied during the fatigue life at a strain level corresponding to a fatigue life of N_i cycles.

The damage D_i caused by a sequence of cycles or "loading block" can therefore be estimated from:-

$$D_i = n_i / N_i \quad - 2.18$$

Obviously using equations 2.17 and 2.18 failure occurs when $D_i = 1$

If the component is subjected to a number of loading blocks then the number of loading blocks to cause failure is $1/D_i$ [51].

2.6 Extracting Hysteresis Loops (Cycle Counting)

The objective of all cycle counting methods is to reduce an irregular load history to a series of constant amplitude cycles and to compare these with the S-N or ϵ -N curves obtained with uniformly repeated simple load cycles. The application of the linear damage rule $D = 1/N$ requires a knowledge of the condition (mean and amplitude of stress or strain) to which the damaging event should be compared.

The only meaningful method among those which are currently used to extract hysteresis loops from a strain signal is the "Rainflow Count" method proposed by M. Matsuiski and T. Endo [39, 52]. The operation of the rainflow method is shown in Fig. 2.7 for a history consisting of four peaks and four valleys.

The rules are:

1. Rearrange the history to start with the highest peak.
2. Starting from the highest peak go down to the next reversal, proceed horizontally to the next downward range, if there is no range going down from the level of the valley at which you have stopped, go upward to the next reversal.
3. Repeat the same procedure upward instead of downward and continue these steps to the end.
4. Repeat the procedures for all the ranges and parts of a range that were not used in previous procedure.

Thus assume that the highest peak is more extreme than the lowest valley. If not, start with the lowest value and go up instead of down. In figure 2.7a, the first traverse is shown. Remaining ranges are in figures 2.7b. The procedure applied to figure 2.7b again leaves a pair of range unused. They are shown in figure 2.7c.

Another technique which gives the same results of cycle counting is that of imaginary rainflow on fictitious multi-farious overlapped pagoda roofs[48] as shown in figure 2.8. The strain-time history is plotted so that the time axis is vertically downwards, and the lines connecting the strain peaks are imagined to be a series of pagoda roofs so that cycles and half cycles are defined. the rain starts at the top of the history and also at the inside of each peak and trough. The flow is stopped by striking flow descending from above, or passing a point opposite a peak or trough with a greater magnitude than that which the flow started. Flow also stops when it reaches the bottom of the history. Each flow is a half cycle, and there is a complementary half cycle of opposite sign elsewhere in the complete history, except for the beginning or the end of the history.

The advantage of a rainflow count comes when it is combined with a strain analysis as shown in figure 2.9. The damage can then be computed for each cycle as soon as it has been identified in the counting procedure and the corresponding reversal points can be discarded.

2.7 Energy Density Approach For Elastic/Plastic Stress And Strain Calculation At The Notch Root

An alternative method to Neuber's equation for the calculation of local stresses and strains is based on the energy density approach developed by Glinka [37, 62, 63].

Due to non-uniform stress distribution at a notch root, each point of the notched body absorbs different strain energies. Assuming uniaxial stress conditions at the notch root and linear elastic behaviour of the material we can calculate that:-

$$WS = \int_0^e S(e)de$$

$$WS = \int_0^e E.e.de$$

$$WS = \frac{E.e^2}{2}$$

$$WS = \frac{s^2}{2E} \quad - \quad 2.19$$

$$W\sigma = \int_0^{\epsilon} \sigma(\epsilon).d\epsilon$$

$$W\sigma = \int_0^{\epsilon} E.e.de$$

$$W_{\sigma} = E \left(\frac{\epsilon^2}{2} \right)$$

$$W_{\sigma} = \frac{\sigma^2}{2E} \quad - \quad 2.20$$

Where:-

WS = The elastic strain energy per unit volume due to the nominal remote stress S.

W_σ = The strain energy per unit volume due to local stress and strain at the notch root.

In entirely elastic cases the stress at the notch tip can be calculated as:-

$$\sigma = K_t \cdot S \quad - \quad 2.21$$

The following equation is obtained by substituting equations 2.19 and 2.20 in equation 2.21.

$$k_t = \left(\frac{W_{\sigma}}{WS} \right)^{\frac{1}{2}} \quad - \quad 2.22$$

It means that the elastic energy density W_σ at the notch tip is equal to the strain energy WS due to the nominal stress s multiplied by the square of the stress concentration, K_t.

In the presence of localised yielding at the notch tip, the strain energy, W_σ is calculated using cyclic stress/strain relationship.

$$W_{\sigma} = \frac{\sigma^2}{2E} + \frac{\sigma}{n'+1} \left(\frac{\sigma}{k'} \right)^{1/n'} \quad - \quad 2.23$$

If plastic yielding occurs equation 2.22 is given in the form:-

$$K_t = \frac{\frac{\sigma^2}{2E} + \frac{\sigma}{n'+1} \left(\frac{\sigma}{K'} \right)^{1/n'}}{\frac{s^2}{2E}} \quad - \quad 2.24$$

Equation 2.24 can be rearranged into:-

$$\frac{(K_t \cdot s^2)}{2E} = \frac{\sigma^2}{2E} + \frac{\sigma}{n'+1} \left(\frac{\sigma}{k'} \right)^{1/n'} \quad - \quad 2.25$$

For fatigue applications the strain energy equation is written in terms of the ranges of stress and strain which results in:-

$$\frac{(K_t \cdot \Delta s^2)}{4E} = \frac{\Delta \sigma^2}{4E} + \frac{\Delta \sigma}{n'+1} \left(\frac{\Delta \sigma}{2k'} \right)^{1/n'} \quad - \quad 2.26$$

Equations 2.26 and 2.12 make it possible to calculate the local elastic/plastic stresses and strains needed for fatigue life evaluation.

2.8 Multiaxial Fatigue

A number of approximation methods for multiaxial fatigue life evaluation have been proposed, but as yet no universally acceptable approach exists [57]. The traditional approach relies on characterisation of ^{the} multiaxial fatigue process by a single parameter (e.g. equivalent stress). This equivalent stress or strain is subsequently processed

with an appropriate fatigue life prediction technique [53,64,59]. Therefore, the fatigue damage is accounted for by a single stress or strain variable without regard to the simultaneous presence of other stresses and strains. The modern approach to fatigue life evaluation adopts two parameters. These parameters may be stress or strain based. Uniaxial fatigue data is then used in the form of stress-life or strain-life curves to obtain a relationship between fatigue life and calculated stress or strain amplitude. Obviously fatigue life estimation based on strain is more appropriate than that based on stress since the former is more suitable for modelling the plasticity which the component undergoes at the critical site of failure.

Multiaxial fatigue theories can be generally divided into three categories [57, 64]. One commonly used approach is based on the extension of static yield criteria to fatigue life evaluation. The most often used criteria in this group include the maximum shear theory (Tresca), the octahedral energy criterion (von Mises), and the maximum principal stress theory (Rankine). In order to improve the accuracy of the results, modifications have been developed by other researchers and incorporated in the analyses. These have included consideration of such factors as hydrostatic stress effect, normal stress effect and surface anisotropy [57]. Another approach to fatigue life prediction has been the use of energy as a correlating parameter for multiaxial data. A third and more recent

method of multiaxial fatigue life evaluation has been the critical plane approach [37, 63], described earlier.

Close examination of the published data shows that successful multiaxial fatigue life assessment requires replacement of uniaxial quantities σ and ϵ by the equivalent quantities σ_{eq} and ϵ_{eq} , by consideration of the following steps [53, 59]:-

- i) Knowledge of external loads or nominal stresses and strains which causes failure.
- ii) A yield criterion (e.g. Tresca or von Mises') to reduce the multiaxial elastic/plastic stress system to an equivalent stress or strain.
- iii) An approximation formula (e.g. Neuber's equation) to relate the external loads or nominal stresses and strains to notch root stresses and strains causing failure.
- iv) Geometric information, K_t .
- v) The material fatigue properties.

Since there are no universally acceptable standard techniques for fatigue life assessment, a brief review of some of the more popular traditional and more radical modern techniques are out-lined below:

2.8.1 Principle Of Static Yield Criteria To Fatigue

This approach has been developed from theories of strength of materials under static biaxial loading [53, 54]. When using these techniques the Multiaxial stresses are reduced at some critical location on the structure, to three principal stresses, the failure criterion is then applied which will reduce these principal stresses to a single equivalent stress, σ_{eq} or strain, ϵ_{eq} . This is then used in conjunction with an approximation formula and material fatigue properties to obtain the fatigue life of engineering components. Therefore, principle of static yielding criteria has been adopted for dynamic loading of the structures. For random loading of the structure, the first step is to calculate an equivalent stress/strain from the principal stress histories. This equivalent history is subsequently processed with any of the available uniaxial techniques. A brief description of each method is outlined below.

a) Tresca's Method: (Maximum Shear Stress Theory)

This theory states that failure can be assumed to occur when the maximum stress in the complex stress system becomes equal to that at yield in the simple tensile test. Since the maximum shear stress is half the greatest difference between two principal stresses the criterion of failure become [55, 56]:-

$$\tau = \frac{\sigma_1 - \sigma_3}{2}$$

And for yield

$$\frac{\sigma_1 - \sigma_3}{2} = \frac{\sigma_{yt}}{2}$$

$$(\sigma_1 - \sigma_3) = \sigma_{yt} = \sigma_{eq} \quad - \quad 2.27$$

b) von Mises' Method (Shear or Distortion Strain Energy Theory)

The total strain energy, U_t , of an element of material is made up of two parts, that due to change in volume and that due to change in shape. These will be termed volumetric strain energy, U_v and distortion or shear strain energy, U_s . The conditions are determined by equating the strain energy of distortion at yield in the general case with the strain energy of distortion under simple tension thus [55, 56]:-

$$\frac{1}{12G} (\sigma_1 - \sigma_2)^2 + (\sigma_2 - \sigma_3)^2 + (\sigma_3 - \sigma_1)^2 = \frac{\sigma_{yt}^2}{6G}$$

$$(\sigma_1 - \sigma_2)^2 + (\sigma_2 - \sigma_3)^2 + (\sigma_3 - \sigma_1)^2 = 2\sigma_{yt}^2 \quad - \quad 2.28$$

In two-dimensional systems,

$$\sigma_3 = 0$$

Therefore:-

$$\sigma_1^2 + \sigma_2^2 - \sigma_1 \cdot \sigma_2 = \sigma_{yt}^2 = \sigma_{eq}^2 - 2.29$$

c) Rankine's Method: (Maximum Principal Stress Theory)

This theory states that yielding will occur in a material under complex stress when σ_1 attains a value equal to the yield stress, σ_{yt} , measured in a simple tension test on the same material [55, 56].

$$\sigma_1 = \sigma_{yt} = \sigma_{eq} \quad - 2.30$$

For yielding to occur.

Rankine's method defines the fatigue limit in terms of maximum principal stress. The component is judged safe if the principal stress remains below that of the yield stress under uniaxial tension. A cumulative damage sum under random loading can be calculated by using the principal stress and the service history [53].

The maximum principal stress theory has successfully been used for brittle materials, while both the Tresca and von Mises' criteria have been shown to result in good correlations for ductile materials at long lives [53, 64].

The above techniques a, b and c, can be used to reduce the multi-axial stress system to an equivalent stress σ_{eq} which can then be used in conjunction with an approximation equation to calculate the local stress/strain values needed for fatigue life estimation.

2.9 Critical Plane Approach

Brown and Miller [42] have postulated that cracks initiate and grow on certain planes and that the normal strains to those planes assist in the fatigue crack growth. The general form of this theory is expressed with the aid of figure 2.10.

$$(\epsilon_1 - \epsilon_3)/2 = f \left(\frac{\epsilon_1 + \epsilon_3}{2} \right) \quad - 2.31$$

Where:-

$\epsilon_1, \epsilon_2, \epsilon_3$ are principal strains ($\epsilon_1 > \epsilon_2 > \epsilon_3$)

$$(\epsilon_1 - \epsilon_3)/2 = \frac{\bar{\gamma}}{2} \quad \text{maximum shear strain}$$

$\frac{(\epsilon_1 + \epsilon_3)}{2} = \epsilon_n$ tensile strain normal to the plane of maximum shear.

f = Functional relationship

There are two possible cases of crack growth under biaxial fatigue conditions [64, 65]. Case A arises for negative values of $\lambda = \sigma_2/\sigma_1$ where the crack propagates along the surface and the surface strains are ϵ_1 and ϵ_3 . Case B arises for positive values of $\lambda = \sigma_2/\sigma_1$ where ^{the} crack propagate inwards and the surface strains are ϵ_1 and ϵ_2 .

Case B is more severe than case A as shown in figure 2.11. Brown and Miller have shown that data from all kinds of biaxial and multiaxial fatigue tests can be plotted on Γ planes. It is to be noted that for all possible combinations of biaxial loading, no points can lie outside a wedge shaped area, the top edge of which corresponds to the uniaxial loading. The horizontal axis is the plane strain state and pure torsion condition and lastly the bottom edge of the wedge corresponds to equiaxial loading as shown in figure 2.12.

A similar approach has been proposed by McDiarmid [66, 67, 68] although his approach is based on maximum shear and normal direct stress. McDiarmid has proposed that the important parameters for long life fatigue in the unnotched specimens are the alternating and mean stresses, both normal and shear, occurring on the plane of maximum range of shear stress.

McDiarmid has shown that:-

$$\tau_a = C_1 - C_2(\sigma_\tau)^{1.5} \quad - 2.32$$

where:-

τ_a = Shear stress amplitude on plane of maximum range of shear stress.

σ_τ = Normal stress amplitude on plane of maximum range of shear stress.

$C_1 = t =$ Fatigue strength in twisting.

$$C_2 = (t - b/2) / (b/2)^{1.5}$$

$b =$ Fatigue strength in bending

Hence:-

$$\tau_a = t - [(t - b/2) / (b/2)^{1.5}] \cdot \sigma_r \quad - 2.33$$

The allowable amplitude of shear stress on the plane of maximum shear stress can be predicted using equation 2.33.

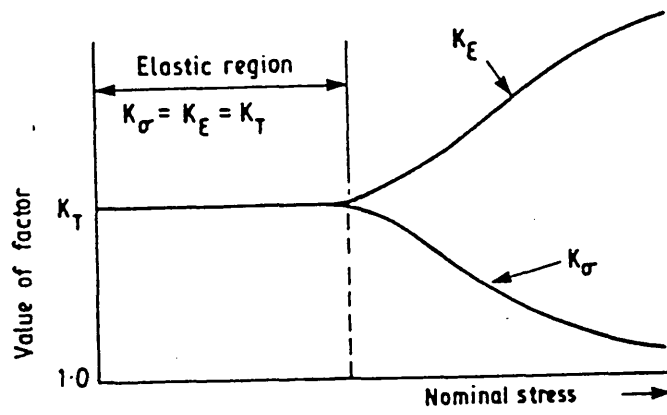


Fig. 2.1 Variation of Stress Concentration Factor and Strain Concentration Factor as Stress Increases.

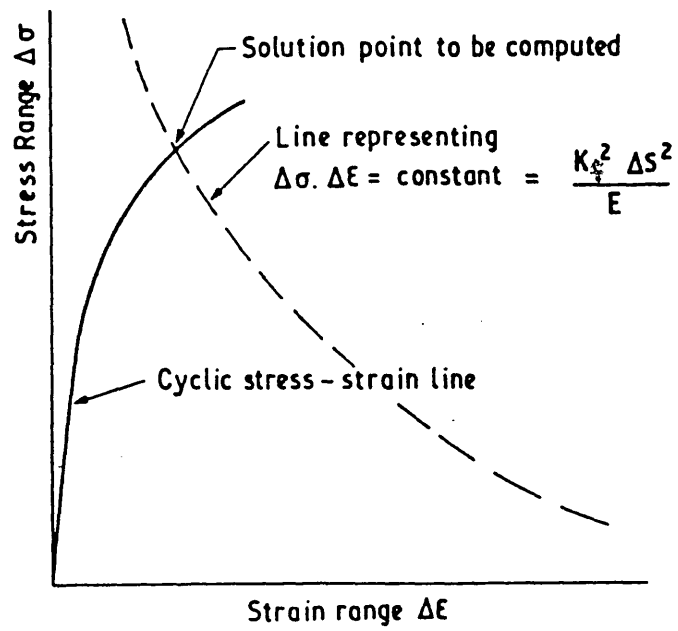


Fig. 2.2 Solving the Neuber Equation.

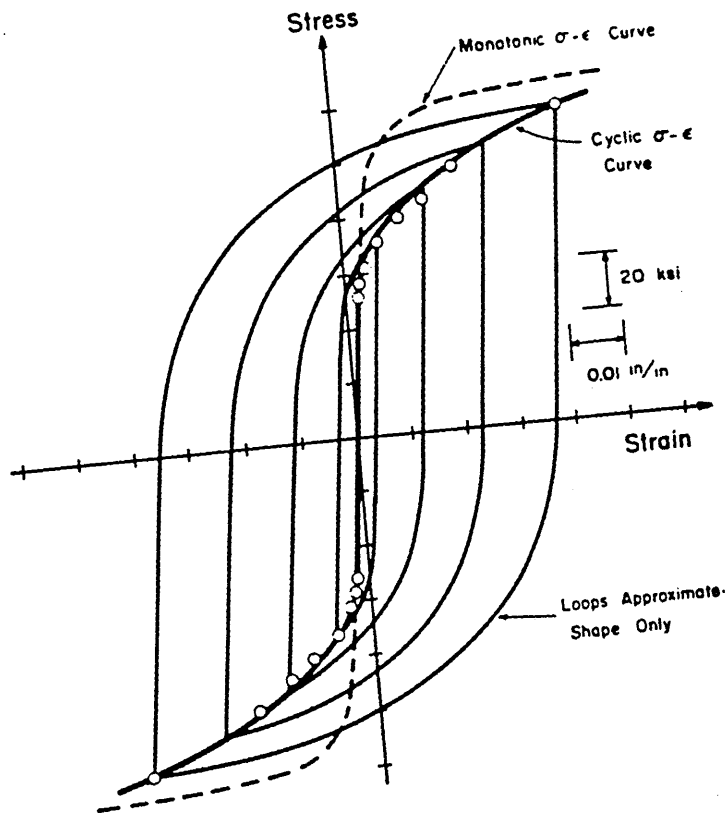


Fig. 2.3 Monotonic and Cyclic Stress/Strain Curve.

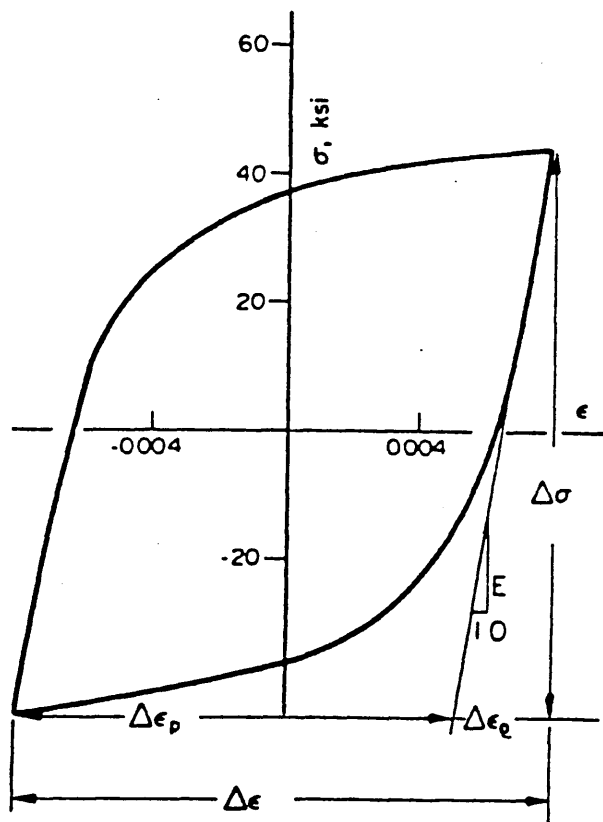
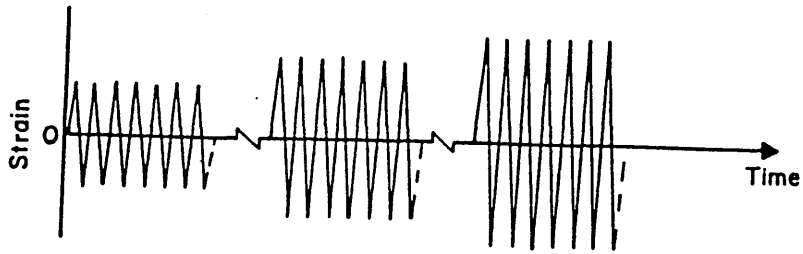
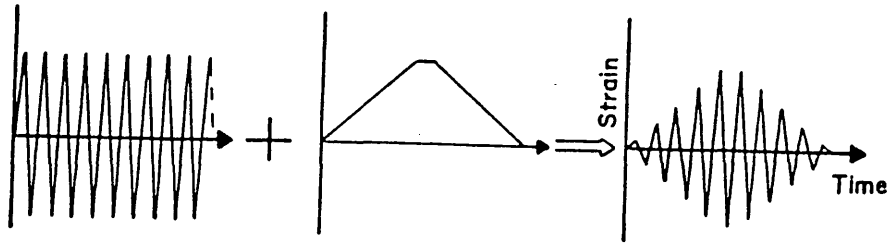


Fig. 2.4 Stable Stress/Strain Hysteresis Loop.



a) Multiple Step Test Program



b) Incremental Step Test Program

Fig. 2.5 Strain Control Programmes for Obtaining An Approximate Cyclic Stress/Strain Curve From One Specimen

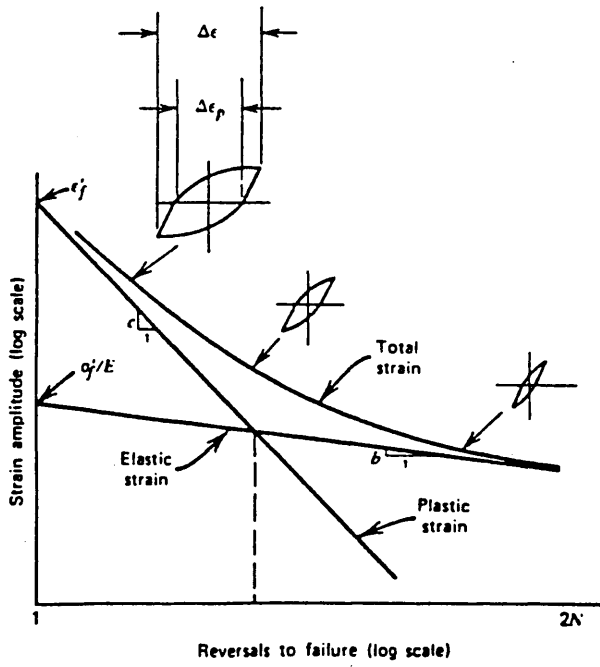


Fig. 2.6 Strain-Life Curves Showing Total Elastic and Plastic Strain Components.

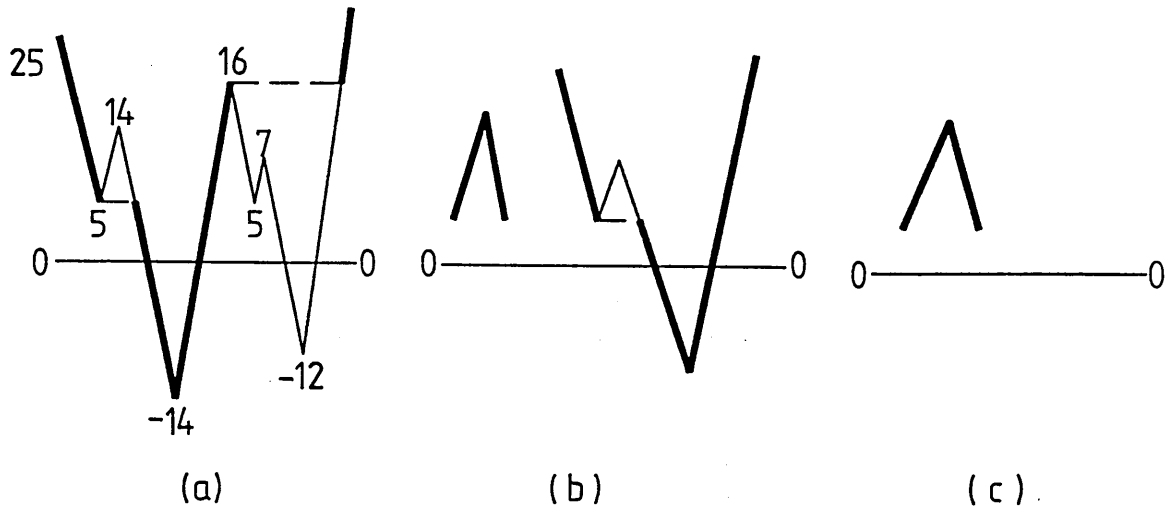


Fig. 2.7 Rainflow Cycle Counting.

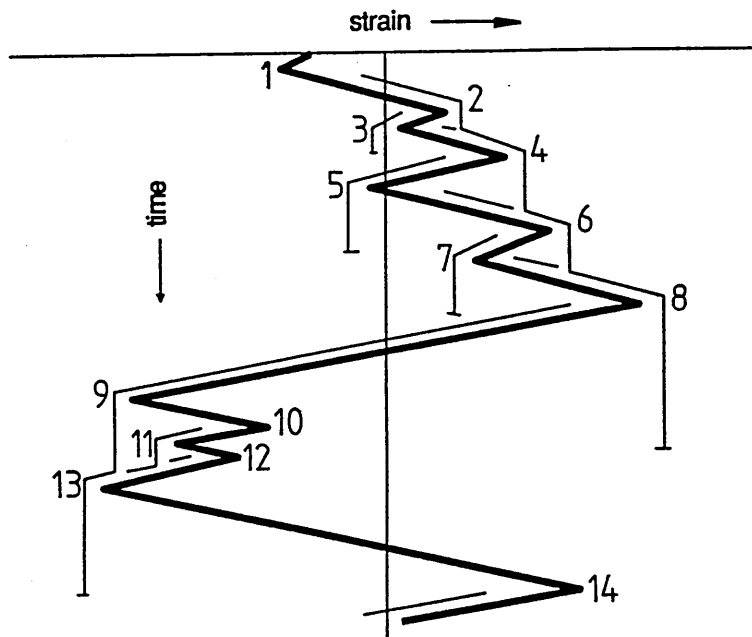


Fig. 2.8 Example of Rainflow Cycle Counting Method.

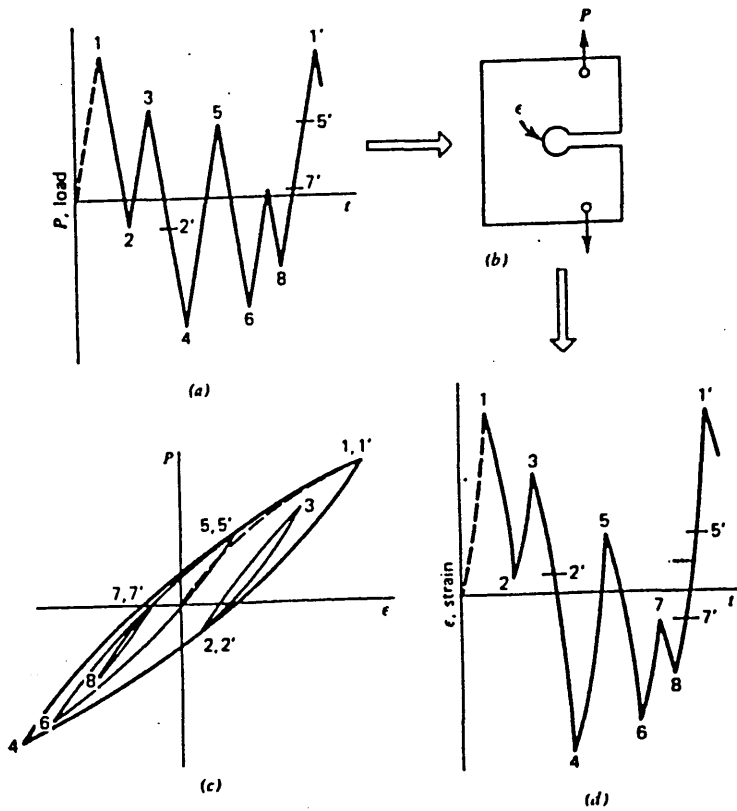


Fig. 2.9 A Load Versus Time History Repeatedly Applied To A Notched Component and the Resulting Notch Strain Response.

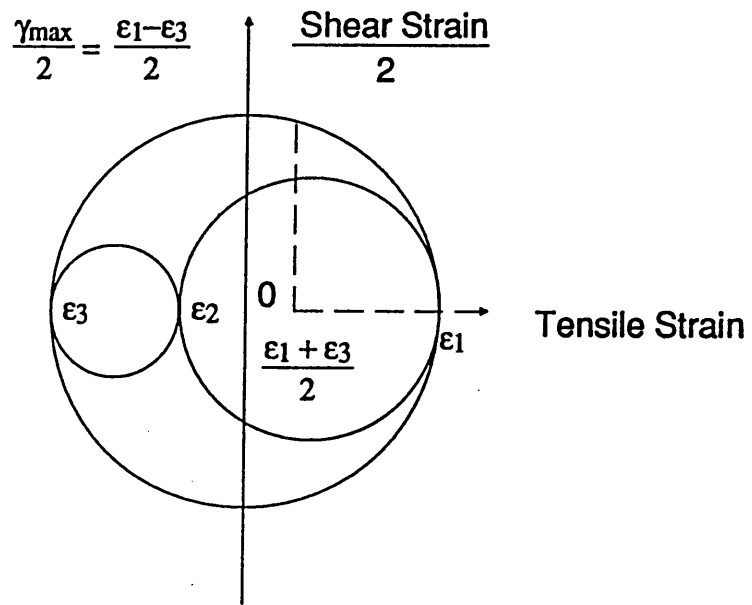


Fig. 2.10 Mohr's Circle of Strain.

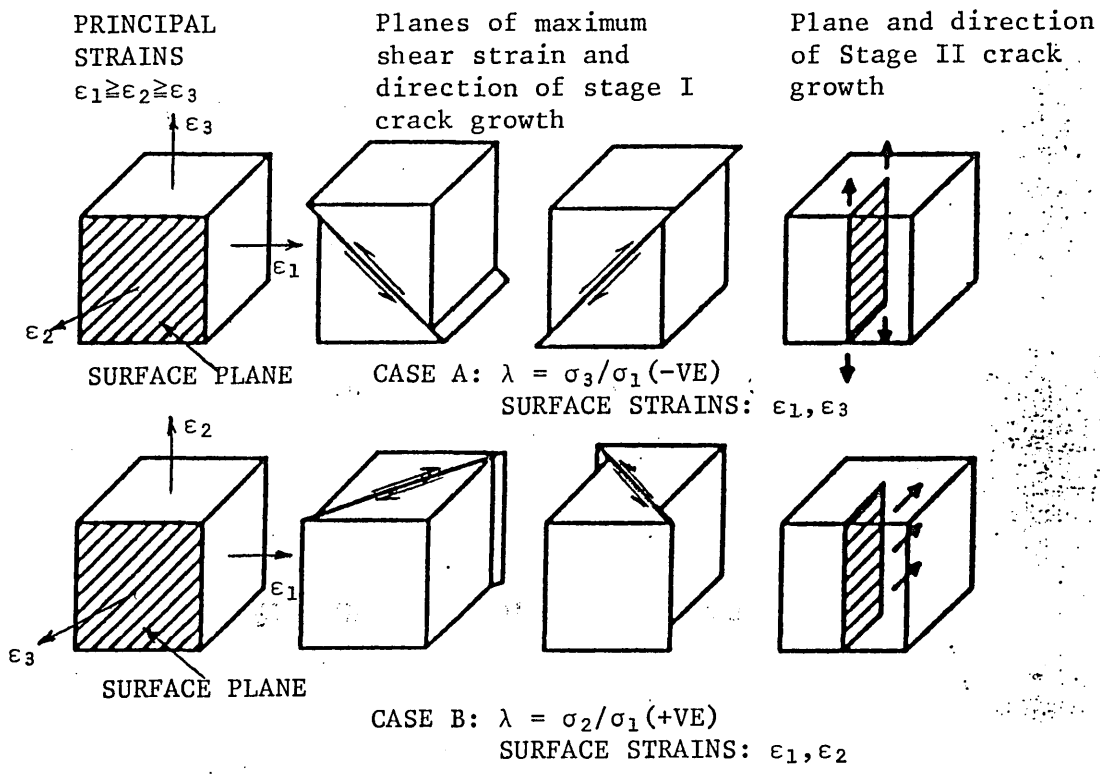


Fig. 2.11 Case A and Case B Systems of Crack Extension

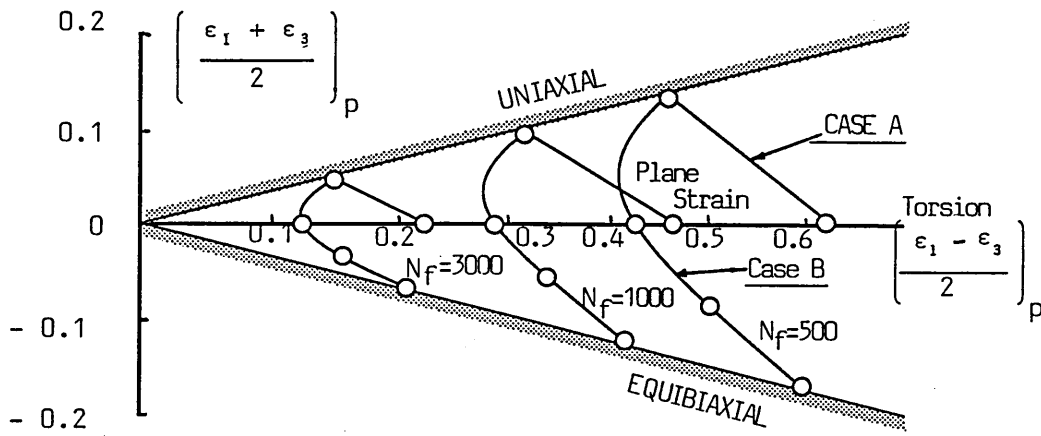


Fig. 2.12 A Typical Γ Plot.

STEERING ARM DESCRIPTION

3.1 Introduction

The selection of a material that gives the longest fatigue life under a given service loading is one of the most important aspects of the design analysis process. The designer must be able to match the material behaviour to the expected loading condition. This is only possible if a great deal is known about every proposed material and the required service conditions. Therefore, a full knowledge of all aspects of the mechanical properties of proposed materials is essential before they can be used efficiently.

This chapter discusses the important properties that should be considered during the design process to predict the fatigue life of the component. Macro/Micro examination and the chemical analysis of the component material was undertaken to identify the following aspects:

- a) Non-uniform composition due to the segregation of alloying elements.
- b) Non-metallic inclusions such as slag, sulphides and oxides.
- c) Method of manufacture.
- d) Mechanical properties.

- e) Physical defects due to manufacture and uniformity of heat treatment.
- f) The distribution of phases.
- g) The number of micro-constituents present.
- h) Identification of the equivalent British Standard specification.

3.2 Steering Arm

During prototype testing of a new 32 ton truck the heavy goods vehicle manufacturer identified a fatigue problem with the steering arm shown in figure 3.1. This is a typical problem faced by the automotive industry. To analyse the fatigue behaviour of the component, basic software was obtained from engineering software specialist, nCode International Limited. In the current work the possibility of combining finite element analysis and durability assessment software packages are under investigation.

The steering arm has been used to test the validity of the proposed approach in the design and development stage before commitment to expensive prototype development is made. Study of this component will lead to an understanding of the application of the proposed method to a wider range of components experiencing uniaxial, biaxial and triaxial states of stress during service.

3.2.1 Function Of A Steering System

The function of a steering system is to enable a vehicle to change its direction of travel and negotiate corners. The main requirement of a good steering system is to ensure geometrically precise rolling of the wheels (without slip) when travelling in bends. Figures 3.2 and 3.3 show the overall dimensions and an exploded view of the kingpin steering system for a 32 ton truck. In this steering system each wheel has its own pivot point, namely, kingpin, to which is attached the stub axle on which the wheel rotates. Each stub axle is connected to the steering arm. The two track arms are inter-connected by the track rod.

3.3 Chemical And Mechanical Properties

The steering arm was manufactured of forged 41 Cr 4V material (DIN standard). The equivalent British Standard specification for the above material was found to be BS 970 530 M40 (EN 18). This is a general purpose steel which may be heat treated to produce a tensile strength of 700 MPa and upwards depending on the section size, with good ductility and resistance to shock. It is used in the automobile industry for gears, connecting rods, steering levers, spindles, axles and crank shafts. Table 3.1 compares the range in chemical composition for the steering arm tested with standard data for actual material EN 18. The typical monotonic mechanical properties of the material are listed in table 3.2.

The fatigue test data for the component material was provided by the manufacturer. The cyclic properties are described in tabular form in table 3.3, and the cyclic stress/strain, strain-life and STW (Smith-Topper-Watson)-life curves are shown in figures 3.16 to 3.18. The material has a considerable amount of plasticity. The cyclic strain hardening exponent of the material is less than 0.1 ($n'=0.097$), and under the experimental cyclic loading conditions the material softens [72].

3.4 Micro-structure Examination

The micro-structure examination of the component was undertaken to identify the phases present, and their shape and size distribution.

A Zeiss Ultraphot metallurgical microscope was used for this purpose. The magnification was set at X500 for all the tests. When investigating the properties of a metal it is essential that the specimens used be representative of the whole mass. The usual procedure is to obtain samples in two directions; longitudinal and transverse. These were obtained from the critical location of the component and mounted in bakelite. Fine grinding of the specimens was carried out on a series of silicon carbide papers of increasing fineness. The fine scratches were then removed by polishing on an alumina loaded selvyt stretched on a flat disc. The polished specimens were mounted on a glass slip with plasticine. These were examined under an optical microscope. A uniform bright surface with some small dark

areas were observed as shown in figure 3.4. Micro-structure examination of the surface showed the dark areas to be non-metallic inclusions such as oxides and manganese sulphides as can be seen from the X-ray spectra produced for manganese sulphides inclusion as shown in figure 3.6. The specimens were then immersed in etching solutions for 30 seconds, removed, swilled in running water, rinsed in methylated spirits and dried in hot air. These were examined under the microscope, and the structure of the material was found to be upper bainite as shown in figure 3.5.

The time for the beginning and completion of the transformation of austenite have been plotted against temperature to give the "S-curve" known as time-temperature-transformation (T T T) curve of figure 3.7. The T T T curve was then used to predict the transformation and heat treatment operations undertaken to form the bainitic micro-structure.

Ac1 and Ac3 lines represent the equilibrium transformation temperature. Austenite is completely stable above Ac3, partially unstable between Ac3 and Ac1, and below Ac1 it is completely unstable and transforms in time.

The decomposition of austenite occurs according to three separate but sometimes overlapping mechanisms and results in three different reaction products, pearlitic (700°C to 500°C), bainitic (500°C to 350°C) and martensitic (350°C to 250°C). For detailed account of each reaction product see [73, 74].

At quench temperatures slightly above Ms (Martensite start), a micro-structure forms that is distinctly different from fine pearlite. This micro-structure is called bainite. Bainite has a two-phase micro-structure composed of ferrite and iron carbide. There is a variation in the morphology of bainite and in the type of carbide (Fe_3C or ϵ carbide $\text{Fe}_{2.5}\text{C}$) depending upon the quench temperature and composition.

A distinct change in morphology occurs between high and low quench temperature. These two morphologies are referred to as upper bainite (high quench temperature) and lower bainite (lower quench temperature). The micro-structure of lower bainite is finer than that of higher bainite.

The centre scale in figure 3.7 represents the logarithmic scale bar dimensions of oil quenched materials.

The maximum sectional dimensions of the component body is 42 x 46 mm. A line is projected vertically from the appropriate point along the scale to the undersection of the T T T curve. This determines the percentage bainite available with in the martensitic matrix, which is found to be approximately 50%.

3.5 Manufacturing Processes

It is difficult to establish precisely the manufacturing processes carried out to produce the aforementioned micro-structure. However, examination of the component material suggested that the following manufacturing and heat

treatment processes must have been carried out.

a) Forging	1200°C	finish above 850°C
b) Hardening	850°C - 880°C	oil quench
c) Tempering	600°C	air cool
d) Surface treatment	sand-blasted	surface cleaning

3.6 Test Track Trials

Several methods are available for assessing the fatigue of engineering components prior to their incorporation into products in the market place. At the conceptual stage simple calculations can be performed to give approximate load and stress histories, which in conjunction with material data such as S-N curves, provide an estimate of fatigue life. These can be refined by the manufacture of prototype products which when subjected to realistic loading can provide accurate component measured load histories. For new components where previous load histories have been established then simulated testing can take place on laboratory equipment and data thus generated be used to predict the real fatigue life of the component using computer methods such as the FATIMAS program. Finally real life tests would normally follow for confirmation.

The importance of component testing was recognised as early as the 19th century. One of the earliest published papers by Albert, 1838, discusses tests carried out to investigate the fatigue life of mine cables [70]. Other

examples of component testing are reported in the work by Wohler [14], 1860, and Andrew, 1890, which investigated the effect of fatigue damage on railway axles [71].

The concept of component testing on proving grounds can be traced to The Dodge brothers, who built the earliest test track in 1915 [31]. The construction was built of split logs, which is known today as a corrugated surface. The purpose of the test track was to investigate the suspension systems of automobiles. This form of accelerated testing is a feature of all proving ground tests today.

Today's test track constructions contain a mixture of surfaces designed to represent typical customer usage. The criterion is often based on the vehicle surviving a given distance, usually 1000 miles, over such surfaces.

3.7 Durability Assessment

Automotive industries have numerous road endurance test routes which they use for evaluating components and vehicles. The test circuits contain a number of different surfaces. These routes have all been prepared following past experience and historical usage. The general feeling being that the routes simulate closely conditions met in service.

It is the manufacturer's practice to select a mix of test track surfaces as shown in figure 3.8 to evaluate ride and handling, noise, vibration and harshness of prototype vehicles.

During the durability assessment of a new 32 ton prototype truck on manufacturer's proving grounds in 1983, fatigue failure of the steering arm occurred. The expected life was specified to be 10,000 circuits of the test track. However, failure occurred after approximately 120 circuits; considerably less than that desired for the life of the component. Figure 3.9 shows the recorded strain-time history from the road test.

The component was manufactured from forged SAE 1046 V with a tensile strength of 890 MPa. The test information was fed back to the material engineering department to initiate modifications to the component. It was decided to change the material. Two alternative materials were considered, namely; 41 Cr 4V and 42 Cr S4 with tensile strength of 940 and 1100 MPa, respectively. These were fitted to the truck and the above test was repeated. The life remained approximately 120 circuits of the test track.

Tests were then undertaken to consider the possible changes in mechanical properties that cyclic loading may induce. The test results showed the cyclic properties of the above materials to be almost the same as shown in figures 3.10 to 3.18 consequently the materials selected were unsatisfactory. The chemical composition of the three materials are shown in tabulated form in table 3.1. Examination of the chemical composition of the three materials shows that they are almost identical.

Geometric modifications were implemented by engineers in an attempt to overcome the above problem. Material 41 Cr 4V was selected. The blend radii around the bosses were increased at the critical location and consequently the desired fatigue life was achieved.

3.8 Discussion

The procedure followed by the manufacturer in developing the steering arm component is typical of many industrial organisations, where decisions on physical shape and material are not confirmed until very late in the development cycle. Clearly the ultimate confirmation of any component is the final road test but it is necessary to increase the reliability of the decision making process at the early stages of the design cycle, where costs accrue at a relatively slow rate. Having decided upon the best available concept, detailed design and analysis procedures follow. At this stage of the design process the level of commitment to the development of a new artefact is high. Consequently, long term decisions for the manufacturing processes and tooling are made. At this stage in the design process the rate of spending is very high. It is at this late stage when the engineering prototypes are made and tested for integrity and durability that any design changes are expensive, since modifications will lead to further testing and may even lead to major tooling changes.

During the analysis process the manufacturer had made a number of wrong decisions which led to the premature

failure of the steering arm. They fell into the trap of endless material changes and repeated testing without asking the question, why? After much research it emerged that a design modification of the steering arm at the critical location was required.

It is difficult to be specific concerning which method of analysis has been used by the designer. However, it is suggested that because a material with a higher tensile stress was usually selected, then one can conclude that the designer used a S-N curve approach to estimate the fatigue life of the component.

Figures 3.19 and 3.20 show the three dimensional outputs of cycle distributions and associated fatigue damage distributions for the above materials for the recorded data shown in figure 3.9. Several comments can be made of the graphs.

- 1) Figures 3.19 and 3.20 shows that in all cases only a small number of the cycles caused any damage.
- 2) Figure 3.20 shows that all the fatigue damage was caused by the washboard road surface.

It is clear that the company should have recognised that only the washboard road surface was causing damage and the follow up tests should have been carried out only on that surface. This would have reduced the testing time.



Fig. 3.1 The Steering Arm.

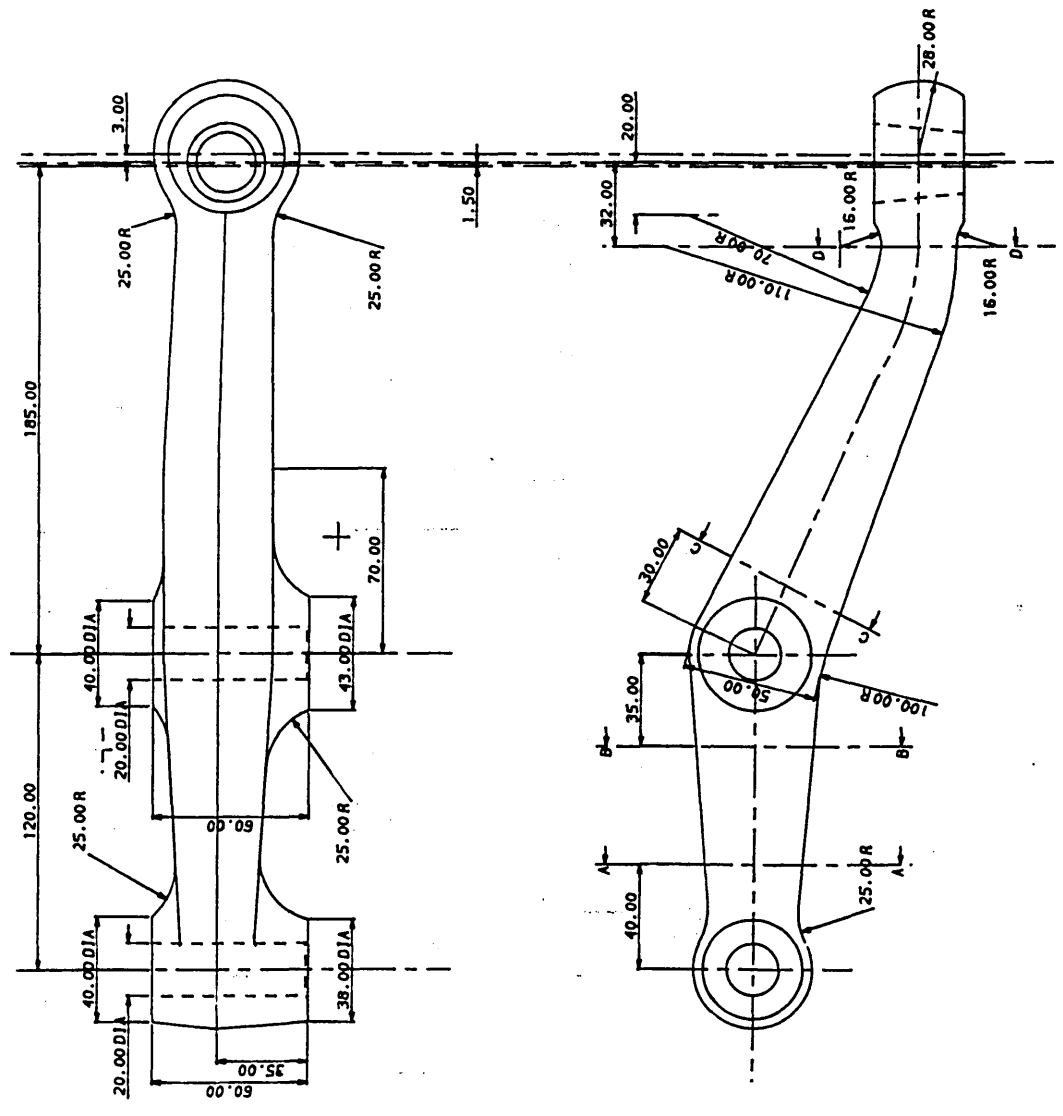
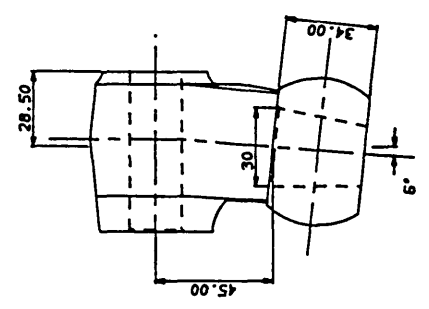
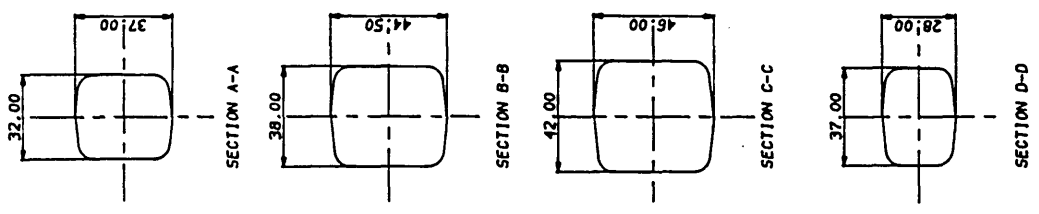


Fig. 3.2 Steering Arm Dimensional Details.

Percentage Element Material	C	Mn	Si	S	P	Ni	Cr	Mo	Cu	V	Al
SAE 1046	0.43 to 0.5	0.7 to 1.0	-	0.05	0.04	-	-	-	-	-	-
42 Cr S4	0.38 to 0.45	0.5 to 0.8	0.15 to 0.35	0.035	0.035	-	0.9 to 1.2				
41 Cr 4V	0.41	0.69	0.35	0.016	0.011	0.18	1.08	0.05	0.21	0.02	0.016
Standard (EN 18)	0.38 to 0.44	0.50 to 0.80	0.15 to 0.35	0.035 to Max	0.035 to Max	-	0.90 to 1.20	-	-	-	-

Table 3.1 Chemical Composition Of The Forged Sheering Arm

Yield Point, MPa	:	813
Tensile Strength, MPa	:	940
Elongation	:	24%
Reduction in Area	:	63.5%
Hardness, Vickers	:	250

Table 3.2. Mechanical Properties

MATERIALS ENVIRONMENT

Fatigue Strength Coefficient (MPa)	$S_f' = 840$
Fatigue Strength Exponent	$b = -0.041$
Fatigue Ductility Exponent	$e = -0.694$
Fatigue Ductility Coefficient	$\epsilon_f' = 0.387$
Elastic Modulus (MPa)	$E = 2.148 \times 10^5$
Cyclic Strain-Hardening Exponent	$n' = 0.097$
Cyclic Strength Coefficient (MPa)	$k' = 944$
Cut-off (reversals)	$R_c = 1E7$

Table 3.3 Cyclic Properties of the Steering Arm
(41 CR 4V)

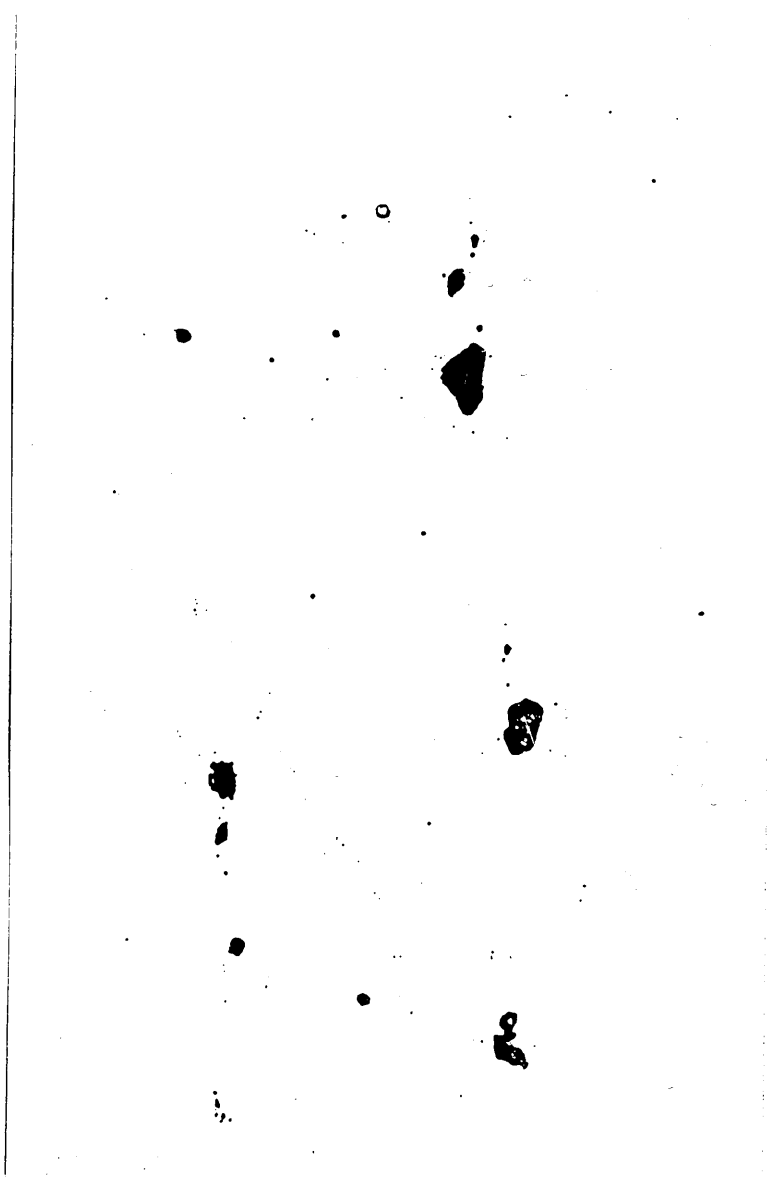


Fig. 3.4 Unetched Micro-Structure Showing The Inclusions.

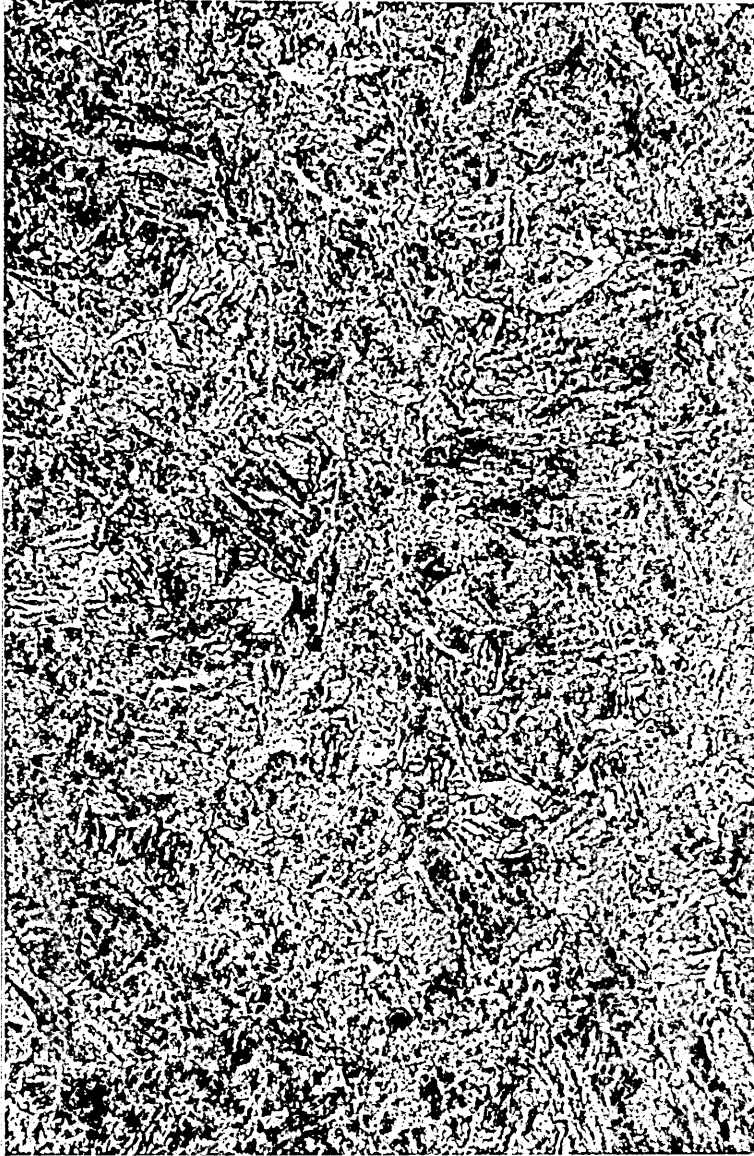


Fig. 3.5 Etched Micro-Structure Showing
Bainite in a Matrix of Martensite.

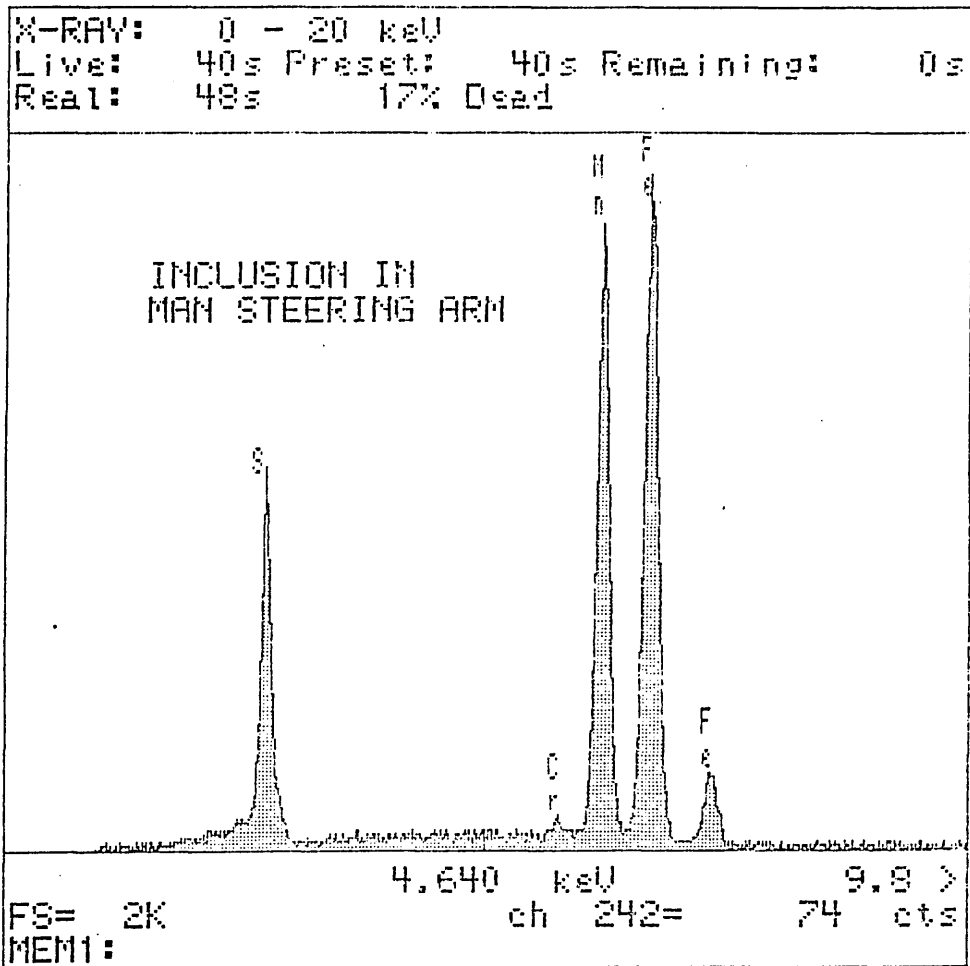


Fig. 3.6 The Spectra Of Inclusion Plot.

CONTINUOUS COOLING TRANSFORMATION DIAGRAM

1 Cr

AUSTENITISED AT 870°C

PREVIOUS TREATMENT ROLLED

ANALYSIS Wt % (See note on page 8)

C	Si	Mn	P	S	Cr	Mo	Ni	Al	Nb	V
0.39	0.20	0.70	0.020	0.020	1.05	—	—	—	—	—

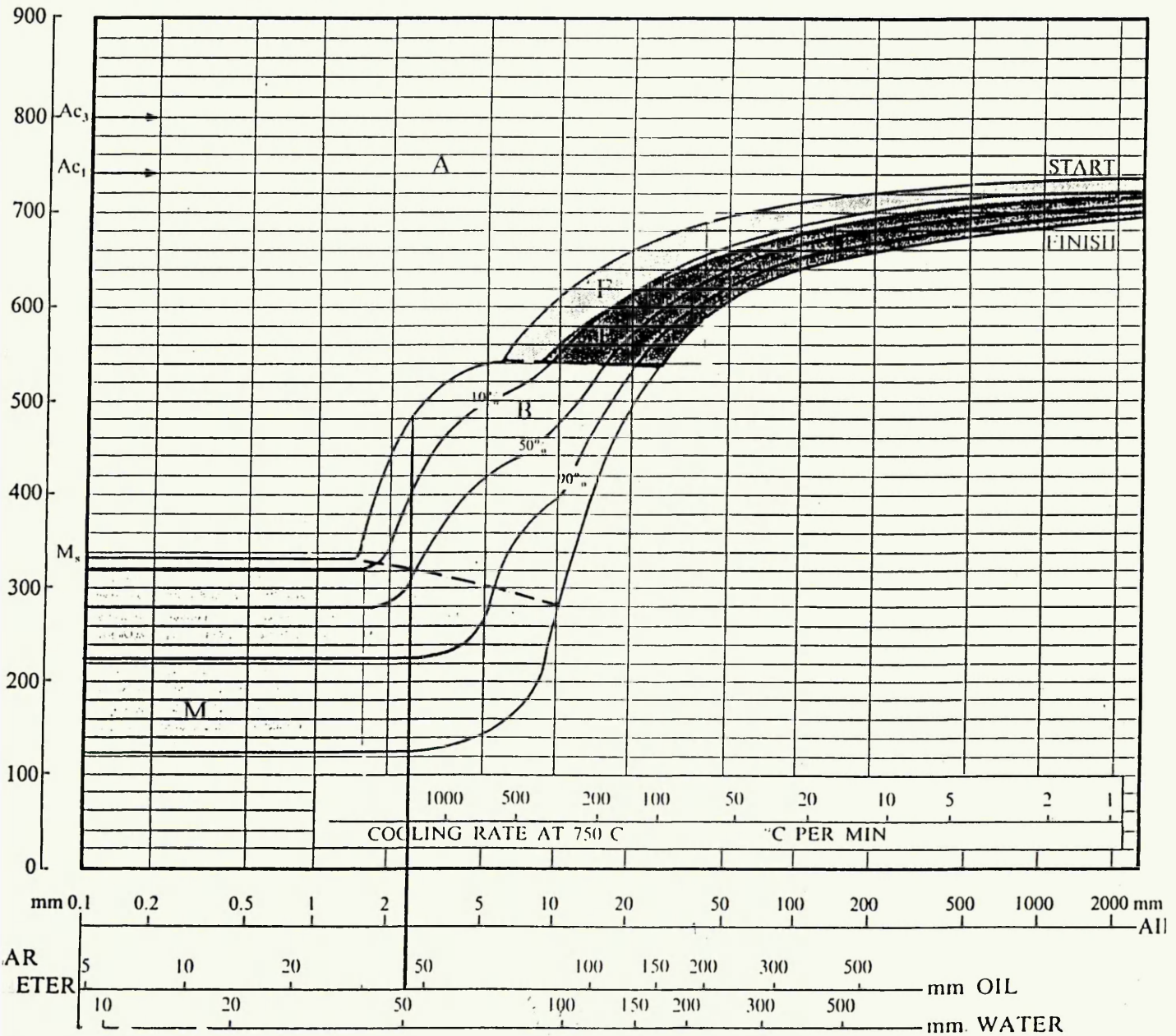


Fig. 3.7 Time Temperature Transformation Curve.



Fig. 3.8 Manufacturer's Test Track Surfaces.

DISPLAY OF SIGNAL : STUBAXLE

Full file data :

214641 points.

370.4 pts/Secs

Max = 2740

at 50.33 Secs

Min = -3846

at 103.8 Secs

Mean = -421.2

S.D. = 675.5

Displayed :

214641 points.

from pt 1

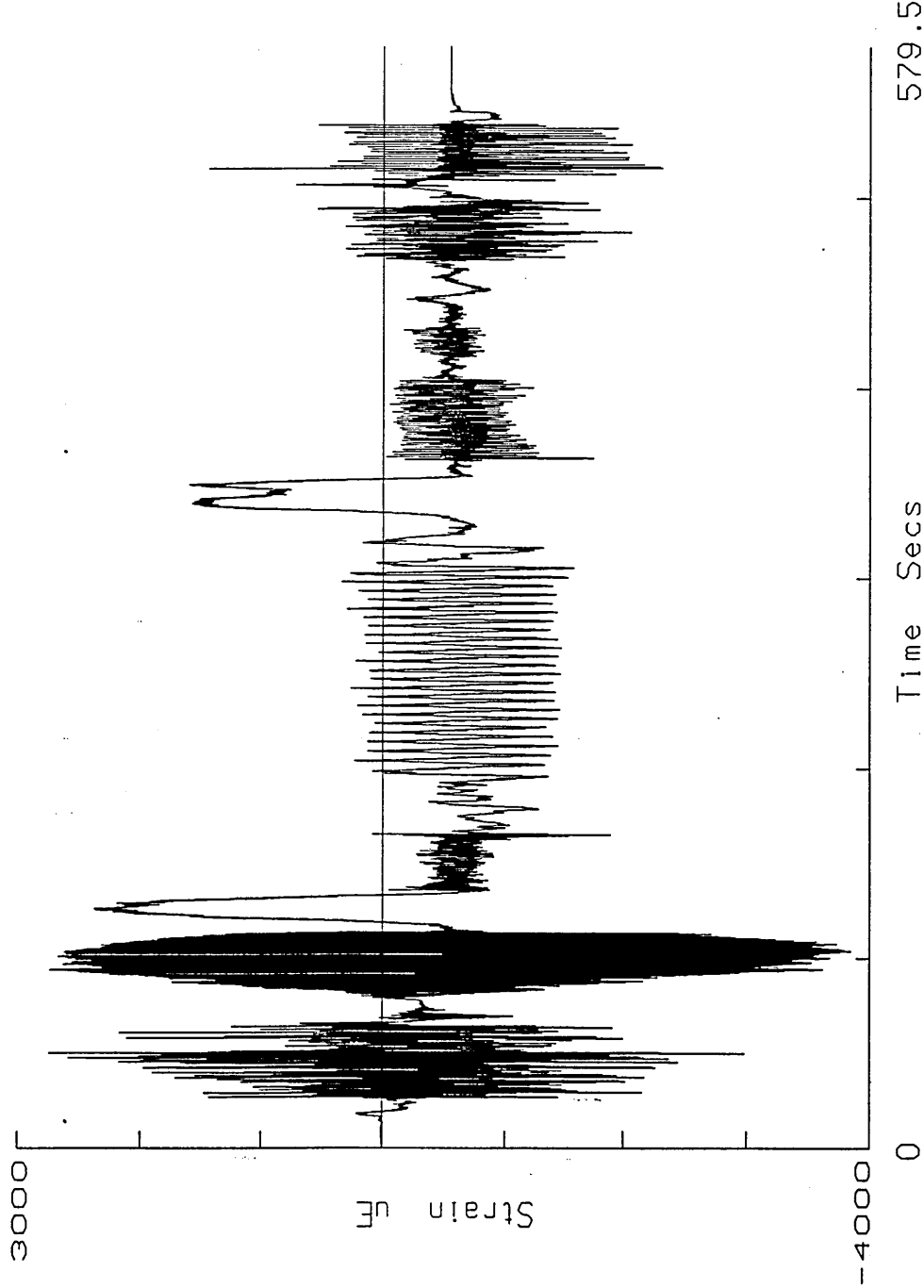
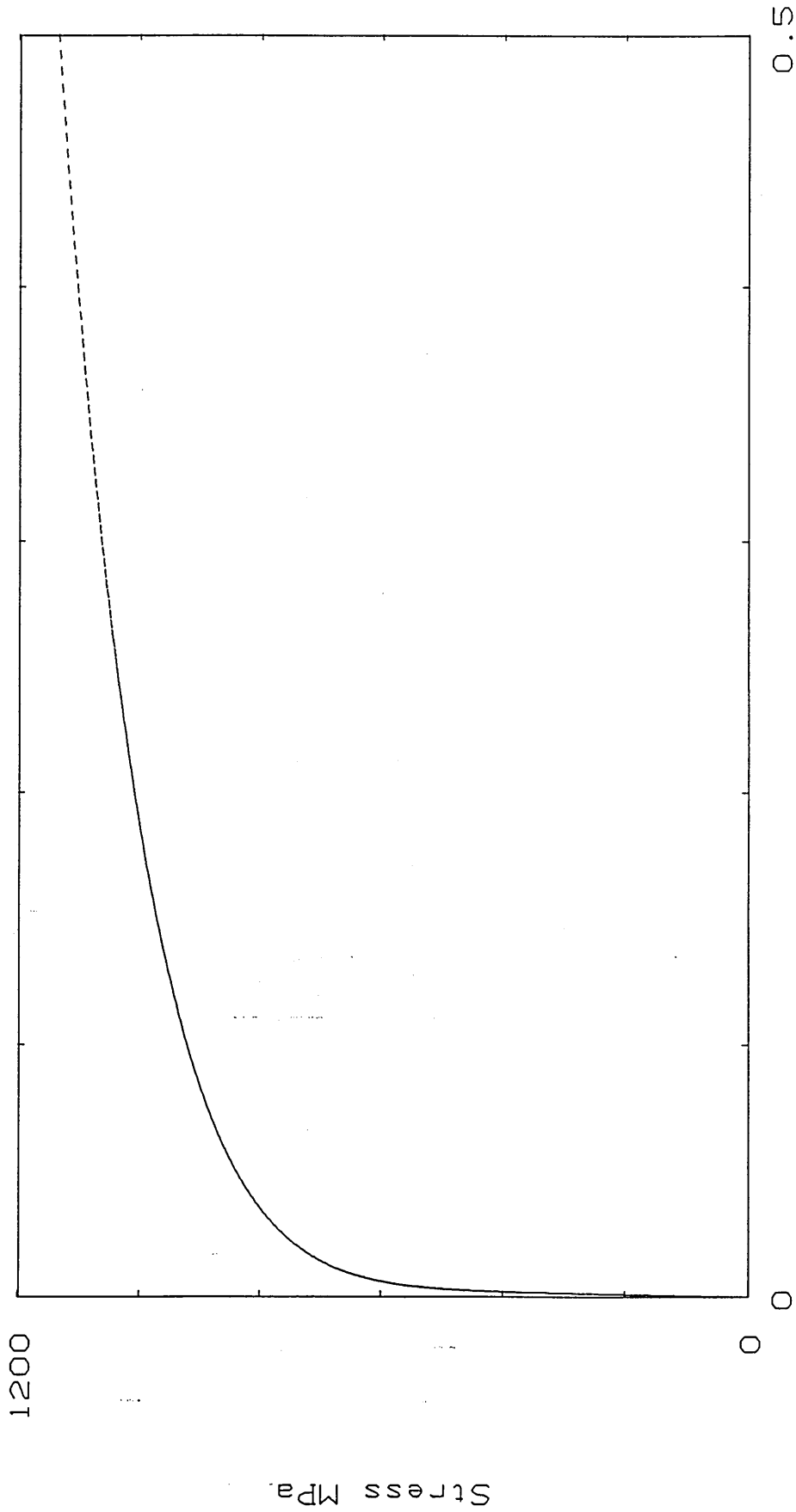


Fig. 3.9 Recorded Stubaxle Strain-Time History.

Cyclic Stress-Strain Plot

----- SAE1046V n' : 0.127 K' : 1241 E : 204000

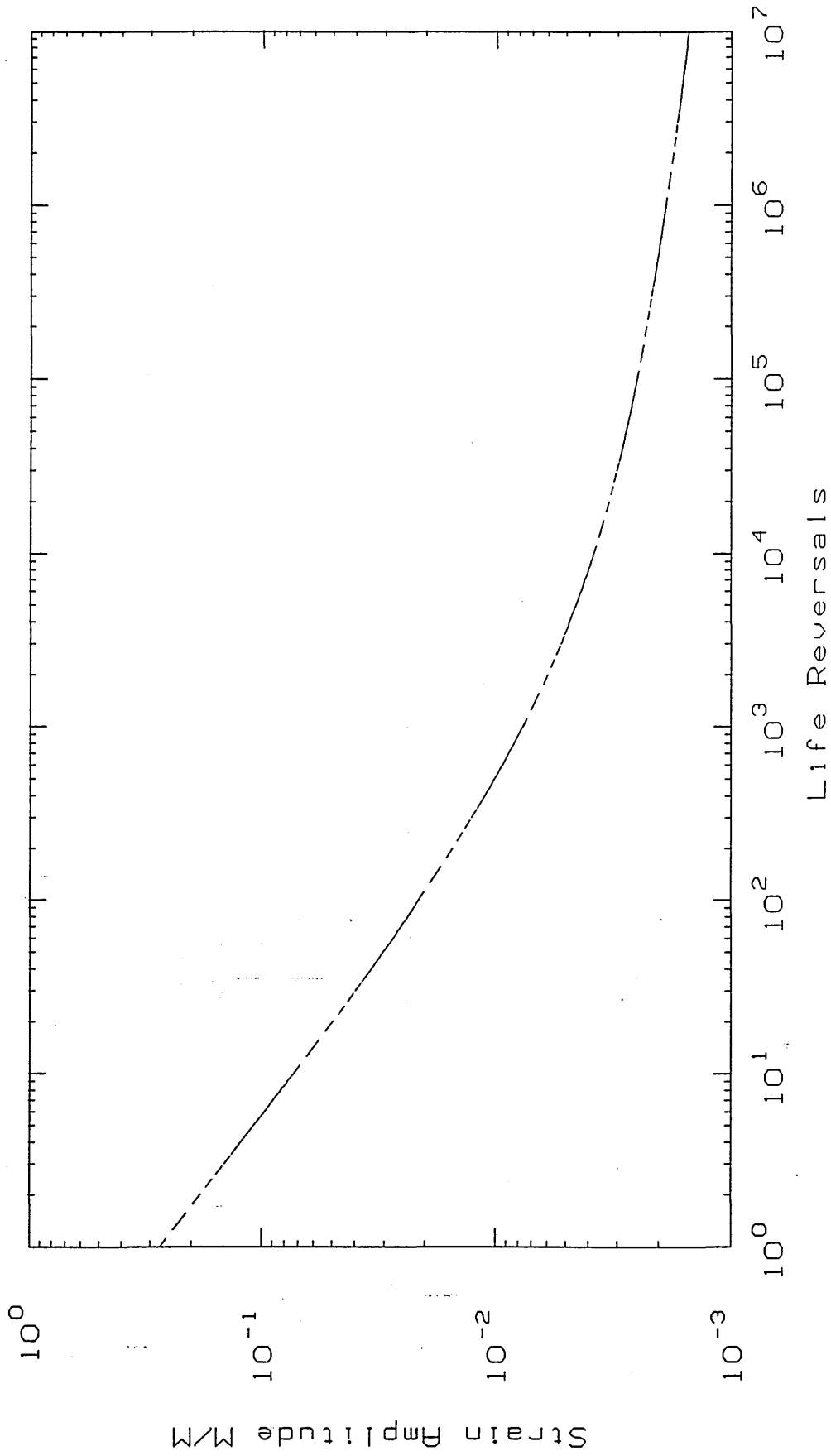


Strain M/M

nCode NSOFT Fig. 3.10 Cyclic Stress/Strain Curve (SAE 1046 V).

Strain Life Plot

----- SAE1046V SF' : 1200 b : -0.085 Ef' : 0.268 c : -0.595



nCode NSOFT

Fig. 3.11 Strain/Life Curve (SAE 1046 V)

STW Life Plot

----- SAE1046V Sf' : 1200 b : -0.085 Ef' : 0.268 c : -0.595

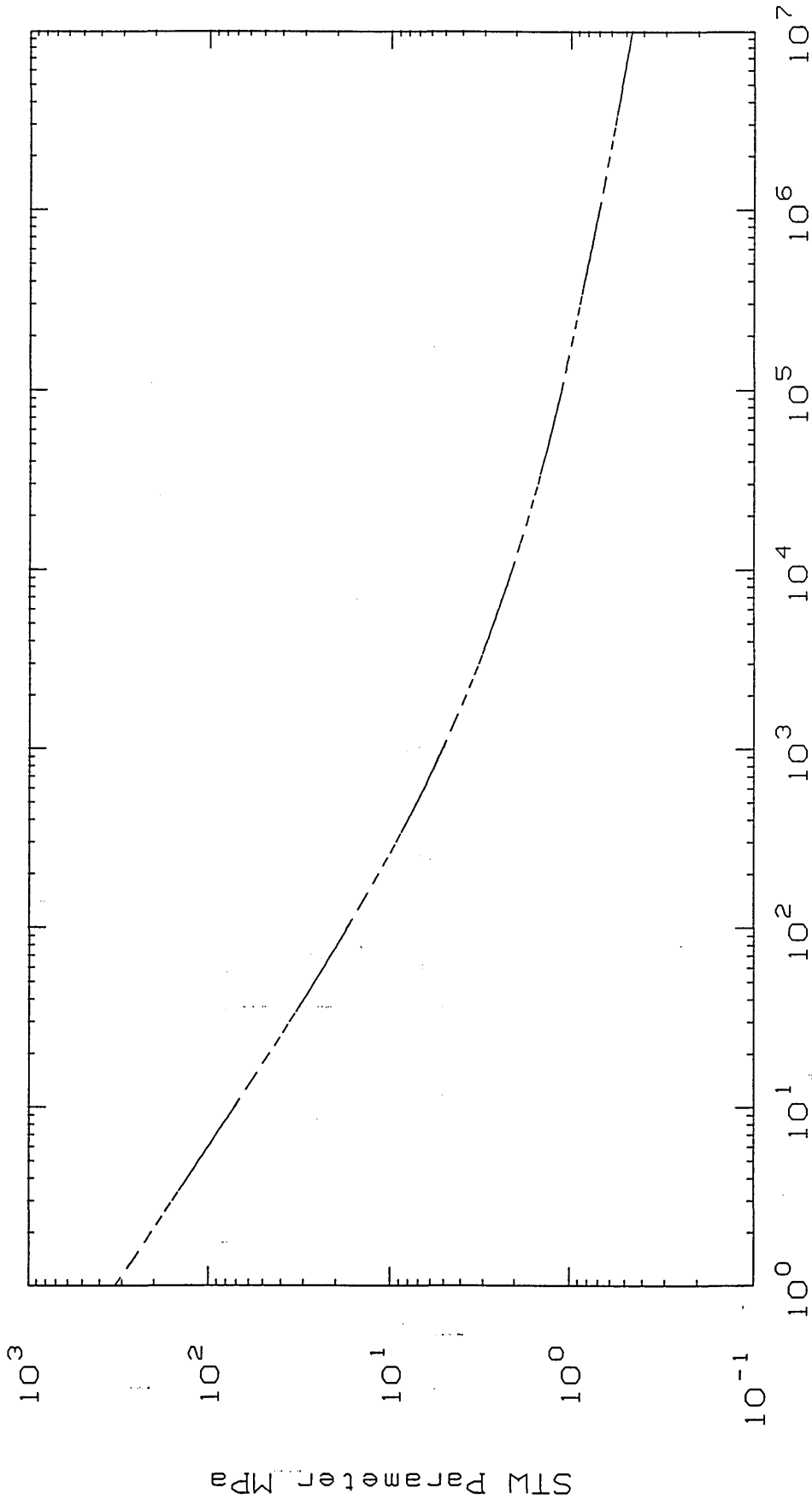
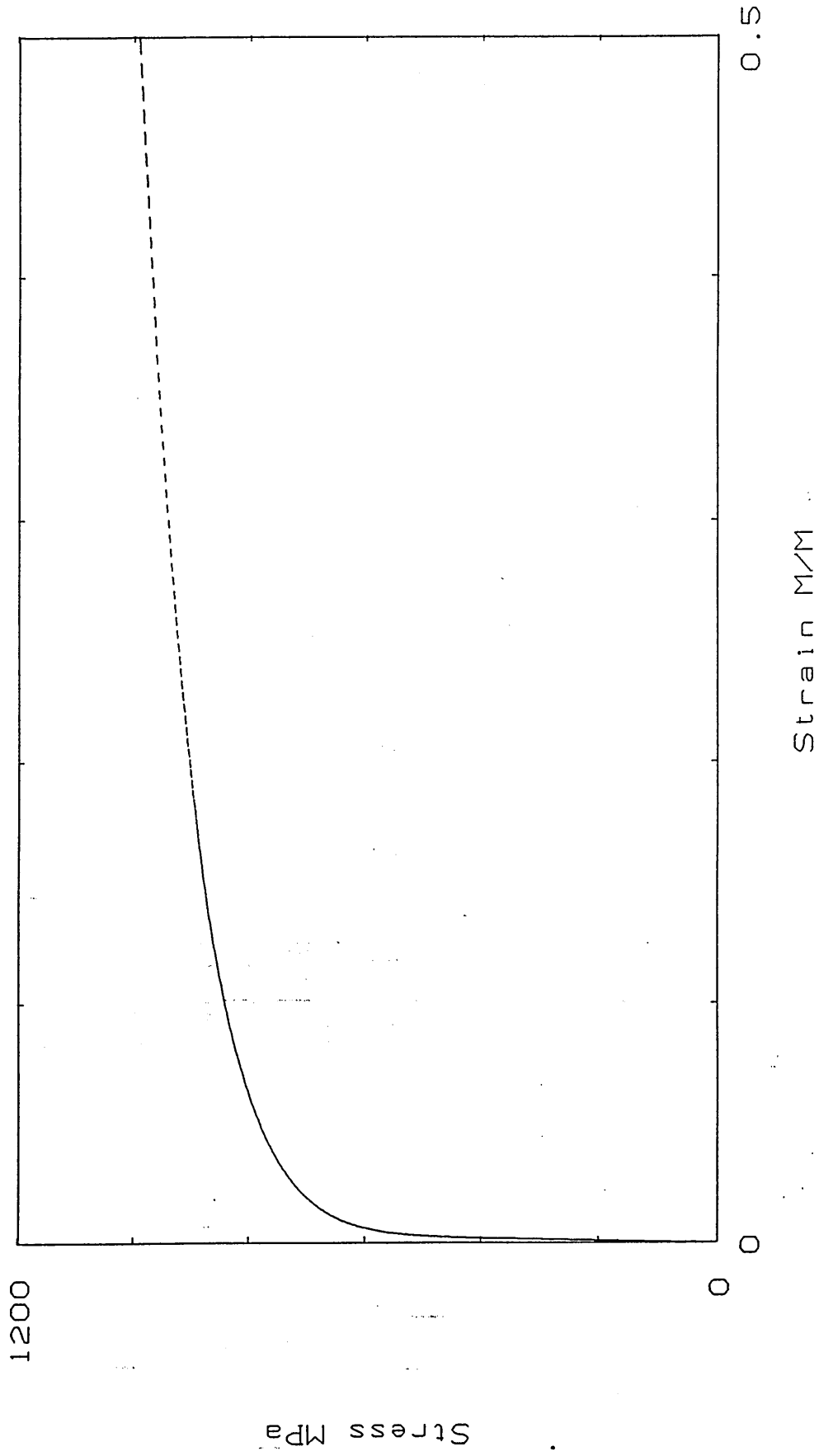


Fig. 3.12 STW/Life Curve (SAE 1046 V).

nCode NSOFT

Cyclic Stress-Strain Plot

----- 41CRS4 $n' : 0.1$ $K' : 1063$ $E : 210000$



nCode NSOFT Fig. 3.13 Cyclic Stress/Strain Curve (41 Cr S4).

Strain Life Plot

----- 41CRS4 Sf' : 1040 b : -0.066 Ef' : 1.22 c : -0.71

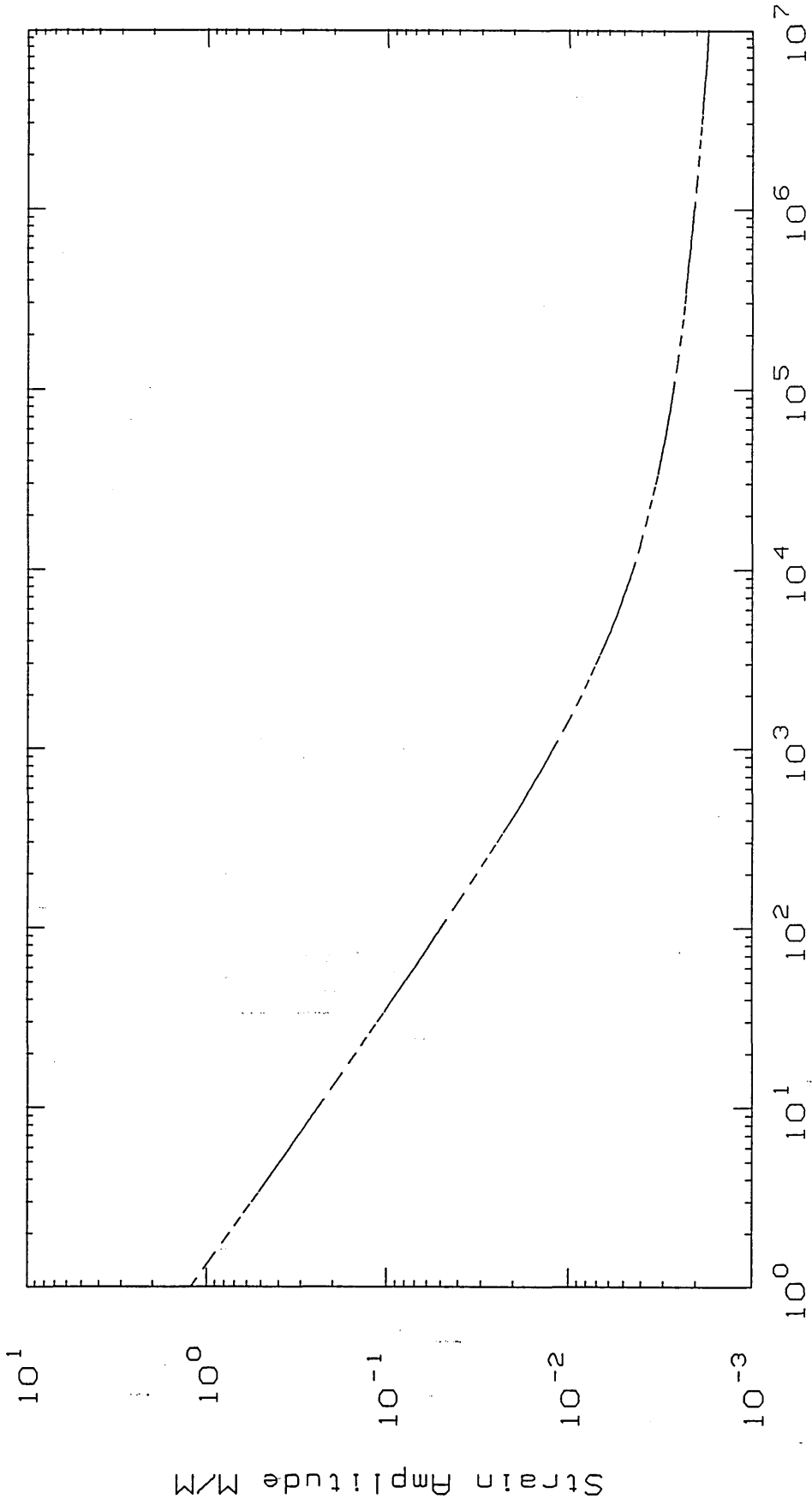


Fig. 3.14 Strain/Life Curve (41 Cr S4). Reversals

nCode NSOFT

STW Life Plot

----- 41CRS4 Sf' : 1040 b : -0.066 Ef' : 1.22 c : -0.71

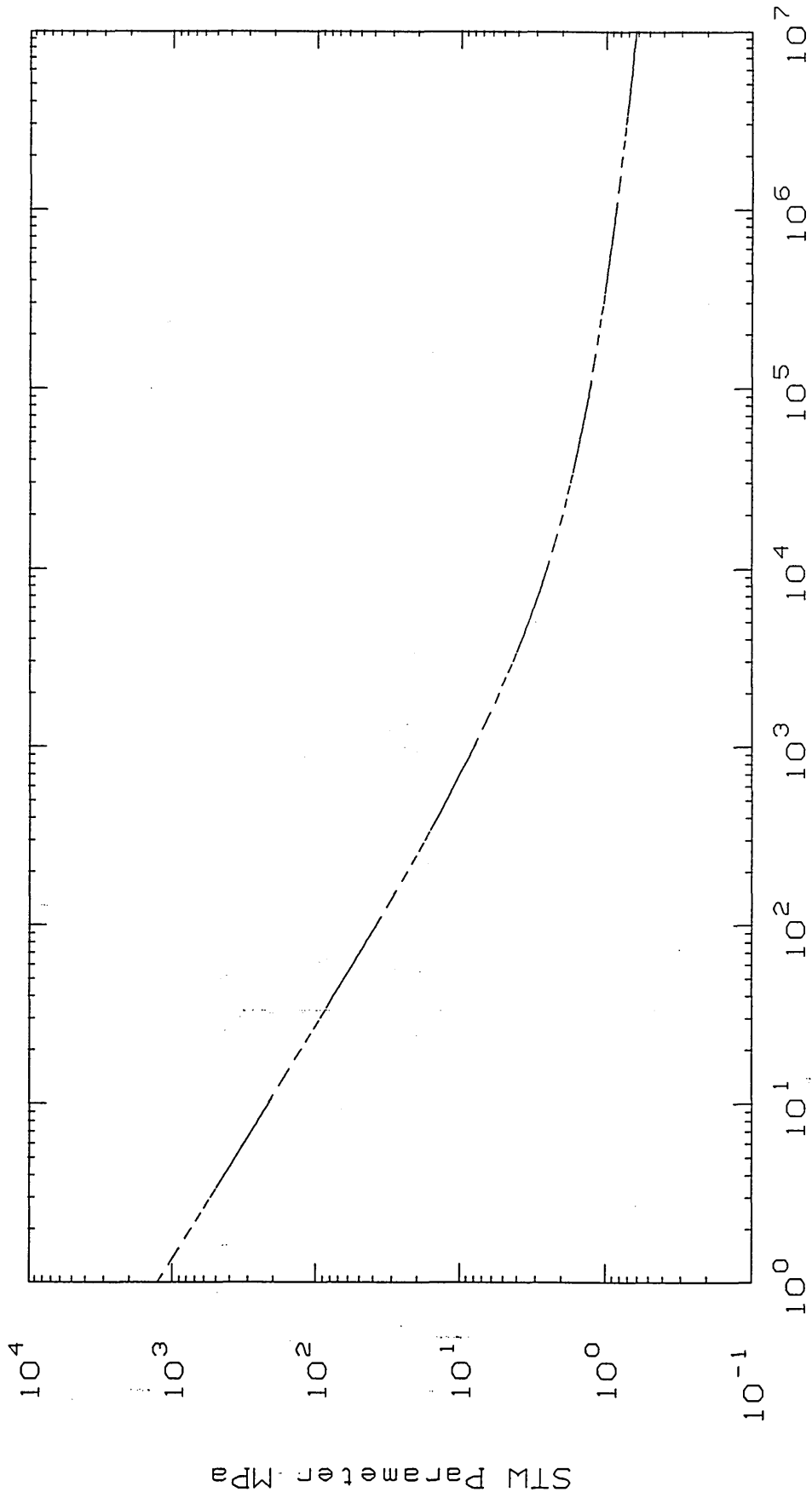


Fig. 3.15 STW/Life Curve (41 Cr S4).

nCode NSOFT

Cyclic Stress-Strain Plot

----- 41CR4V n' : 0.097 K' : 944 E : 214800

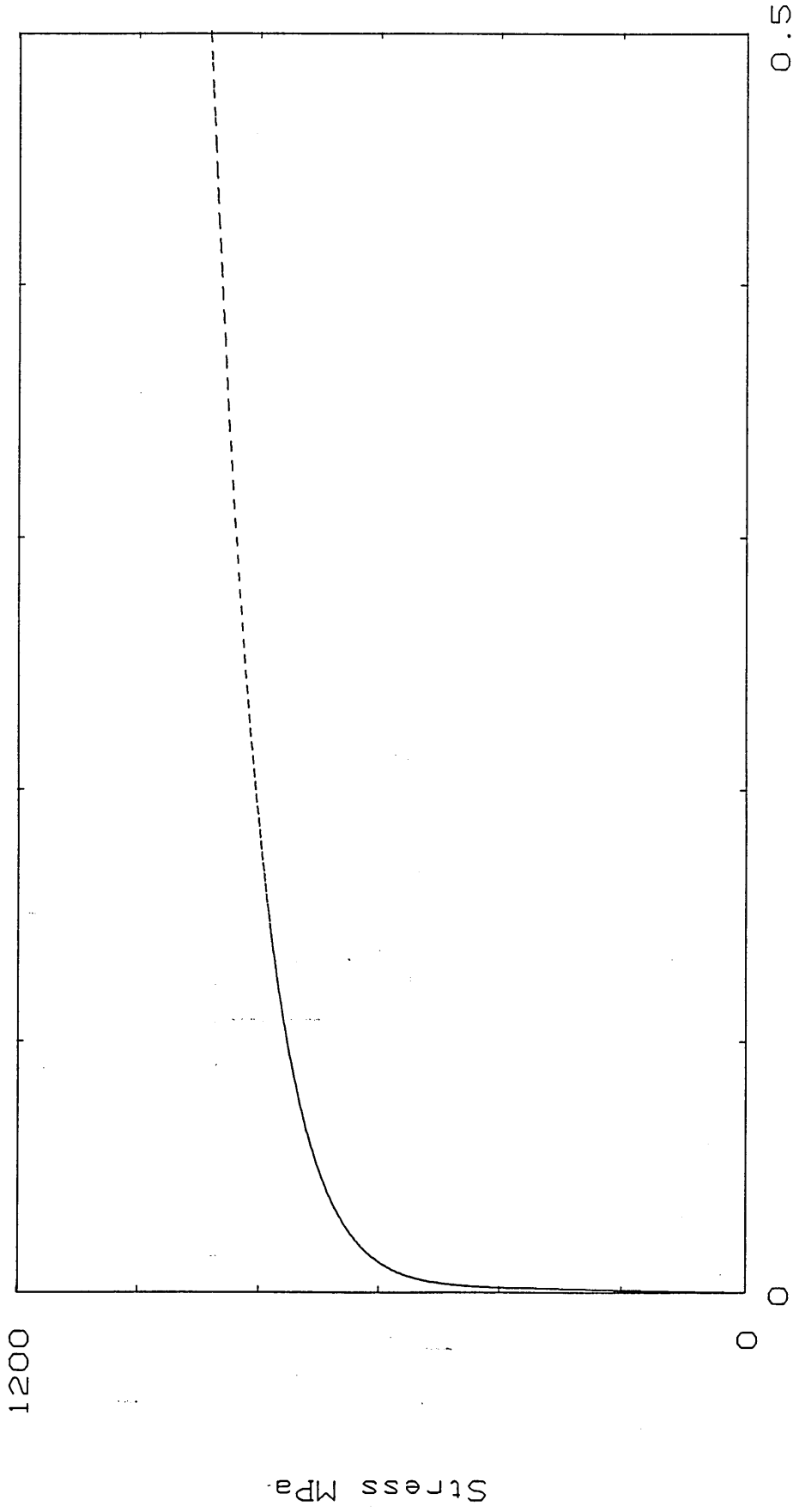


Fig. 3.16 Cyclic Stress/Strain Curve (41CR4V) M/M

nCode NSOFT

Strain Life Plot

----- 41CR4V Sf' : 840 b : -0.041 Ef' : 0.387 c : -0.694

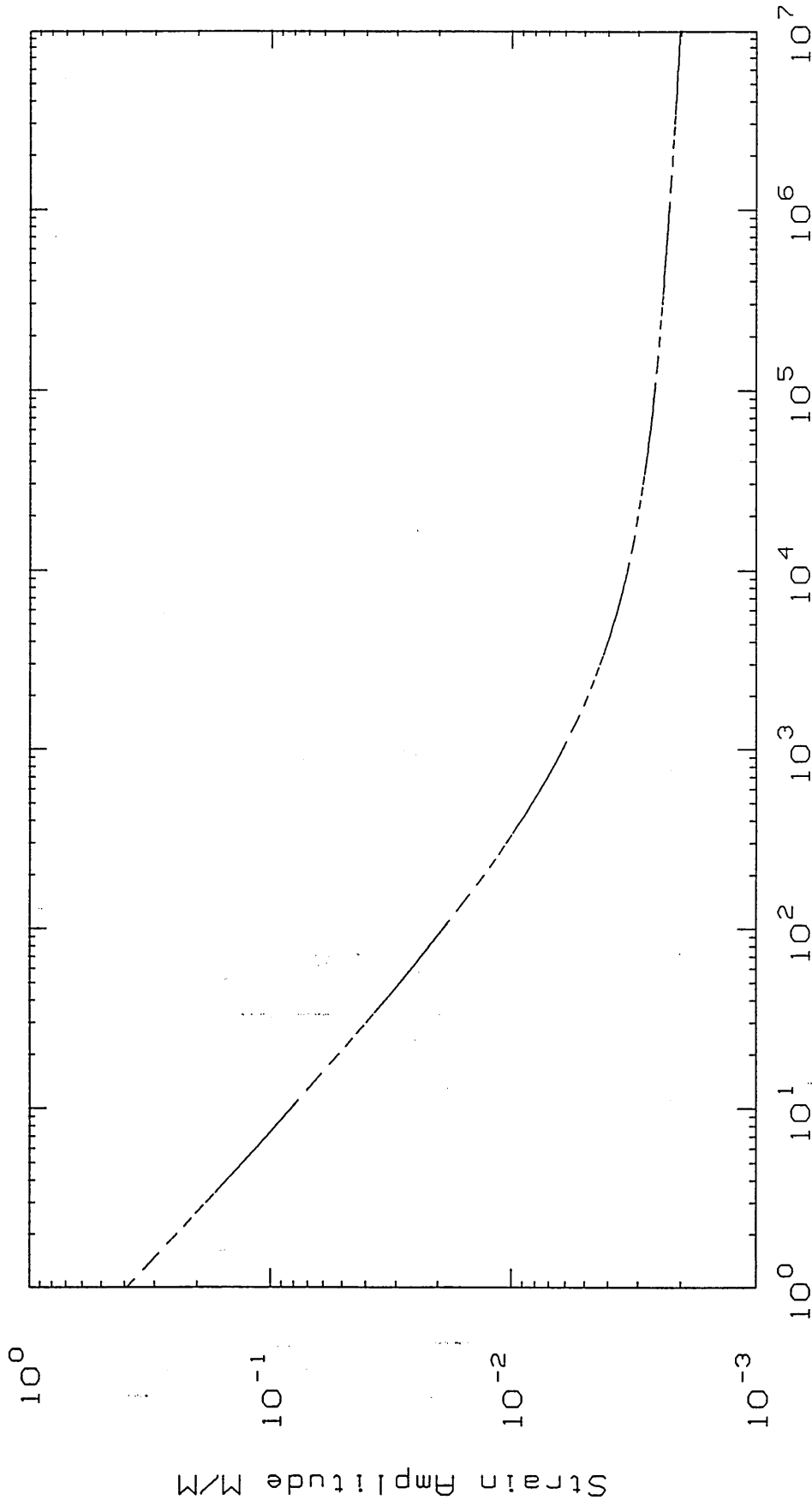


Fig. 3.17 Strain/Life Curve (41 Cr. 4V) Reversals

nCode NSOFT

STW Life Plot

----- 41CR4V Sf' : 840 b : -0.041 Ef' : 0.387 c : -0.694

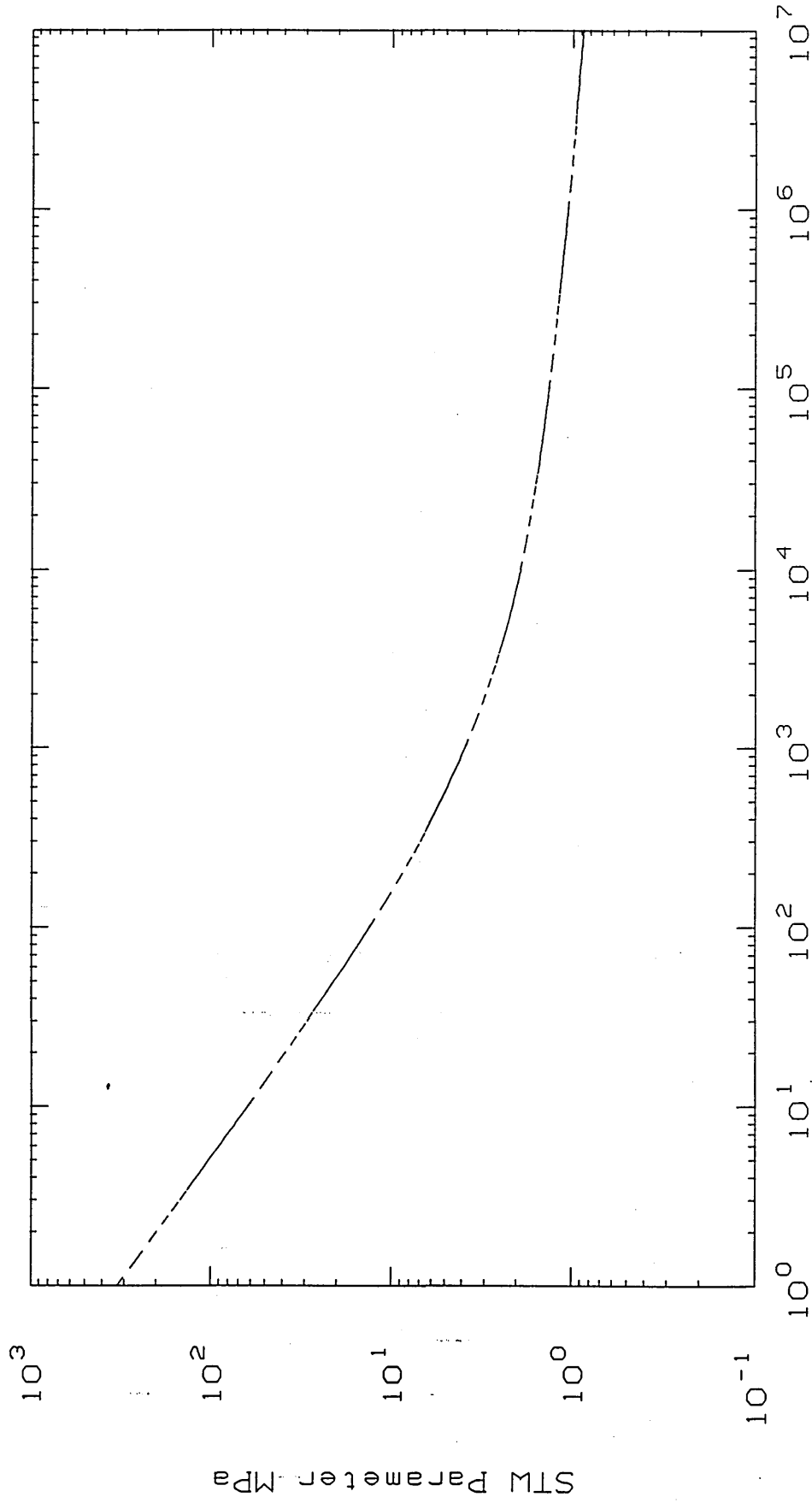
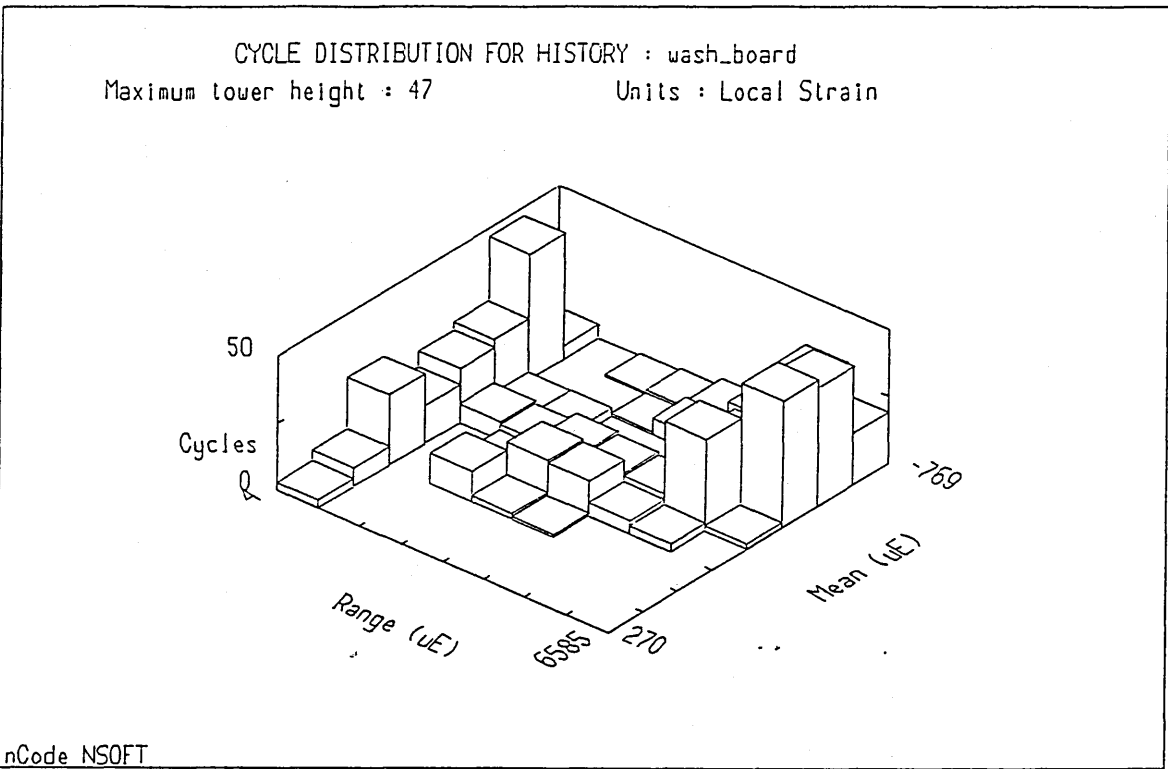
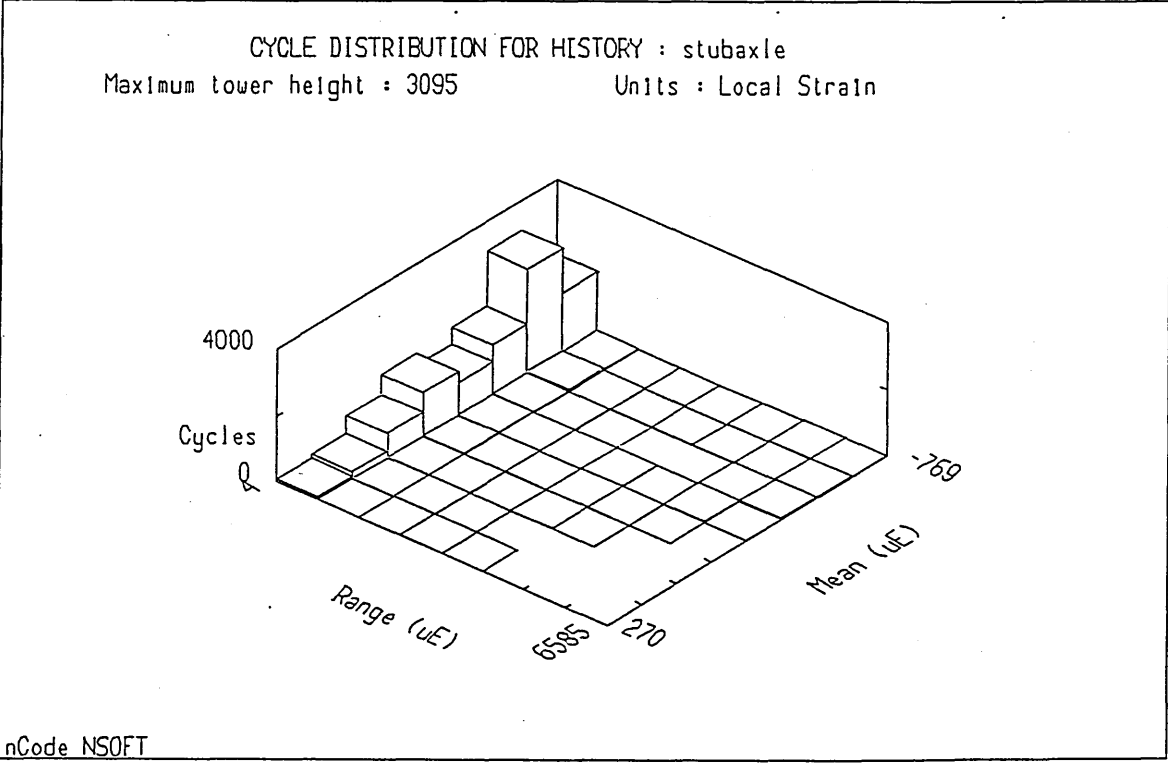


Fig. 3.18 STW/Life Curve (41 Cr 4V) Reversals

nCode NSOFT

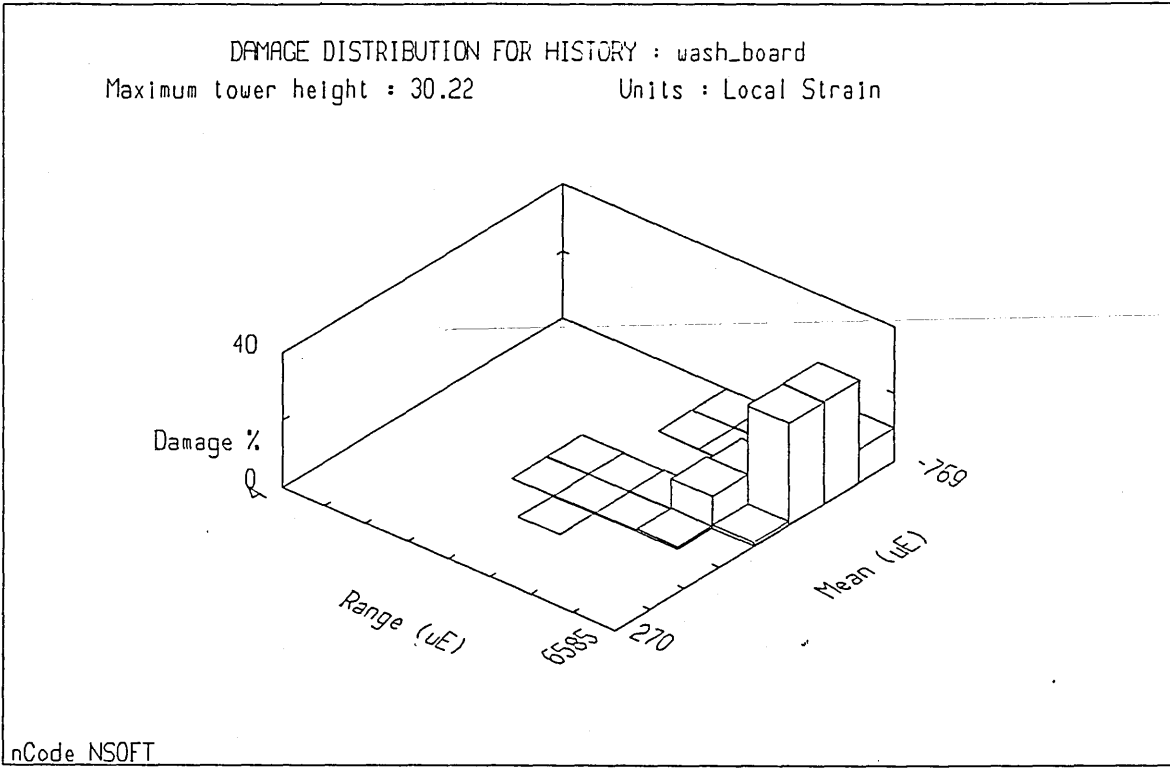


Turning point history : washboard.dac
 Number of cycles used : 479
 Fatigue life : 58 repeats of history

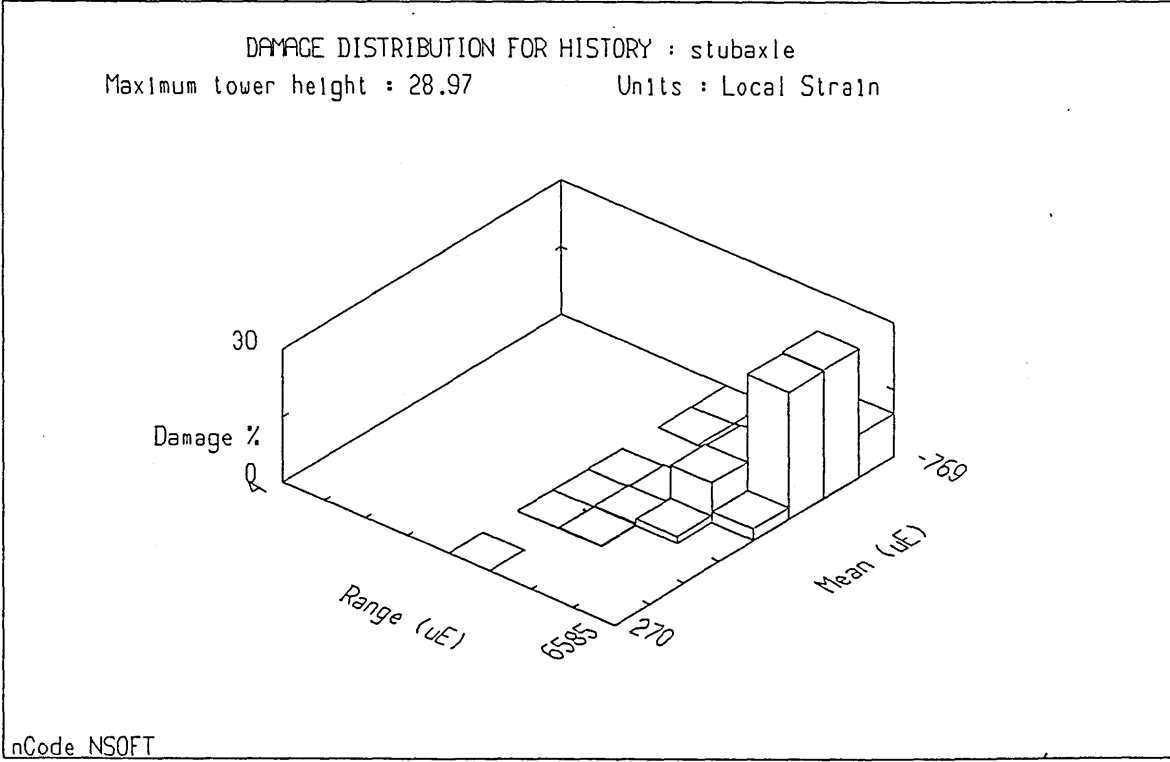


Turning point history : stubaxle.dac
 Number of cycles used : 12991
 Fatigue life : 58 repeats of history

Fig. 3.19 Cycle Distribution (Micro-strain).



Turning point history : washboard.dac
 Number of cycles used : 479
 Fatigue life : 58 repeats of history



Turning point history : stubaxle.dac
 Number of cycles used : 12991
 Fatigue life : 58 repeats of history

Fig. 3.20 Damage Distribution (Micro-Strain).

COMPUTER BASED ANALYSIS OF STEERING ARM

4.1 Introduction

The aims of this section of the programme of work were:-

- i) To develop two and three dimensional computer models of the steering arm. The former was used to locate the relevant boundary co-ordinates as required for the development of a finite element mesh and the latter was for automatic mesh generation using the FAMbuild software package [82, 6].
- ii) To undertake a full three dimensional elastic finite element analysis to identify the most critically stressed areas of the component, and also establish a full description of the static load stresses and strains under elastic conditions.
- iii) To use the elastic stress field information obtained to predict local elastic/plastic strains in the component for inclusion in a fatigue life prediction computer package [83].

Typical of available methods for determining the plastic strains is the one associated with Neuber [3, 38]. This uses the nominal stress, the stress concentration factor and Young's Modulus of Elasticity to determine the plastic strains as follows;

$$\sigma \cdot \epsilon = \frac{(K_f \cdot S)^2}{E}$$

For an elastic finite element analysis σ is the plastic stress at the critical location and $K_t = 1$;

$$\sigma \cdot \epsilon = \frac{(S)^2}{E}$$

Another approach which can be used to determine the local elastic/plastic strain behaviour is the energy method [37, 63]. This also uses the nominal stress, the stress concentration factor and Young's Modulus of Elasticity;

$$\frac{(S)^2}{4E} = \frac{(\sigma)^2}{4E} + \frac{\sigma}{n'+1} \left[\frac{\sigma}{2K'} \right]^{1/n'}$$

The results obtained from the above techniques were used to develop a series of critical location load/strain calibration curves for the component. These were used to load scale the washboard service strain history. The fatigue life evaluation package FATIMAS was then used to assess the fatigue life of the steering arm through a range of scaled load histories. The lowest factored load history was 20 kN and the highest factored load history was 40 kN which resulted in respective strain fields which varied from totally elastic to highly plastic. These are discussed in chapter 6.

4.2 Software Summary

Three individual software packages were used in this phase of the project. A brief description of each is outlined.

4.2.1 MEDUSA

A Prime 9750 mini computer using Medusa [33] software is typical of commercially available CAD systems. The work station consists of a graphics screen and keyboard, and a graphics menu. The screen displays the drawing, as it is being developed or modified. The menu is divided into segments, each labelled with the name of a frequently used command. A command is activated by moving a pen to the relevant entry in the menu and pressing the pen. The screen cursor can be moved by means of a joy-stick. The keyboard can also be used to enter commands, instructions and data to the system, and to input any text, labelling, titles or notes which are to be appear in the drawing. Completed drawings are stored as a data file on magnetic tape and paper copies made on plotters or printers.

A solid model consists of one or more objects. An object is a single continuous piece of material or, more formally, a number of polygons that bound part of space. A complex model is usually created by a build up of simple primitives (blocks, cylinder, cone, wedge, sphere etc), with Boolean operations.

Prime Medusa geometric modelling systems consist of three programs the modeller, the viewer and the reconstructor. A model is created by processing a three dimensional file through the modeller. The modeller scans the sheet and interprets the primitives on the sheet and creates a model. The viewer generates one or more orthogonal and isometric views of a specific model. The orientation of

the model and the direction from which it will be viewed are determined by the view prim in that box. The reconstruction program projects the generated views back on to the sheet.

4.2.2 PAFEC

The finite element package PAFEC (Program for Automatic Finite Element Calculation) [34, 35] together with PIGS (PAFEC Interaction Graphics Suite) is typical of commercially available finite element systems. The package consists of ten definite phases, each carrying out a specific task, towards a solution. In phase one the data modules are read in, the other nine phases including the solution, determination of the stresses, etc. can be included depending on the output required.

The PAFEC program is modular in nature, and due to its flexibility, requires a control file to guide a particular problem towards the required solution. The control module starts with the word CONTROL and ends with CONTROL.END. In between these a number of command statements can be entered. This informs the computer what will be required in the subsequent analysis. Each module within the data file is defined by its heading. After this there will normally be a 'contents' card giving the headings for the information columns. There are over one hundred data modules available and descriptions of each module is outlined in PAFEC Manual [34, 35]. However, some of the most frequently used modules are:-

geometry, mesh, restraints, loading, material.

PAFEC data validation takes place in phase 2; here each element is checked for distortions from the basic shape. Limited distortions are acceptable, and these limits vary with the element type. Four basic checks are made;

- i) Angles between adjacent element sides.
- ii) Ratio of longest to shortest sides.
- iii) Radius of curvature on each side.
- iv) Nodes out of the plane of the elements.

If any of the above fails, warnings or errors result.

4.2.3 PIGS

PIGS is a powerful and valuable pre-processing and post-processing package. It is used for the production of F.E. models and files and also examination of the PAFEC output profiles. The following advantages are associated with PIGS:-

- a) Fast F.E. data production
- b) Mistakes can be viewed and rectified on the screen at all times
- c) Results can be processed quicker than through PAFEC plots.

4.2.4 FAMbuild

FAMbuild is a finite element mesh generation program [36]. It may be used to interface almost any CAD to finite element analysis program. The interface between FAMbuild and CAD systems is achieved by FAM from CAD system commands.

The first level of the problem is the transformation from a CAD model into a numerical model suitable for finite element analysis. The second level of the problem is the actual transfer of geometry between the systems.

Any data transferred must be selected carefully in CAD systems and must represent information that can be used in FAMbuild. The processing in FAM from CAD can not add geometrical information that is not supplied to an unstructured sequence of points and lines.

For a well prepared numerical model, the FAM from CAD processor can significantly contribute to the building of a finite element model in FAMbuild and avoid the extremely labour intensive manual inputting of data, hence saving time and money.

4.3 Two And Three Dimensional Geometric Modelling

The Medusa software package was used to create both a two and three dimensional model of the steering arm. These were then used to accurately locate the boundary coordinates needed for the development of the finite element mesh.

Initially a two dimensional drawing of the steering arm was produced as shown in figure 3.2. This was found to be a relatively easy task. A three dimensional solid model of the component was also generated as shown in figure 4.1. Due to the complexity of the component geometry, in particular the blend radii surrounding the bosses, it was necessary to create the model in two separate stages.

To reduce the degree of complexity, the component was modelled in three separate parts, namely; the steering control shaft, and the two regions surrounding the two bosses. Three separate facilities were used to create the model:-

- a) Volume of revolution
- b) Slide
- c) Surface network.

A Boolean addition operation was then undertaken to combine the individual models to form the complete component.

Overall, the software package was found to be user friendly. However, the creation of a 3-D model was found to be a very complicated and time consuming process. It was found impossible to create an exact replica of the actual shape of the component. This was mainly due to the limitation of the Medusa software package. It was found that the software is incapable of handling coincident faces of the primitive shapes during the Boolean operation. To overcome this major deficiency the primitives had to be overlapped, which was then accepted

by Medusa software. This is a very serious problem particularly when combining a number of three dimensional solid models at common faces or edges.

The accuracy of a solid model is dependent upon chord tolerance selected for cylindrical primitives in the model. The finer the chord tolerance given to a model the better the accuracy. However, more time is consumed by the computer to generate such a model. For the steering arm the chord tolerance was set at 0.1 mm.

In order to avoid the tedious manual inputting of data, an integrated solid modelling and finite element analysis software package (CAD-FAM) was used to transfer the solid model of the component and carry out finite element analysis using the automatic mesh generator package (FAMbuild). This was unsuccessful due to the complex geometry at the change of section around the bosses. An attempt was made to produce a simplified solid model of the component. However, further problems were encountered with coincident face of the primitive shapes during the Boolean operation. Therefore this technique was abandoned. Manual data input to the F.E. package was then undertaken. The three dimensional solid model of the steering arm was found to be of no real value at the later stages of the project.

Having created a solid model, the colour shader facility was used to produce a shaded image of the component as shown in figure 4.2.

4.4 Finite Element Analysis

4.4.1 Component Geometry And Material Properties

Due to the complexity of the component geometry in particular the blend radii around the bosses, the generation of a three dimensional finite element model was necessary. There were however, considerable constructional difficulties in undertaking such a task. Restrictions on element geometry presented the largest problem. Within such a complex mesh it was difficult to avoid the generation of elements which violated the basic elemental rules.

Distorted elements even far removed from the region of immediate interest can lead to the introduction of quite considerable inaccuracies.

The biggest problems encountered were at the changes of section around the bosses, where the adjacent angles were outside the acceptable limit. To minimise the above difficulties some geometric modifications were necessary. These will be described in the next section.

The material properties used for input to PAFEC data file were:-

Young's Modulus, E = 214800 MPa

Poisson's ratio, ν = 0.3

Density, ρ = 7850 Kg/mm

4.4.2 Development Of The Finite Element Model

Initially the full component was modelled. To overcome the difficulties posed by the complex geometry of the component the geometric model in Medusa was modified in order to simplify the finite element discretisation process. The diameter of the bosses were made the same (40 mm), this increased the blend radii around the bosses from 25mm to 25.73mm.

The component was split into several suitable blocks [82] and the boundary co-ordinates were entered using a global axis set. PIGS was used to fill these blocks with 892 individual elements.

The elements used were standard twenty noded isoparametric brick elements (37110) and fifteen noded isoparametric prism elements (37210) as shown in figure 4.3 [82]. These elements have three degrees of freedom at each node and the stress/strain varies linearly in each direction. This also has the advantage that the displacement and boundary shapes are quadratic in nature. The midside nodes allow curved boundaries to be represented accurately if necessary.

A point load of 20 kN was applied to the area XY in figure 4.4. Since the stress/strain varies linearly, unit load may be applied. This value of load was chosen to obtain reasonable stress values for comparison with strain gauge results.

The lower surfaces AB and GH of the component were restrained in the Z direction. The end AC was fully restrained in the X direction. The upper surface CD and EF were subjected to a uniform pressure of 87 MPa in Z direction representing fastening bolt pressure in both the rig and the real location. This value was derived using the following method:-

$$\text{The clamping force of bolt and washer} = \frac{2}{3} \sigma_y$$

where:-

$$\sigma_y = \text{yield stress of the bolt} \approx 640 \text{ MPa}$$

$$\text{Clamping force of the bolt} = \frac{2}{3} \times 640 = 427 \text{ MPa}$$

$$\text{bolts diameter} = 18 \text{ mm}$$

$$\text{Area of bolt} = \pi r^2 = 254.54 \text{ mm}^2$$

$$\text{Load} = F = \sigma \cdot A$$

$$\text{Load} = 108.6 \times 10^3 \text{ N}$$

$$\text{Diameter of the washer} = 40 \text{ mm}$$

$$\text{Area of the washer} = 1256 \text{ mm}^2$$

$$\text{Pressure} = \sigma = \frac{F}{A} = 86.5 \approx 87 \text{ MPa}$$

The data file was created in PIGS and the material properties were entered via the keyboard.

The basic output from the computer was in digital form. For every node or element in the structure the print out gave the values of stress and displacement in X, Y and Z directions. The computer also calculated the principal stresses and their directions. Whilst the printed output was required for detailed analysis, a clear picture of the state of stress was given on the graphics terminal. The

results were also plotted as stress contours, to highlight the highly stressed regions as shown in figure 4.5.

Close examination of the stress contours and stress data file revealed that the component does not carry any appreciable load between A-A and B-B. Hence, this part was discarded and the component was restrained in the X direction at the section of cut to enable a finer mesh to be produced at the critical location.

Again the blend radii were increased from 25 mm to 25.73 mm to enable the element geometry to be within acceptable limits of PAFEC. At this point the remainder of the component was remodelled. A point load of 20 KN was applied to the kingpin, area XY shown in figure 4.6.

To ensure the accuracy of the solution a finer mesh was defined at the section of the component which exhibited high stress gradients, identified by the previous model. The new model resulted in a total of 600 elements and 3156 nodes.

The lower surface of the component, AB, was restrained in the Z direction as shown in figures 4.6. The section of cut, AC, was clamped in the X direction. The upper surface, CD, was subjected to a uniform pressure of 87 MPa to represent the fastening pressure exerted by the bolt. The data file was created in PIGS and material properties were input via the keyboard.

4.5 Results And Discussion

Contours of the maximum principal stresses were plotted using the facility within PIGS. The 'rainbow' plots highlighted the areas of high stress gradients, referred to as 'hot spots', which are shown in figure 4.7.

Output from the FE analysis is shown in Table 4.1 in the form of principal stresses.

At the point of highest principal stress (node 12) a triaxial state of stress prevails. The percentage biaxiality was found to be 9% for principal stress values of $\sigma_1 = 355$ MPa, and $\sigma_2 = 32.2$ MPa and $\sigma_3 = 23.3$ MPa.

Since maximum principal stress/strain values at the surface of the component are of interest in fatigue life evaluation, only these were initially considered. The elastic stress/strain relations given by equations 4.1 to 4.3 were used to calculate the elastic principal strains from the F.E calculated principal stresses and are shown in Table 4.2.

$$\epsilon_1 = \frac{1}{E} \{ \sigma_1 - \nu (\sigma_2 + \sigma_3) \} \quad - \quad 4.1$$

$$\epsilon_2 = \frac{1}{E} \{ \sigma_2 - \nu (\sigma_3 + \sigma_1) \} \quad - \quad 4.2$$

$$\epsilon_3 = \frac{1}{E} \{ \sigma_3 - \nu (\sigma_1 + \sigma_2) \} \quad - \quad 4.3$$

For an applied end load of 20 kN the finite element analysis predicted a maximum principal strain value of 1571 micro-strain at node 12.

For prediction of the elastic/plastic strain values at the critical location both Neuber's rule and the energy density approach were used. Since the measured strains were obtained using the unstabilised component, the initial plastic strain calculations were carried out using the monotonic stress/strain curve, listed in table 4.4. These strains were then compared to measured strains. For use in fatigue life predictions the method was repeated using the cyclic stress/strain curve, listed in table 4.5.

The elastic finite element critical location principal stress values, listed in table 4.1, were reduced to an equivalent stress (σ_{eq}) using maximum principal stress, Tresca, von Mises' and maximum principal strain methods and the results are listed in table 4.3 [55, 56].

The elastic finite element principal stresses vary within the region of the critical location. Consequently when equivalent values are calculated there is a degree of variation in magnitude and position of the critical node. Using the maximum principal strain and the maximum principal stress methods node 12 is the most critical node, whereas using the other two methods node number 19 is the most critical node.

Neuber's rule was then applied to each equivalent stress to construct Neuber's hyperbola. The intersection of

Neuber's hyperbola and the uniaxial monotonic stress/strain curve gives the required elastic/plastic strain values. As an example the procedure for solving the Neuber's equation for a 30 kN load is shown in figure 4.8.

The energy density approach was also used in conjunction with the monotonic stress/strain curve to calculate the plastic strain values using the equivalent stresses (σ_{eq}) described above. A number of calculations were carried out in load increments of 10 kN from 10 kN to 70 kN and the results are included in table 4.4.

The component monotonic load/notch root strain calibration curves using F.E. calculated equivalent values and both Neuber's rule and the energy density method are shown in figure 4.9. It is apparent that for low values of load, both methods give results very close to each other. For high values of load the calibration curves obtained from both methods deviate from each other. As the amount of plasticity increases the degree of correlation decreases between Neuber's estimated strains and the energy density estimated strains.

For a load of 10 kN, the estimated total strain values obtained using maximum principal stress, Tresca, von Mises and maximum principal strain methods together with Neuber's rule were found to be respectively 845, 763, 734 and 783 micro-strain. For a 70 kN load these values increase to 7077, 6539, 6494 and 6679 micro-strain. For the same load variation the calculated strain values using

maximum principal stress, Tresca, von Mises and maximum principal strain methods together with energy density technique were found to be 815, 776, 771 and 789 micro-strain and 6070, 5731, 5678 and 5822 micro-strain. Thus, the lowest 70 kN total micro-strain of 5678 is obtained using the energy density and von Mises method, whilst the highest value of 7077 micro-strain occurred with Neuber's method and maximum principal stress equivalent. The latter is 20% greater than the former.

The above calculations were repeated using the F.E. calculated equivalent values and the cyclic stress/strain curve. The results are shown in tabulated and graphical form in table 4.5 and figure 4.10.

For a load of 20 KN, the estimated elastic/plastic strain values obtained, using maximum principal stress, Tresca, Von Mises and maximum principal strain methods in conjunction with the cyclic stress/strain curve and Neuber's rule were found to be respectively 1800, 1665, 1640 and 1730 micro-strain. This variation increased with increasing load to 4415, 4095, 3955 and 4150 micro-strain for a 40 KN load. For the same load variation the calculated strain values using maximum principal stress Tresca, Von Mises and maximum principal strain methods together with the energy density method and cyclic stress/strain curve were found to be 1653, 1547, 1539 and 1569 micro strain, and 3276, 3079, 3064 and 3127 micro-strain.

The onset of cyclic yielding (σ_y) appears to occur at a load of approximately 20 KN. At this load the material experiences slight plastic deformation as shown in figure 4.8. Close agreement was found between the Neuber's estimated strains and those obtained using the energy density method for a 20 KN load (the elastic range). However, it can be seen that the estimated strains based on Neuber's rule and equivalent methods are grossly over-estimated for a 40 KN load in the plastic range when compared to those obtained using the energy density method.

In the case of the 20 kN load, the highest elastic strain (approximating the cyclic yielding) of 1800 micro-strain is obtained with Neuber's method and maximum principal stress method, whilst the lowest value of 1539 micro-strain occurred with the energy density and von Mises equivalent method. The former is 14.5% greater than the latter. The highest strain of 4415 micro-strain comes from using Neuber's method with maximum principal stress for 40 kN. For the same load increment the lowest plastic strain of 3064 micro-strain is produced by combination of the energy method and von Mises' equivalence. This represents a 31% increase between minimum and maximum values.

The above results show that the accuracy of the above methods depends in general on the extent of the plastic zone at the notch root. The smaller the plastic zone in comparison with the elastic area surrounding the notch

root, the closer agreement exists between the two methods. The percentage strain difference of 14.5% and 31% for 20 and 40 kN load increment show that Neuber's rule overestimates local strains, ^{as} at the amount of plasticity increases with increasing load in comparison with the energy density method.

4.6 Conclusions

For low values of nominal stress, $K_t.S$, both Neuber's and the energy density methods give results which are in close agreement. For high nominal stress values, Neuber's method in general overestimates the local strains when compared to those obtained using the energy density method. As the load increases to give high levels of plasticity the degree of correlation reduces as shown in figures 4.9 and 4.10.

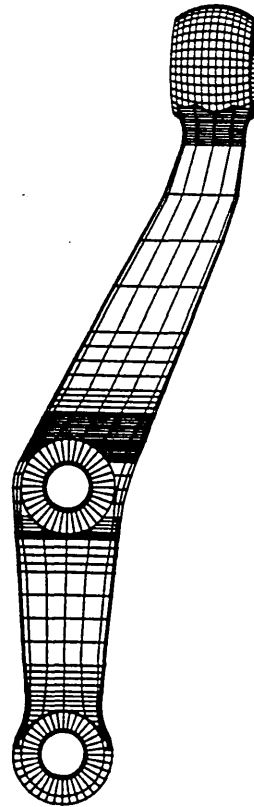
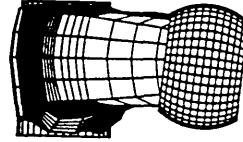
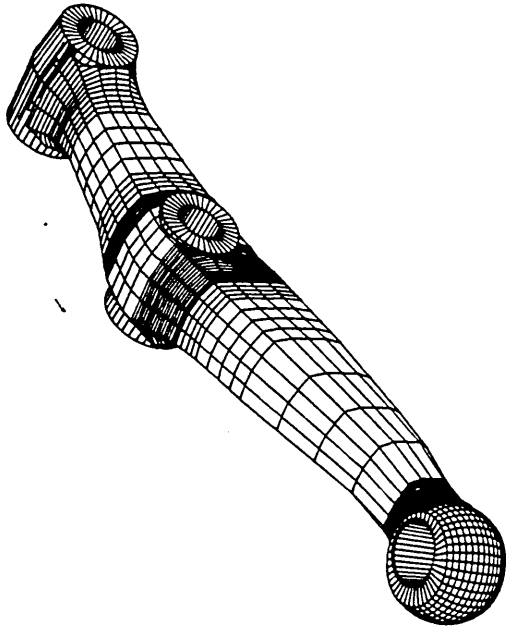


Fig. 4.1 Three Dimensional Geometric Model
Of The Steering Arm

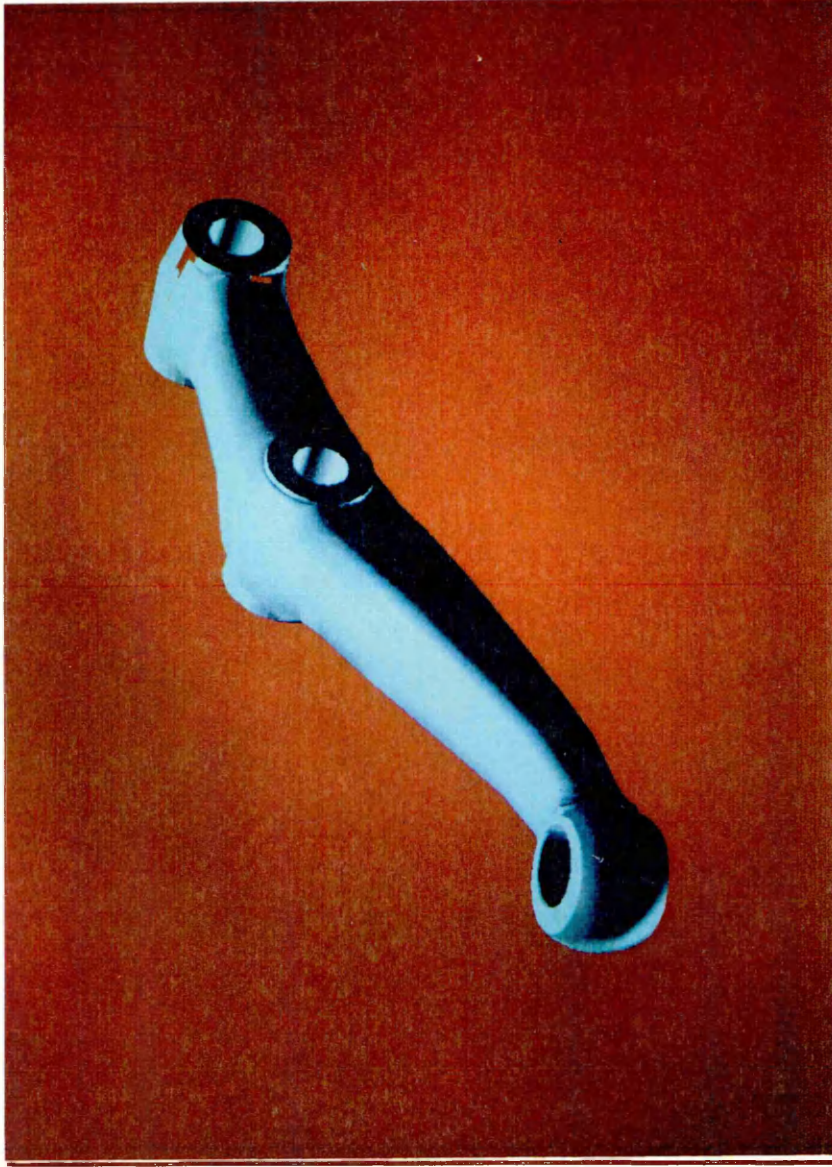
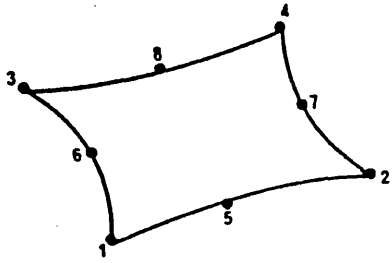
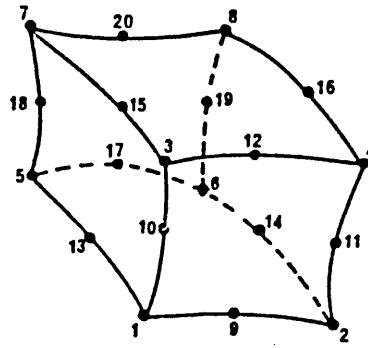


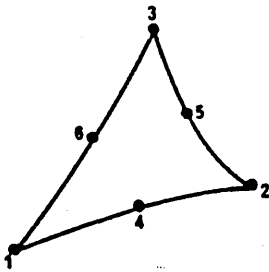
Fig 4.2 Shaded Image of the Steering Arm.



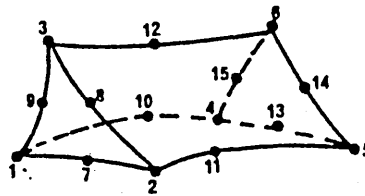
Eight Noded Isoparametric
Quadrilateral Element (36210)



Twenty Noded Isoparametric
Brick Element (37110)



Six Noded Isoparametric
Triangular Element (36110)



Fifteen Noded Triangular Prism
Element (37210)

Fig. 4.3 Element Types.

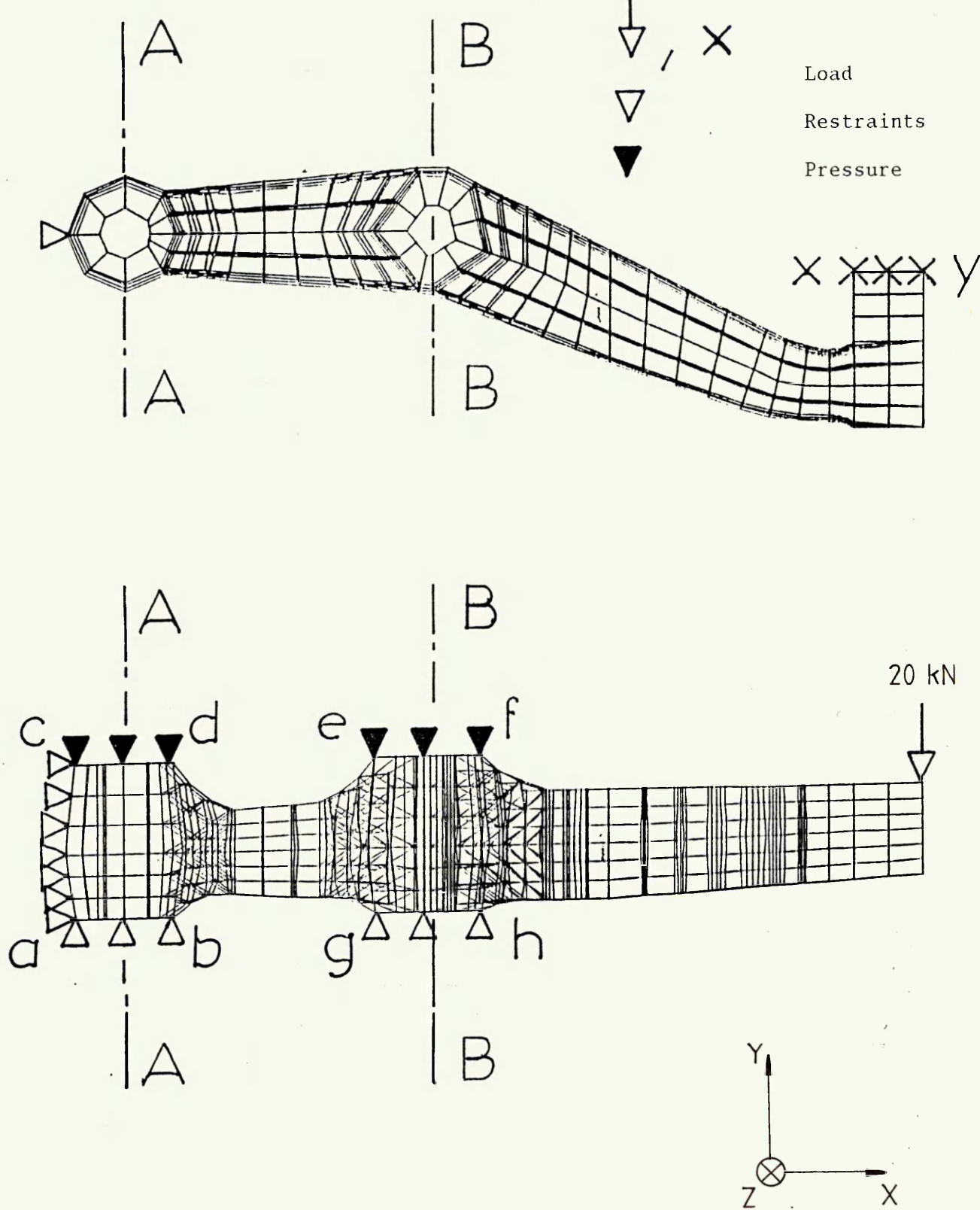


Fig 4.4. A Mesh Used For Three Dimensional Finite Element Analysis Of The Full Component.

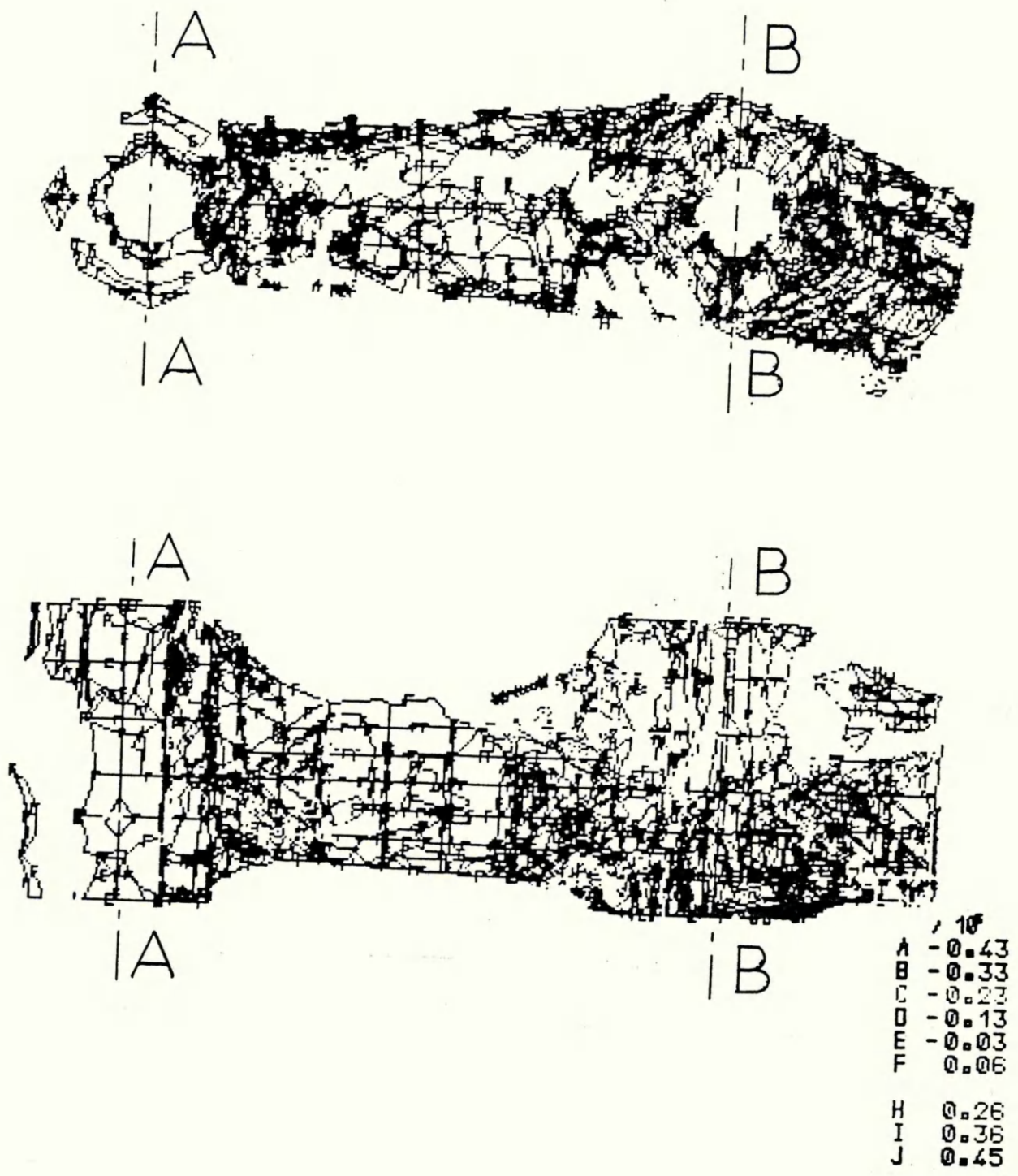


Fig 4.5 Stress Contours Of The Full Component.

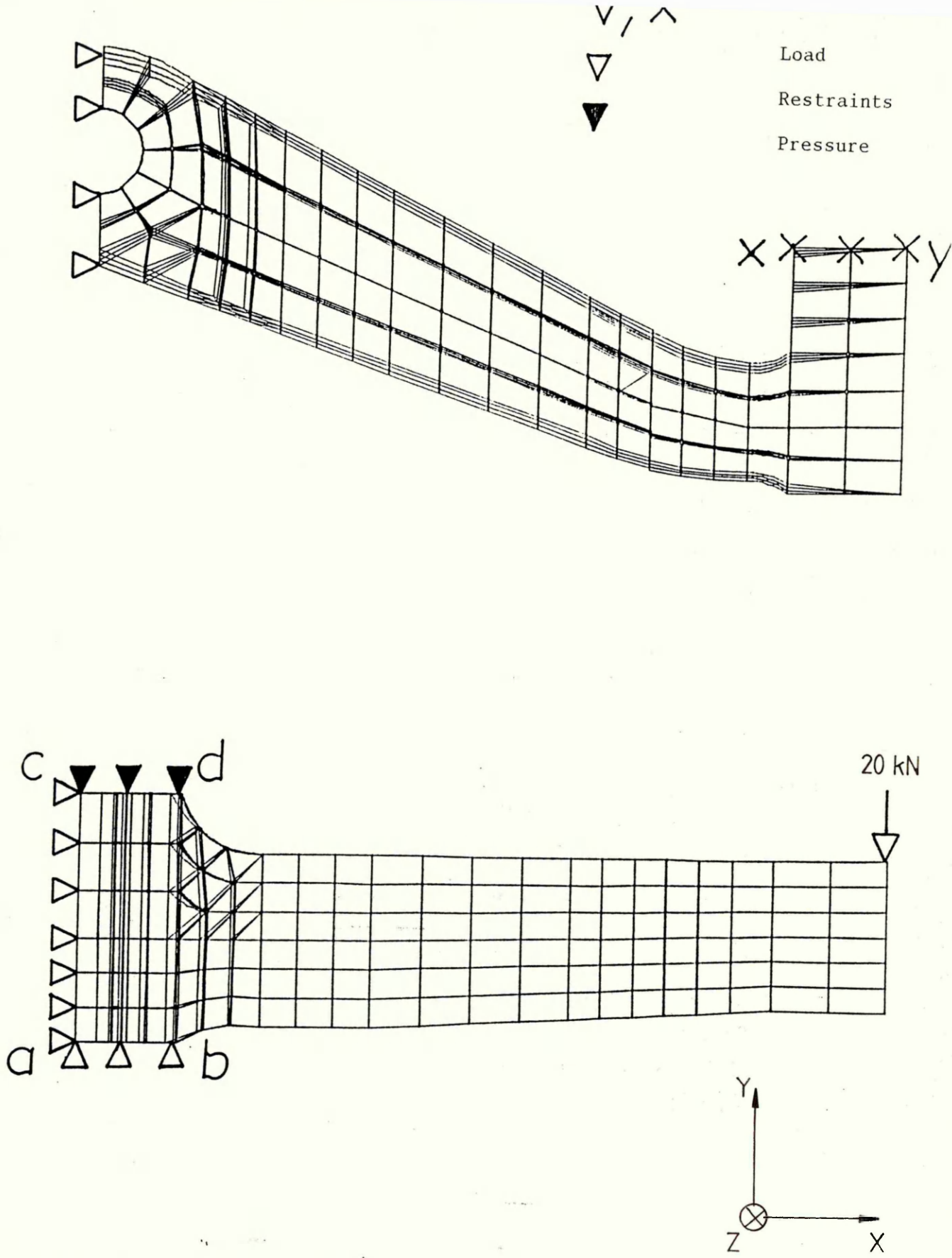


Fig. 4.6 Mesh Used For Three Dimensional Analysis Of The Critical Part Of The Component.

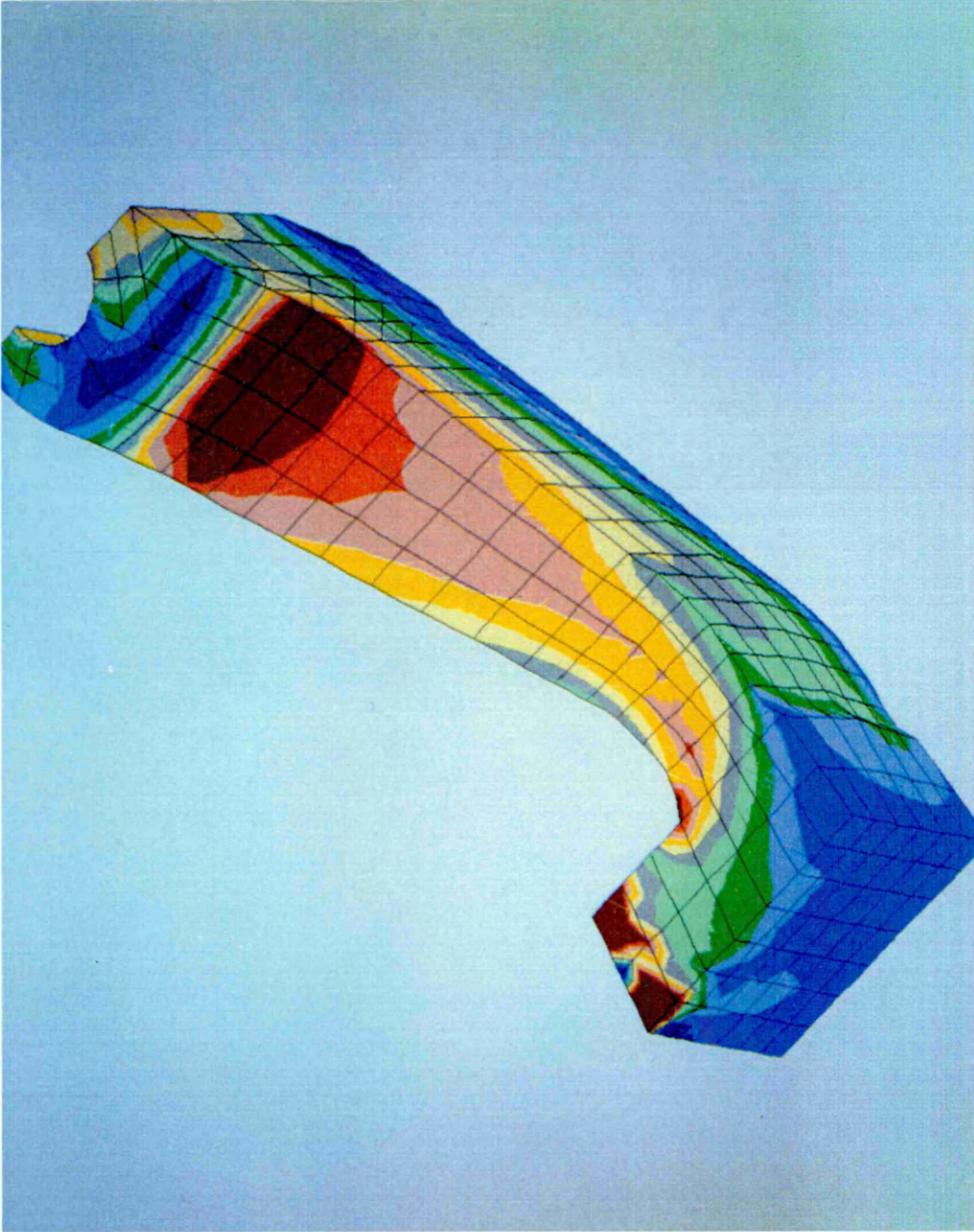
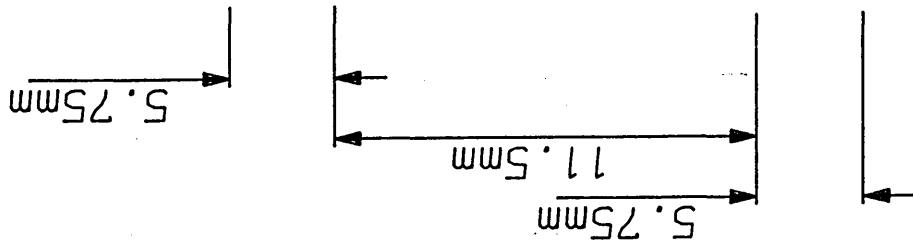
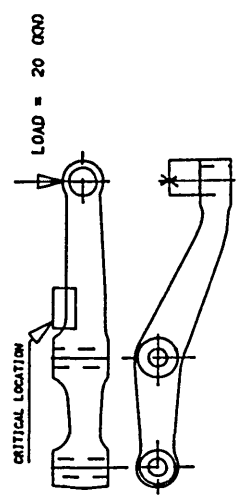
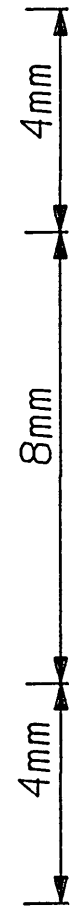


Fig 4.7. Stress Contours Of The Critical Part Of The Component.

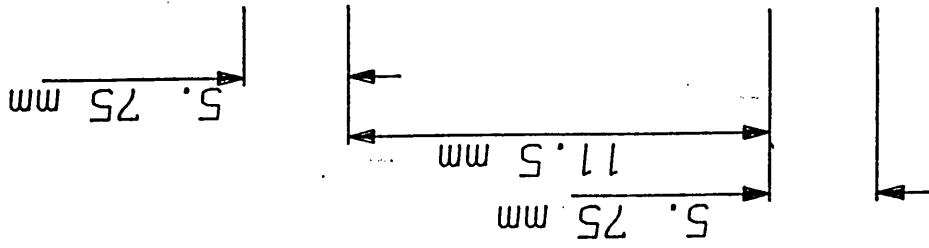


$\begin{Bmatrix} 249 \\ 25.6 \\ 13.6 \end{Bmatrix}$	$\begin{Bmatrix} 231 \\ 41 \\ 16.5 \end{Bmatrix}$	$\begin{Bmatrix} 242 \\ 3 \\ -6 \end{Bmatrix}$	$\begin{Bmatrix} 238 \\ -1 \\ -2 \end{Bmatrix}$
$\begin{Bmatrix} 285 \\ 32 \\ 12.4 \end{Bmatrix}$	$\begin{Bmatrix} 278 \\ 28.5 \\ 20.2 \end{Bmatrix}$	$\begin{Bmatrix} 266 \\ 5 \\ -12 \end{Bmatrix}$	$\begin{Bmatrix} 250.5 \\ -2 \\ -17 \end{Bmatrix}$
$\begin{Bmatrix} 313 \\ 38 \\ 17 \end{Bmatrix}$	$\begin{Bmatrix} 277 \\ 16.2 \\ 7.3 \end{Bmatrix}$	$\begin{Bmatrix} 276 \\ 1 \\ -10 \end{Bmatrix}$	$\begin{Bmatrix} 288.5 \\ 2 \\ -7 \end{Bmatrix}$
$\begin{Bmatrix} 330 \\ 33 \\ 16.4 \end{Bmatrix}$	$\begin{Bmatrix} 299 \\ 14 \\ 7 \end{Bmatrix}$	$\begin{Bmatrix} 282.5 \\ -2.5 \\ -11 \end{Bmatrix}$	$\begin{Bmatrix} 251 \\ 0.05 \\ 12 \end{Bmatrix}$
$\begin{Bmatrix} 332 \\ 28 \\ 16 \end{Bmatrix}$		$\begin{Bmatrix} 288.5 \\ 2 \\ -7 \end{Bmatrix}$	$\begin{Bmatrix} 276 \\ 5 \\ -2 \end{Bmatrix}$
$\begin{Bmatrix} 325 \\ 18 \\ 11 \end{Bmatrix}$		$\begin{Bmatrix} 288 \\ -7.5 \\ -8 \end{Bmatrix}$	
$\begin{Bmatrix} 299 \\ 14 \\ 7 \end{Bmatrix}$		$\begin{Bmatrix} 276 \\ 5 \\ -2 \end{Bmatrix}$	



○ SURFACE NODES
 ELASTIC PRINCIPAL STRESSES (F.E.A) : LEGEND :
 { STRESS 1
 STRESS 2
 STRESS 3

Table 4.1 Surface Maximum Principal Stresses At Critical Location (MPa).



①	{ 947 -270 -421	②	{ 1122 -270 -445
③	{ 990 -154 -299	④	{ 1303 -178 -293
⑤	{ 1414 -365 -401	⑥	{ 1224 -326 -431
⑦	{ 142 -287 -444	⑧	{ 1240 -352 -394
⑨	{ 1501 -327 -472	⑩	{ 1269 -365 -401
⑪	{ 1513 -357 -469	⑫	{ 1287 -359 -408
⑬	{ 1492 -385 -457	⑭	{ 1287 -359 -408
⑮	{ 1386 -387 -426	⑯	{ 1217 -339 -378
⑰	{ 1245 -323 -347	⑱	{ 1175 -333 -399
⑲	{ 1567 -400 -430	⑳	{ 11192 -333 -430
㉑	{ 1571 -371 -444	㉒	{ 11175 -333 -399
㉓	{ 1586 -400 -430	㉔	{ 11175 -333 -399

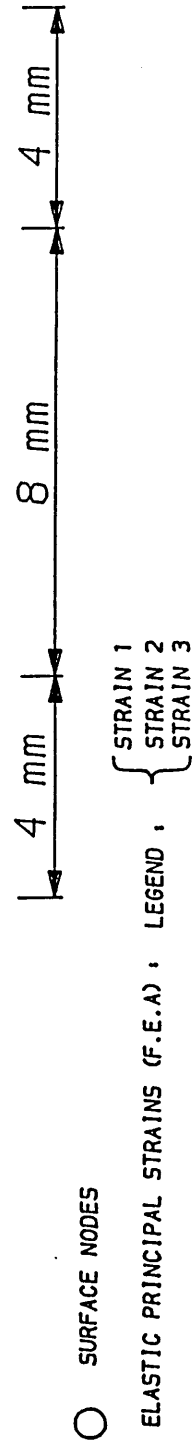
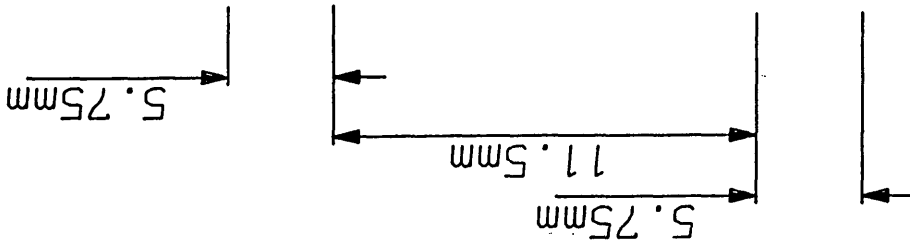
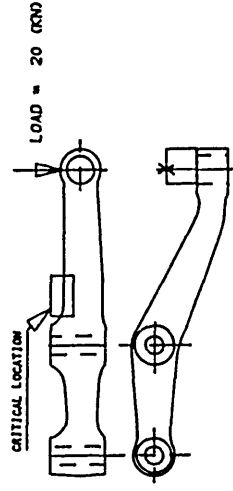
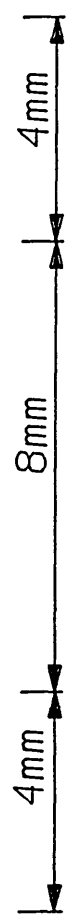


Table 4.2 Surface Maximum Principal Strains at Critical Location Micro-Strain.



	①	②	③	④	⑤	⑥	⑦
	{ 249 236 230 }	{ 242 248 244 }	{ 231 214 203 }	{ 285 273 263 }	{ 316 299 295 }	{ 266 266 264 }	{ 238 237 236 }
	⑧	⑨	⑩	⑪	⑫	⑬	⑭
	{ 313 296 286 }	{ 276 285 280 }	{ 278 258 254 }	{ 330 314 306 }	{ 355 332 327 }	{ 282.5 293 289 }	{ 250.5 267 260 }
	⑮	⑯	⑰	⑱	⑳	㉑	㉒
	{ 332 316 310 }	{ 349 332 330 }	{ 277 269 265 }	{ 288.5 296 291 }	{ 288 293 294 }	{ 251 239 238 }	
	㉓						
	{ 299 277 274 }						



○ SURFACE NODES
 ELASTIC EQUIVALENT STRESSES (F.E.A):
 LEGEND :
 { PRINCIPAL STRESS METHOD
 TRESCA METHOD
 VON MISES METHOD

Table 4.3 Surface Equivalent Stresses At Critical Location (MPa).

LOAD kN	ESTIMATED LOCAL STRAINS F.E. CALCULATED EQUIVALENT METHOD AND NEUBER (MICRO-STRAIN)				ESTIMATED LOCAL STRAINS F.E. CALCULATED EQUIVALENT METH. AND THE ENERGY DENSITY APPROACH			
	Princ. Stress	Tresca	von Mises	Princ. Strain	Princ. Strain	Tresca	von Mises	Princ. Strain
10	845	763	734	783	815	776	771	789
20	1685	1523	1462	1563	1627	1548	1538	1574
30	2445	2325	2275	2405	2441	2321	2307	2359
40	3302	3121	3098	3156	3272	3099	3071	3161
50	4321	4059	4025	4149	4149	3908	3584	3974
60	5591	5196	5123	5301	5053	4778	4741	4853
70	7077	6539	6494	6679	6070	5731	5678	5822

Table 4.4. The Estimated Local Strains For The Steering Arm Using The Monotonic Stress/Strain Curve.

LOAD kN	ESTIMATED LOCAL STRAINS F.E. CALCULATED EQUIVALENT METHOD AND NEUBER (MICRO-STRAIN)				ESTIMATED LOCAL STRAINS F.E. CALCULATED EQUIVALENT METH. AND THE ENERGY DENSITY APPROACH			
	Princ. Stress	Tresca	von Mises	Princ. Strain	Princ. Stress	Tresca	von Mises	Princ. Strain
	20	1800	1665	1640	1730	1653	1547	1539
25	2230	2100	2052	2100	2067	1937	1923	1965
30	2825	2650	2560	2680	2429	2319	2309	2357
35	3590	3315	3285	3350	2882	2705	2686	2741
40	4415	4095	3955	4150	3276	3079	3064	3127

Table 4.5. The Estimated Local Strains based on Cyclic Stress/Strain Curve.

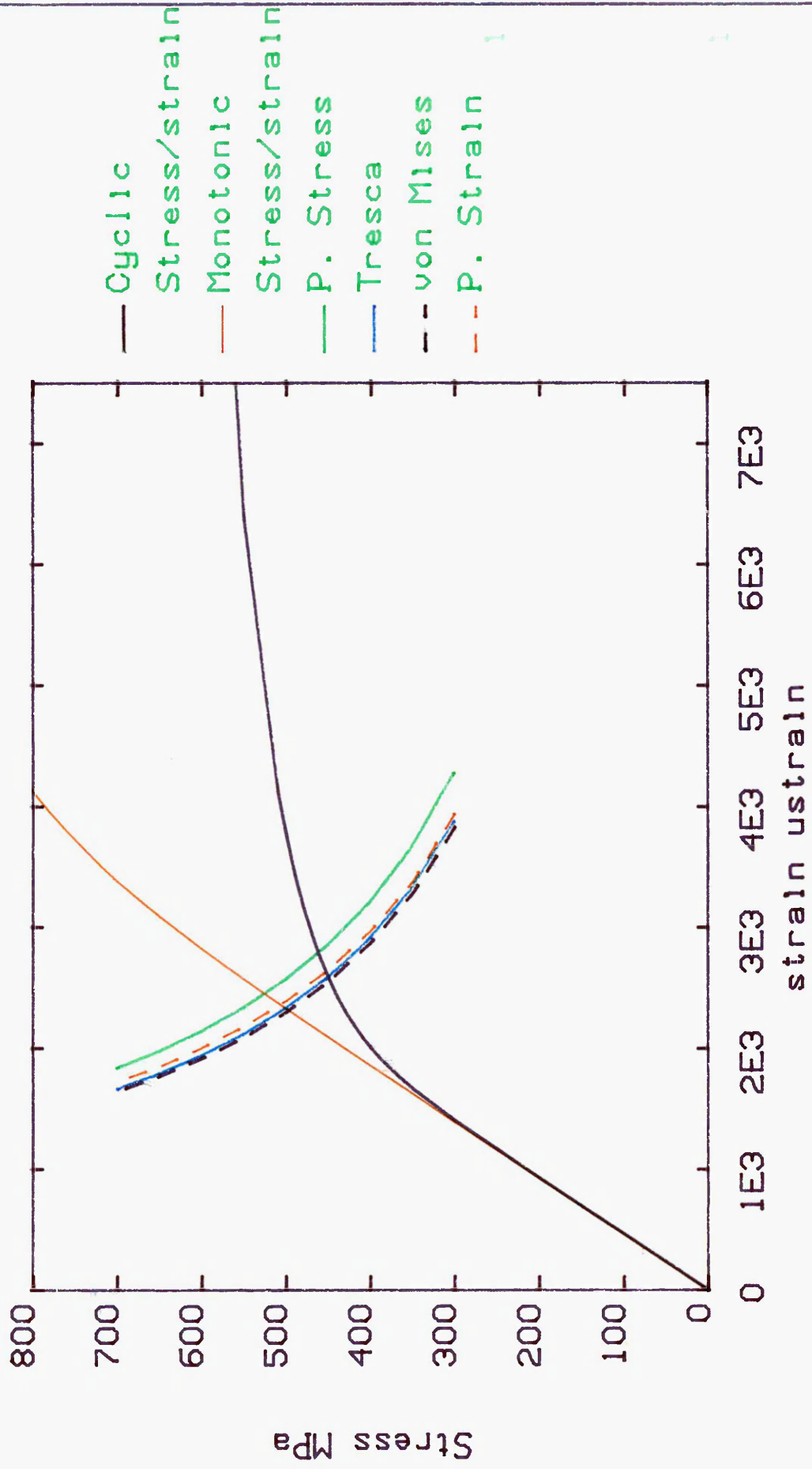


Fig. 4.8 Example of Solving Neuber's Equation.

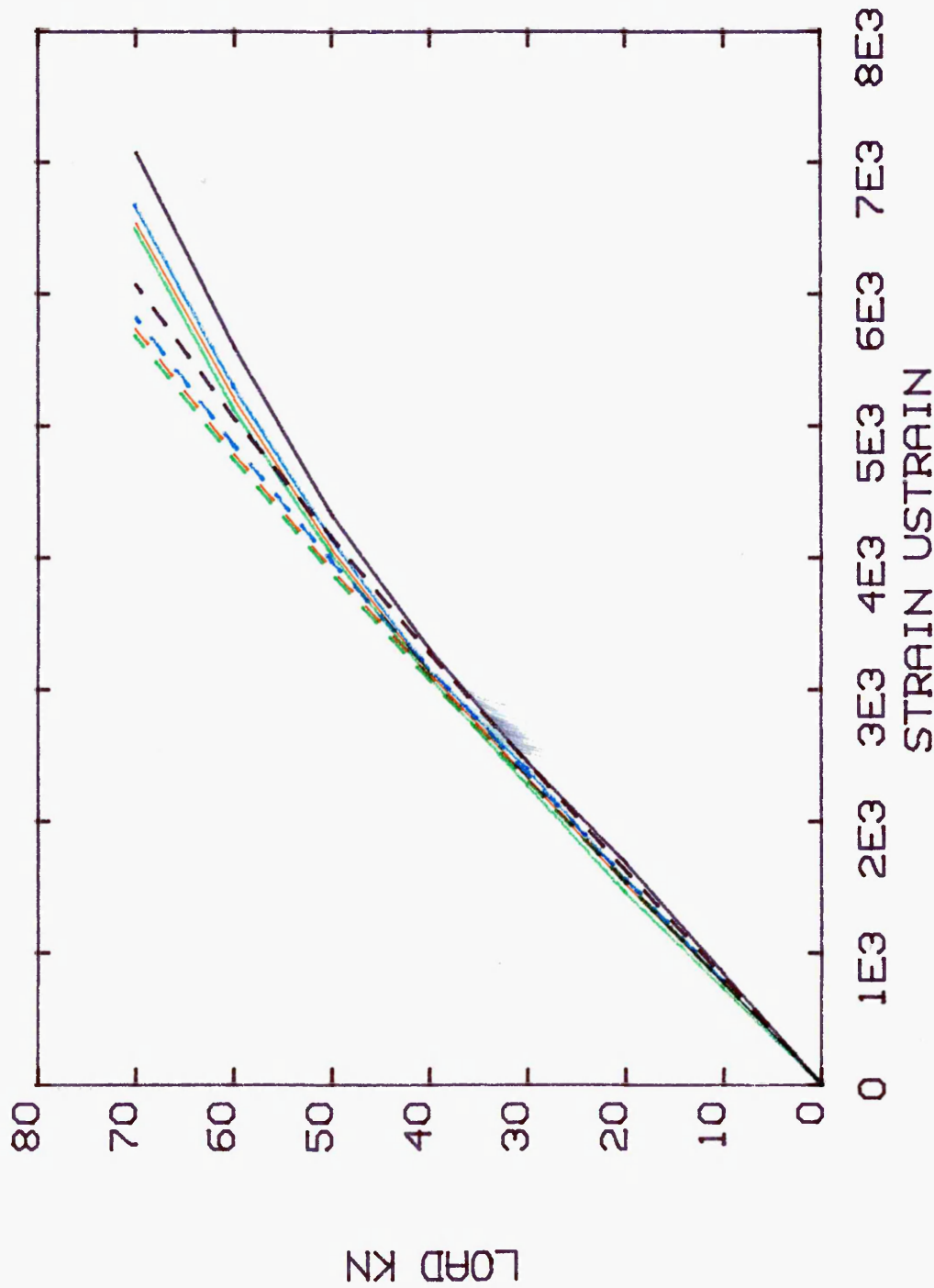


Fig. 4.9 Monotonic Estimated Load/Notch Root Strain Calibration Curves.

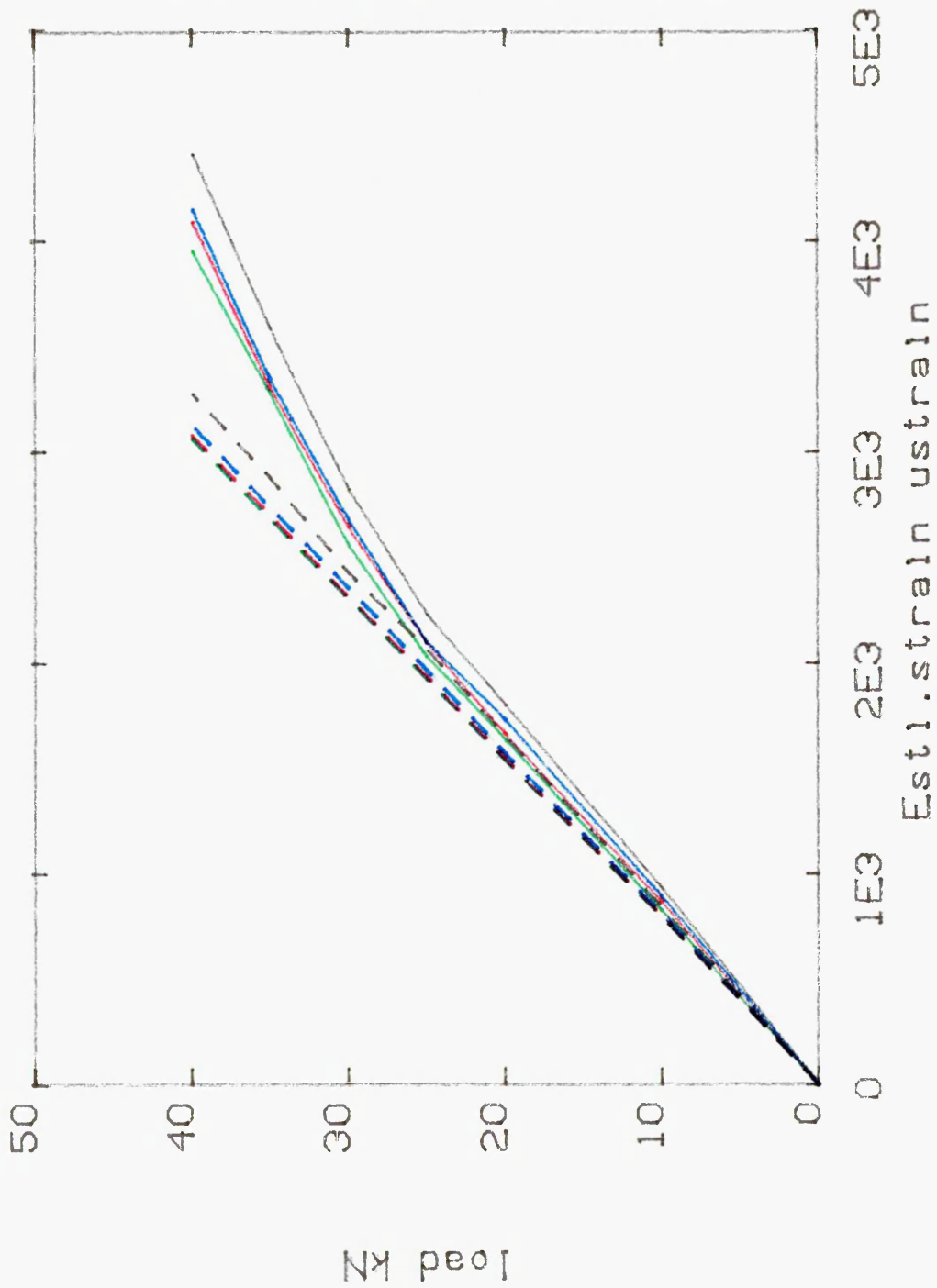


Fig. 4.10 Cyclic Estimated Load/Notch Root Strain Calibration Curves.

STATIC MEASUREMENT OF STEERING ARM STRAINS

5.1 Introduction

The static testing of the component was undertaken to verify the accuracy of the finite element results. Up to the yield-point of the component material, the experimental results were compared with the elastic finite element results. For points where the material yield stress had been exceeded, plastic strains were obtained using both Neuber's rule and the energy method. The resultant elastic-plastic values were compared with post-yield measured data.

5.2 Test Equipment

- 1) Dartec 9500 Computer Controlled Multiaxial Testing Machine:-

This machine can be used for the application of dynamic or static loading of engineering components. The machine can be programmed to run under load, stroke or extension control. For this work it was decided to operate under load control because the actuator has a capacity of +/-250 and +/-200 kN in static and dynamic mode, respectively. The test programme on the 9500 system was programmed and monitored by a IBM A T (E) microcomputer. This was used to apply loading to a test specimen and to store the test results and associated data on disk.

The following modules were used during the testing program.

- i) Profile Generator:- This unit was used to generate command profiles from a large number of turning points. These points were loaded into the memory from the supervisory computer. The origin of the profile was input from a keyboard (manual) or data obtained from service measurement. This program was used to input the load history into the 9500 system.
- ii) Load Program:- This was used to convert the strain based service history supplied by the manufacturer to a load history suitable for the profile generator.
- iii) X-Y program:- This was used to capture and plot the data during the test programme.
- iv) Trip Program:- This facility provided control of the bounds tests, error tests and external tests. The parameters for these tests were read from the 9500 or from a file, as and when required. Maximum and minimum load values were entered and stored if required, also a means of resetting the trip and identifying the cause of a trip was provided. This program was normally loaded before starting a test.

There are several limitations associated with the above facility:-

- a) In its present form the dartec machine will not test under strain control conditions, hence the need to generate a load history from the strain history supplied.
- b) Over heating is a major problem. The pump would often stop, with the profile generator continuing. This made it impossible to run the test program continuously.
- 3) Solartron Data Acquisition System:- This system was micro-processor based. It offered a setting for single gauges as well as rosettes. The system can be programmed to give the principal strains and their directions. This unit allowed 24 individual bridge circuits to be balanced and switched to an output separately. A print out facility was also provided.
- 4) Ferranti Merlin 750 Metrologysystem:- This machine provided measurements in the X, Y, and Z directions. A horizontal bridge X, and a longitudinal granite worktable Y, and a vertical column Z, provided movements of 750, 750, and 500 mm respectively. To ensure precision of movement all axes were fitted with air bearings. The machine was also fitted with an optical scale which allowed measurements to be determined to a resolution of 0.5 micro-metres.

The Merlin machine is micro-processor based, this being fitted and operated as a combined counter and data processing unit. The machine can be part-

programmed by a personal computer. A print-out facility was also provided.

Measurement was carried out by probing the workpiece with a spherically-ended stylus. This operation was carried out manually under Joy-stick control, or computerised using the part-programming facility when undertaking repetitives routines, such as inspection.

This system was used to define the exact position of the strain gauges. Care was taken to position the gauges at points corresponding to the nodal positions of the finite element model around the critical location.

- 5) Dial Test Indicator:- This was used to measure the deflection values at the unsupported end of the steering arm under varying load increments.

5.3 Experimental Rigs

The steering arm was loaded to examine the effects on fatigue life of the stress fields which approximated the actual loading conditions. This was achieved by applying the load through the kingpin, as shown in figure 5.1.

The experimental rig designed to carry out both the static and fatigue tests consisted of two rectangular plates, a circular plate, a T-section and a kingpin manufactured of EN18. The rectangular plates were fastened together with the steering arm bolted securely to the rig. This was then secured to the Dartec 9500 testing machine bed. The

T-section was fastened to the circular plate and this assembly was then secured to the actuator. The kingpin was used to connect the above assemblies. Figures 5.1 and 5.2 show the exploded and the assembled views of the rig.

5.4 Strain Measurements

5.4.1 Strain Gauge Specification

	<u>SINGLE GAUGE</u>	<u>ROSETTE</u>
Type Reference	YFLA -2	FRA -2 -11
Length	2 mm	2 mm
Gauge factor	2.12	2.07
Wire resistance	120 I 0.3 ohm	120 I 0.5 ohm
Orientations	—	0°, 45°, 90°

5.4.2 Static Loading Results

In order to identify the principal planes for attachment of post yield strain gauges, two strain gauge rosettes were attached to the steering arm at the critical location identified from the finite element analysis. One gauge was attached to the radius of the component at a distance of 37 mm to the right of the centre of the middle boss. The second gauge was fixed at an angle of 22° from the first gauge, conforming to the arrangement stipulated by the manufacturer, as shown in figure 5.3. The Dartec 9500 testing machine was used to apply loads from 5 kN to 40 kN in increments of 5 kN, and the strain and deflection values were recorded. The results are shown in table 5.1. A comparison of the measured maximum principal strains

with those obtained from elastic finite element analysis at the highest stressed node (node 12) was made. For a 20 kN load the maximum principal strains were found to be 1608 and 1571 micro-strain for measured and F.E. calculated results, respectively. Therefore the F.E. result was about 2.3% lower than the measured strain.

To obtain the strain values in the plastic range the rosette strain gauges were replaced by two post-yield strain gauges. The post yield strain gauges were attached to coincide with the plane of the maximum principal strain identified by the rosette strain gauges. The Ferranti Merlin 750 Metrology system was used to defined the exact position of the strain gauges. Loads were applied in increments of 10 kN up to a maximum load of 70 kN and the strain values were recorded at each load increment, as listed in table 5.2. Plastic collapse of the component occurred when a load of 80 kN was applied. Two values are useful for comparison; at 20 kN load 1425 micro-strain was recorded and at 70 kN load, 5668 micro-strain was recorded.

The measured strains were compared with the maximum principal strain values obtained using the elastic F.E. analysis at the highest stressed node (node 12), listed in table 4.2 and shown in figure 4.7. For an applied end load of 20 kN in the elastic range the finite element analysis gave a maximum principal strain value of 1571 micro-strain. For the same load the single gauge measured strain was found to be 1425 micro-strain. Thus, the F.E.

calculated results were 9% higher than the measured strains in the elastic region. This is somewhat lower than the strain measured using the rosette and this appears to be true for all experimental strains, which are on average around 10% lower by the single strain gauge than those from the rosette.

Table 5.3 lists the measured and finite element based estimated strains based on both the energy density method and Neuber's equation. The component monotonic load/local strain calibration curves were used with the elastic finite element calculated equivalent values and both Neuber's rule and the energy density method, and the results are compared to the measured load/local strain calibration curve in figure 5.4. It is apparent that for low values of load, both methods give results which are very close to the measured strains. For high values of load, the calibration curves obtained from both methods deviate from the measured strain curve. As the amount of plasticity increases the degree of correlation between measured and Neuber's estimated strains decreases. A range of 6494 to 7077 micro-strain is at least 15% higher than the measured value of 5668 micro-strain. However, the degree of correlation between the measured and the energy density predicted strains remains of the same order of magnitude throughout the elastic and plastic deformation. A measured value of 5668 micro-strain compares well with the energy method upper and lower values of 5822 and 6070 micro-strain.

Figure 5.5 shows a plot of measured strains versus F.E estimated strains. The strain values obtained using both Neuber's and the energy based method fall above the 100% correlation line in all cases, showing both methods to overestimate the strain values in both the elastic and plastic range. Close agreement was found between the measured and predicted strains based on monotonic stress/strain curves up to a 20 KN load (the elastic range). However, it can be seen that the predicted strains based on F.E. calculated equivalent methods and Neuber's equation are grossly overestimated in the plastic range. This contrasts with the close agreement that exist between the measured and predicted strains based on the energy density method.

A reasonable correlation between the measured, and elastic finite element results using both Neuber's and the energy density predicted strains has been achieved when considering that the geometry of the finite element model was modified, as described in chapter 4.4.2. It was considered that the discrepancy between the results could be influenced by the following factors:

- i) The misalignment of the single gauges with the direction of the principal planes during attachment.
- ii) The strain gauge gives the average strain values under the gauge whereas the finite element analysis gives the strain values at a nodal point.

5.5 Conclusions

- i) The predicted strains based on F.E. analysis together with Neuber's rule and the energy density method are overestimated in both elastic and plastic ranges when compared to the measured strains.

- ii) For low values of nominal stress, ($Kt.S$), both methods give results very close to the measured strains. For high nominal stress values, both Neuber's rule and the energy density method over-estimate the local strains, however, better correlation is achieved with the latter.

- iii) The plastic local strains estimated using the energy density method and von Mises equivalent stress exhibit closest correlation to the measured strains. Those estimated using Neuber's equation and equivalent principal stress exhibit least correlation.

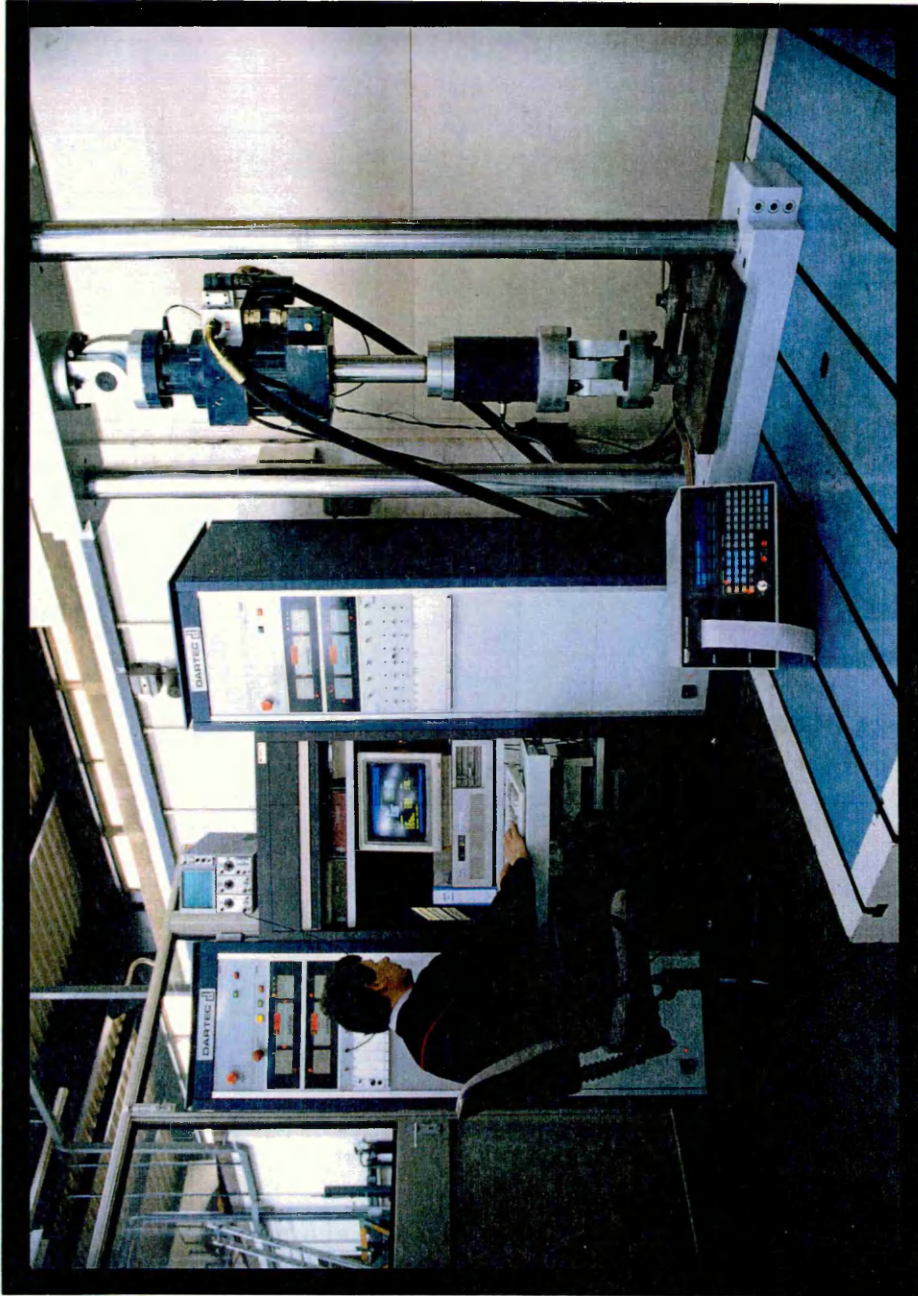


Fig. 5.1 Dartec Fatigue Testing Machine Showing The Swivel Joints, Rig and Component in Position.
(detailed position of the component shown schematically in fig 5.2).

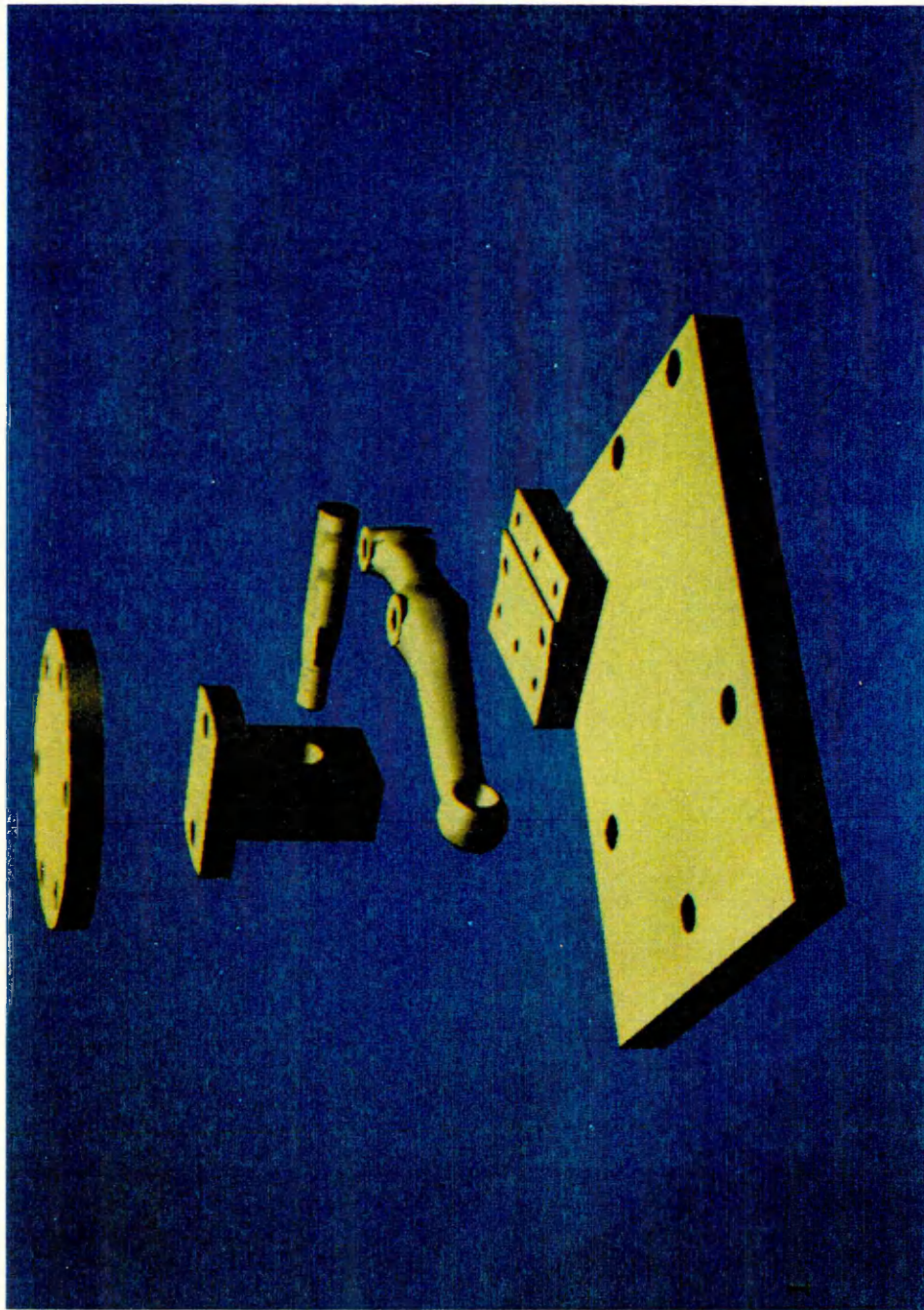


Fig. 5.2 Exploded View of the Testing Rig

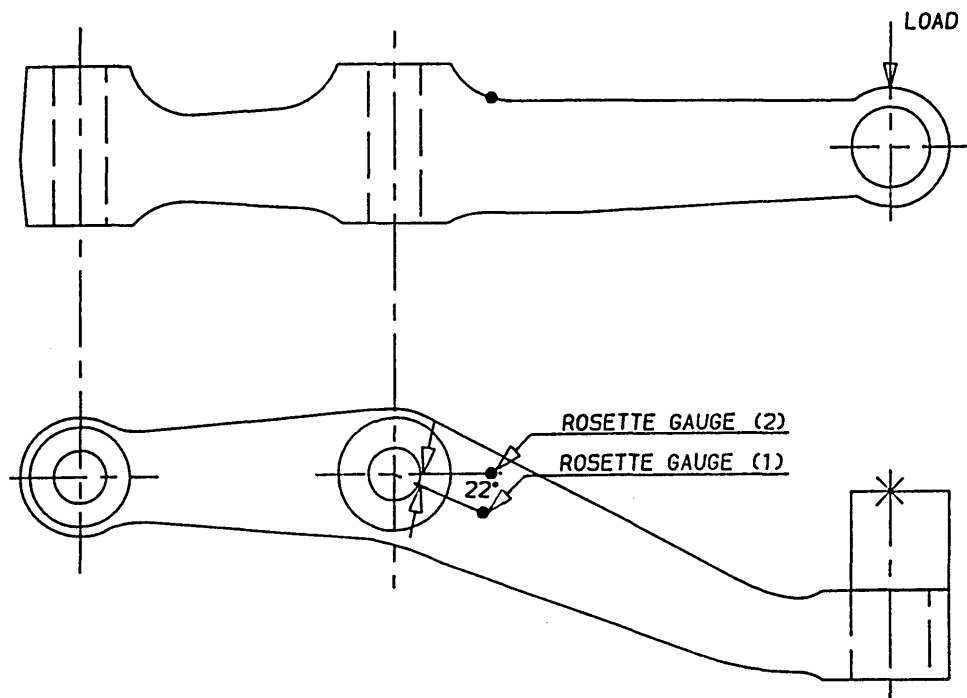


Fig. 5.3 Location of Post Yield Strain Gauges.

LOAD (KN)	ROSETTE 1 (μ STRAIN)		ROSETTE 2 (μ STRAIN)	
5	407	-60	400	-63
10	793	-114	777	-116
15	1204	-108	1174	-168
20	1608	-231	1561	-238
25	2050	-279	2001	-280
30	2435	-328	2382	-325
35	2889	-438.8	2750	-381
40	3295	-502	3195	-482

Table 5.1 The Measured Strains Using Rosette Strain Gauges.

LOAD (KN)	DEFLECTION (mm)	STRAIN GAUGE (μ STRAIN)	
		(1)	(2)
10	1.43	714.4	711.6
20	2.71	1425	1404
30	3.72	2193	2144
40	4.82	2952	2876
50	5.96	3760	3056
60	7.55	4685	4533.6
70	----	5668	5633

Table 5.2 Experimental Strain Values Using Strain Gauges.

LOAD kN	ESTIMATED LOCAL STRAINS F. E. CALCULATED EQUIVALENT METHOD AND NEUBER (MICRO-STRAIN)				ESTIMATED LOCAL STRAINS F. E. CALCULATED EQUIVALENT METH. AND THE ENERGY DENSITY APPROACH			
	Princ. Stress	Tresca	von Mises	Princ. Strain	Princ. Strain	Tresca	von Mises	Princ. Strain
10	845	763	734	783	815	776	771	789
20	1685	1523	1462	1563	1627	1548	1538	1574
30	2445	2325	2275	2405	2441	2321	2307	2359
40	3302	3121	3098	3156	3272	3099	3071	3161
50	4321	4059	4025	4149	4149	3908	3584	3974
60	5591	5196	5123	5301	5053	4778	4741	4853
70	7077	6539	6494	6679	6070	5731	5678	5822

Table 5.3. The Estimated Local Strains For The Steering Arm Using The Monotonic Stress/Strain Curve.

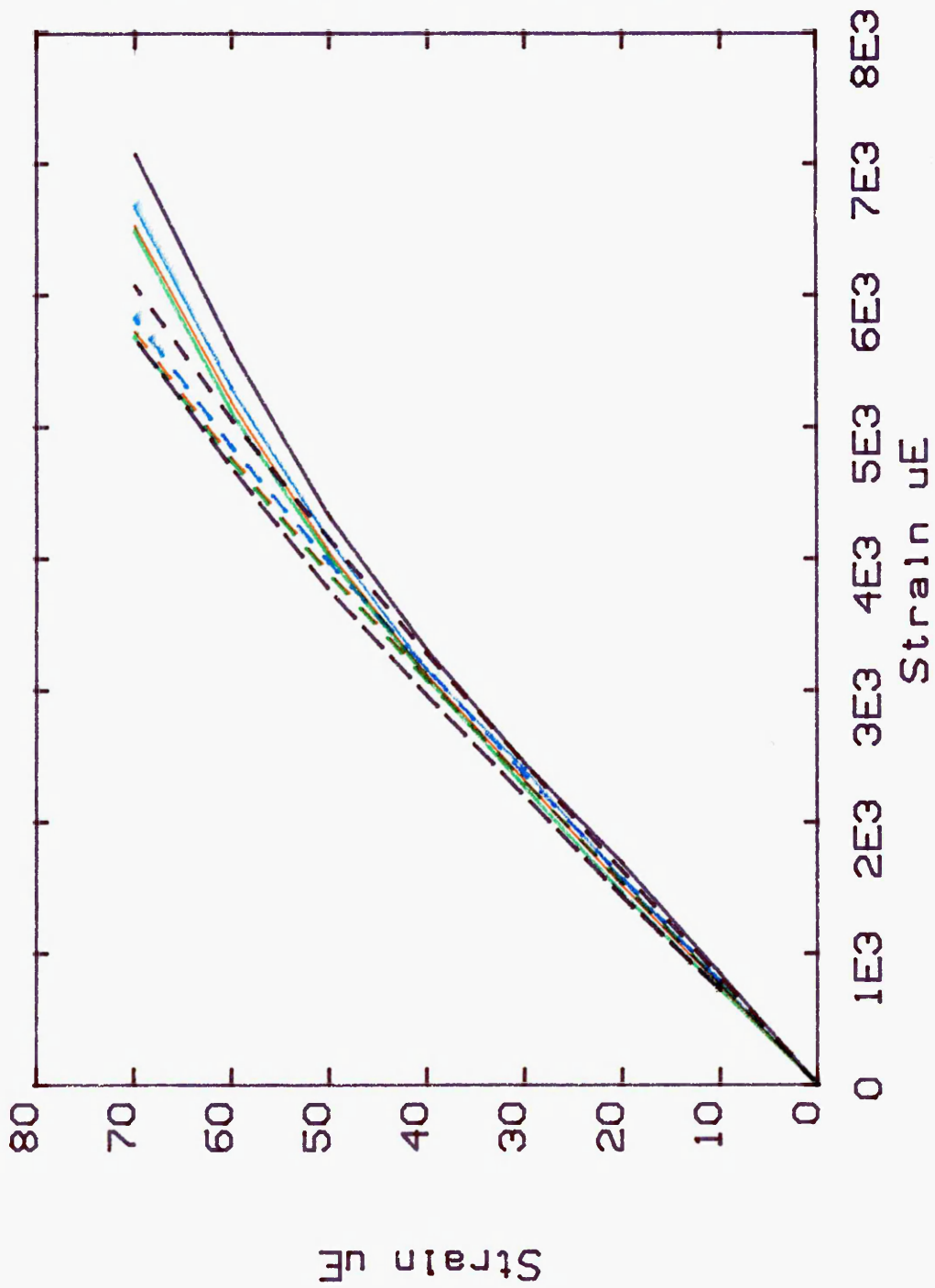


Fig. 5.4 Monotonic, Measured And Estimated Load/Notch Root Strain Calibration Curves.

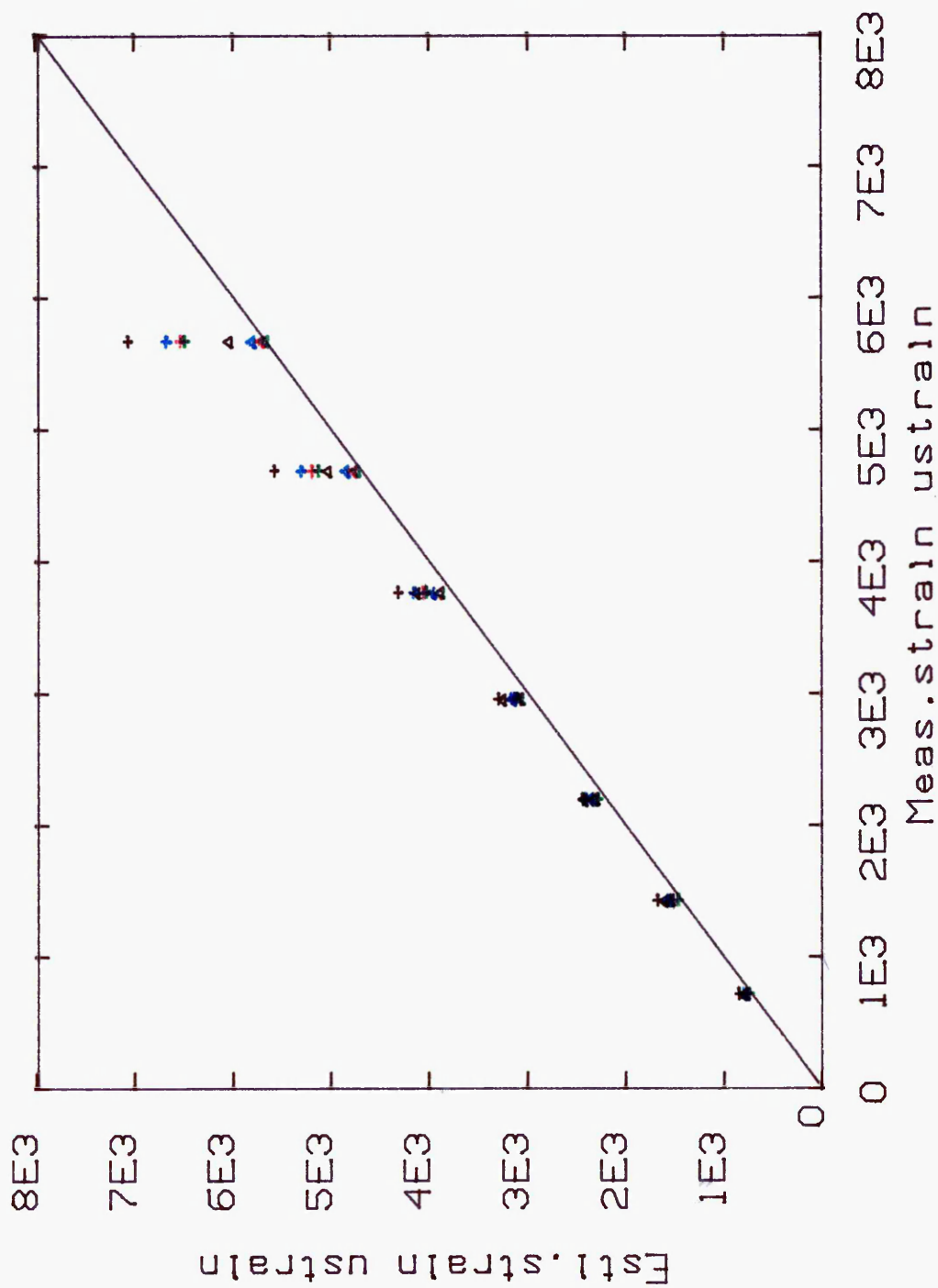


Fig.5.5 Comparison Of Monotonic, Predicted And Measured Strains.

6.1 Aims And Objectives

The critical location technique used to predict the fatigue life of engineering components from the "fatigue environment" (loads, stress, strain, etc) has been discussed in detail in chapter 2. Based on this method, a commercially available computer package (FATIMAS) has been applied to predict the fatigue life of the steering arm. The objectives of this programme of work were:-

- i) To simulate the test circuit fatigue failure of the steering arm using the nCode fatigue analysis software package FATIMAS.
- ii) To assess the components sensitivity to design and manufacturing variables, (K_f) and service loading variables.
- iii) To compare the FATIMAS measured strain-time based service history predicted fatigue life results with full scale load controlled fatigue testing of the component.
- iv) To compare the FATIMAS measured strain-time based service history fatigue life results with FATIMAS predicted fatigue lives based on load calibrated strain-time service histories.

- v) To compare the experimental results with FATIMAS predicted fatigue lives based on load calibrated measured strain-time service histories.
- vi) To compare the experimental results with the Falcon predicted fatigue lives.

It should be pointed out that both the Neuber and the energy density estimated cyclic notch root load/strain calibration curves, figure 4.10, were used to calibrate the washboard measured strain-time history for use in FATIMAS. For the applied load/strain calibration curves an equation of the following form exists.

$$\epsilon = \frac{P}{C_1} + \left(\frac{P}{C_2} \right)^{1/d}$$

where C_1 , C_2 , and d are constants.

Ideally the calibration of the strain-time service history should be governed by the above equation and would take account of the non-linear stress strain relationship. However, it was not possible to include this equation into the FATIMAS package since it is a commercial package and can not be altered without permission. Therefore, for both the experimental and FE estimated applied load/strain curves an approximate linear extrapolation was used. The load-time history for experimental fatigue life evaluation is based on the measured monotonic load/strain curve. An arbitrary reduction in strain of approximately 10% on 36.5 kN load value obtained from the measured monotonic load/strain calibration curve was imposed to compensate for cycle-dependent softening of the component material.

This ensured reasonable lives were likely in tests. The 33 kN load value was used to scale the measured strain-time service history for a maximum strain value of 2734 micro-strain for experimental fatigue life evaluation.

Before discussing the fatigue analysis results, the FATIMAS software is described to present the reader with an understanding of the techniques involved [84].

6.2 Software Summary

The FATIMAS program is modular in nature and consists of the following modules signal display, data manipulation, signal analysis, fatigue analysis, material properties, etc.

The program requires three inputs, the fatigue environment, appropriate materials data, and geometric information.

The fatigue loading on a component is assumed to be obtained from service measurement, or by generation of artificial histories using statistical techniques. An edit facility is also available to remove spikes and gate out noise before extracting the turning points.

Properties for a number of materials are included in the data base and further materials can be added.

The following material properties are used in the analysis:- K' , n' , E , σ_f' , ϵ_f' , b and c . The module MDT enables the graphical display of the following relationships [32].

- 1) stress amplitude versus life
- 2) strain amplitude versus life
- 3) Smith-Topper-Watson (S.T.W) parameter versus life
- 4) cyclic stress/strain curve

Following input of the elastic stress concentration factor, K_t , fatigue damage is calculated using the critical location approach by rainflow and the cycle counting using the cyclic stress/strain curve.

The following output modules are also available:-

SLP - Display of stress/strain hysteresis loops

P3D - Display of cycle and damage histograms

H3D - Formation of cycle and damage histograms

6.3 Measured Strain-Time History

The Washboard signal for the steering arm contains 13705 data points, at a sampling rate of 370.4 points per second. The turning point history contained 884 turning points (442 cycles). Figure 6.1 shows the details of the complete signal.

6.4 Material

The material used for the manufacture of the steering arm was a forging steel DIN 41 CR 4V. The fatigue data was generated by constant amplitude, strain controlled axial push-pull testing of cylindrical specimens by the manufacturer. For full material specification see chapter 3.3, table 3.1 and figures 3.16 to 3.18.

6.5 Fatigue Reduction Factor

A data acquisition exercise has been carried out by the manufacturer using four strain gauges, two of which were affixed at the critical location of the component. Hence, the fatigue strength reduction factor, $K_f = 1$, was used for the analysis.

6.6 Fatigue Life evaluation

6.6.1 FATIMAS Fatigue Life Assessment: Measured Strain-Time Service History

Table 6.1 shows the fatigue life predictions together with a list of the set-up conditions. In this case a life was predicted consisting of 58 repeats (25636 cycles) of signal.

Table 6.2 and figure 6.2a display the tabulated and graphical output showing the effects of adjusting the magnitude of the signal by a "strain factor". Successive 10% reductions were made down to 70% of the strain range. The reduction in strain factor reduced the amount of plasticity which the material experienced.

Table 6.3 shows the sensitivity of fatigue life to variations in stress concentration factor, K_f . Figure 6.2b displays a graphical output of the data from which it is evident that the component is sensitive to small changes in K_f . For example by increasing K_f from 1 to 1.1, an increase in fatigue life of 36% would be achieved.

Figure 6.3 shows the hysteresis loops traced by the material during cycling. It is evident that the material is capable of withstanding a considerable amount of plasticity, by the relatively wide hysteresis loops shown. The life to crack initiation was very short, (58 repeats of strain history), which was not unexpected since the strain data was acquired from the worst durability course. Figures 6.4 and 6.5 show the three dimensional graphical histogram of the cycles and associated fatigue damage using rainflow. It is evident that only a small number of cycles caused most of the fatigue damage. It can be seen that two cycles in particular were responsible for most of the damage.

6.6.2 Fatigue Life Assessment: Load Calibrated Measured Strain-Time Service History

In order to appreciate the potential limitation of the techniques described in section 4.5, it was decided to assess the fatigue life of the steering arm through a range of service histories. Each has the same pattern of loading as the known service history, with the lowest applied load of 20 kN having all strains less than yield and the highest applied load of 40 kN incorporating high yield strains. In all cases the FATIMAS predicted fatigue lives based on FE calculated strains were compared with the FATIMAS washboard history lives and experimental fatigue lives. These are shown in table 7.1. The maximum strain value identified from the washboard service history data was 2734 micro-strain, which was used in subsequent calibration exercises.

The fatigue life evaluation package FATIMAS was used to predict the life of the component for a maximum load of 20 kN, using both the F.E. calculated strains and the measured strains. Load/strain factors of 0.57, 0.59 and 0.52 were applied to the known service history to represent finite element calculated strain and both the rosette and post yield strain gauge results. The fatigue life was found to be infinite in both cases. Clearly, the 2.3% and 9% strain difference between the computerised and measured strains has no effect on the fatigue life of the component under these conditions.

The modification of the radii around the boss, as described in section 4.4.2, may have had a considerable influence upon the results, i.e. an increase of the radii around the boss may have reduced the amount of stress concentration at that area. To examine the effect of such an occurrence the F.E. calculated strain at the highest stressed node was increased by 10%. This gives strain values of 1728 micro-strain. The fatigue life of the component was then predicted using the above strain and was again found to be infinite. Thus, it can be concluded that in this case a 10% difference in finite element strains had no influence on the fatigue life of the component.

For prediction of the post yield strain values at the critical location, the F.E. calculated equivalent stresses were used with both Neuber's rule and the energy approach, as described in chapter 4.5. The results are listed in table 4.5.

In order to judge the real life of the component it was decided to do incremental life evaluations in FATIMAS. This was carried out in load increments of 5 kN from 20 kN to 40 kN. Table 6.4 lists the predicted fatigue lives and figure 6.6 displays the graphical output of the data. The fatigue lives based on the energy method are generally larger than those using Neuber.

For low loads the maximum predicted life is $1.63E7$ cycles which was obtained from Neuber's method combined with maximum principal stress. The highest life was $2.4E9$, cycles, obtained using the energy method and von Mises equivalence. This represents a spread factor of more than 147, but when expressed in logarithmic terms is a factor of 1.3.

At the upper load limit the minimum life is $7.5E3$ cycles and again comes from the combination of maximum principal stress and Neuber's method. When using von Mises and the energy method the highest life of $4.0E4$ repeats is obtained, which is a factor of 5.2 greater than the minimum life. Again when represented in logarithmic terms this is 1.18. Also included are results represented as blocks of service histories, shown in table 6.5.

Table 6.5 lists the predicted fatigue lives obtained using FATIMAS measured strain-time service history and those obtained using load calibrated measured strain-time service history based on F.E. calculated strain with both Neuber's rule and energy density method for load decrements from 33 kN to 23.3 kN. The former represents

the maximum 2734 micro-strain in the service history and the latter represents successive reduction in load history of 10% on the 33 kN load until the load was 70% of the initial value. This represented a maximum total strain of 1914 micro-strain in the strain-time service history. Tables 6.6 and 6.7 lists the predicted number of cycles and blocks of load-time service history to failure of the steering arm and figure 6.7 represents the graphical output of that data.

For load increments from 23.3 kN to 33 kN, the predicted fatigue lives obtained using maximum principal stress, Tresca, von Mises and maximum principal strain methods were found to be non-conservative when compared to the predicted fatigue lives obtained using FATIMAS with the measured strain-time service history. The same is true of Neuber's estimated load-time service histories of Tresca and von Mises. The predicted lives based on maximum principal strain are conservative for a load ranging from 33 kN to 25 kN and below that range are non-conservative when compared to the predictions based on measured strain-time service history results. The predictions based on maximum principal stress equivalence load-history are conservative in all cases when compared to measured strain-time service history results with FATIMAS.

6.7 Conclusions

- i) The predicted fatigue lives based on energy density method were found to be nonconservative when compared

with those obtained using Neuber's load-time service history.

ii) The predicted fatigue lives based on FATIMAS measured strain-time history are found to be conservative when compared with prediction based on both the energy density and Neuber's load-time service histories except for those obtained using maximum principal stress load-time service history.

iii) Of the two methods used the fatigue life predictions based on von Mises equivalent method and energy density were found to be highest. Those predicted using Neuber's load-time service history and maximum principal stress were found to be the lowest and most conservative.

DISPLAY OF SIGNAL : WB

Full file data :

13705 points.

370.4 pts/sec

Max = 2734

Min = -3846

Mean = -367.8

S.D. = 1559

Displayed :

13705 points.

from pt 1

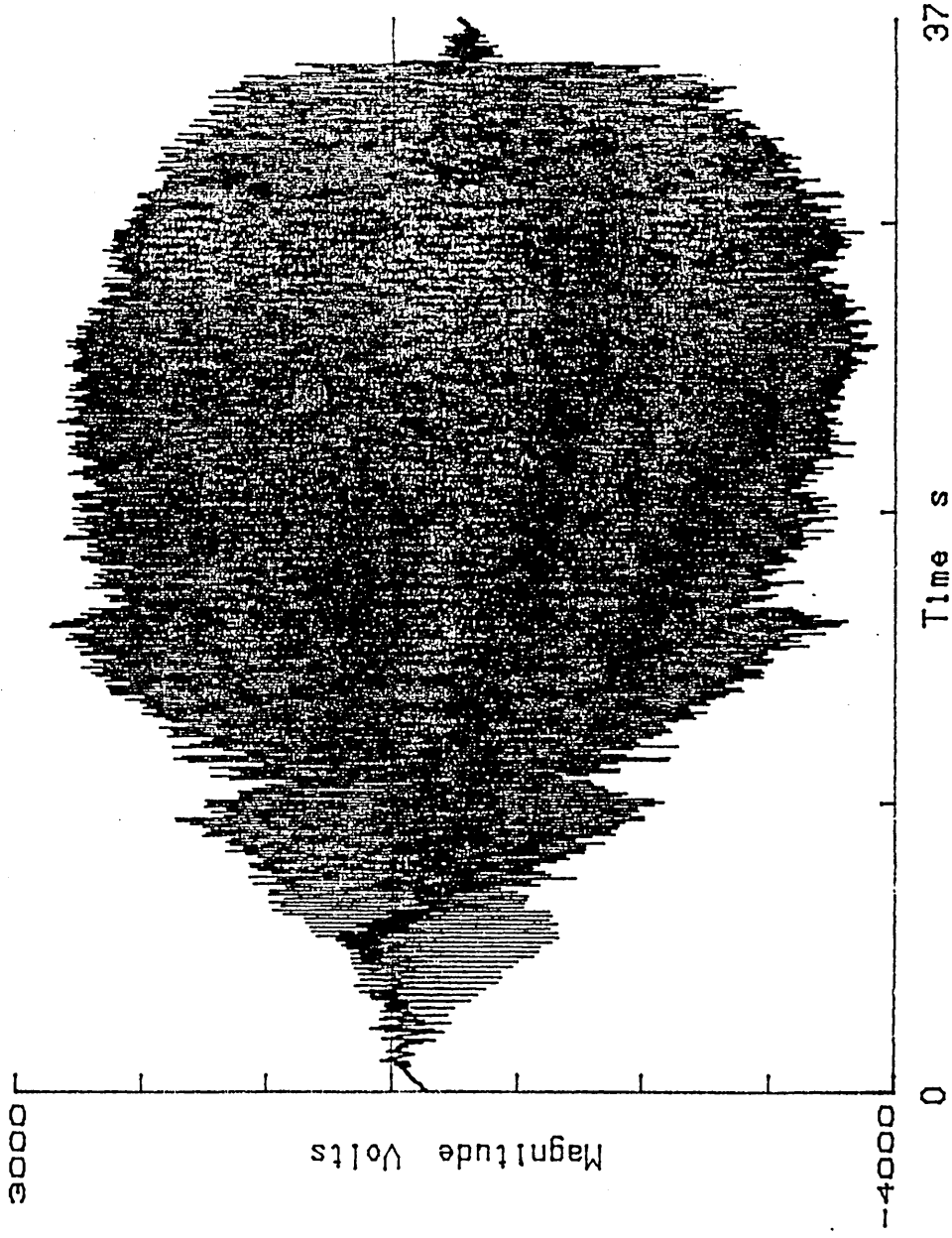


Fig. 6.1 Washboard Strain-Time Service History.

nCode NSOFT

Turning Point History	:	WB.DAT
Material	:	41CR4V
Scaling Factor	:	1
Stress Concentration Factor, Kf	:	1
Damage Parameter	:	Smith-Topper- Watson
Plain Strain Correction	:	Y
Miners Constant	:	1
Number of cycles used	:	442
Fatigue Life	:	58 repeats of history

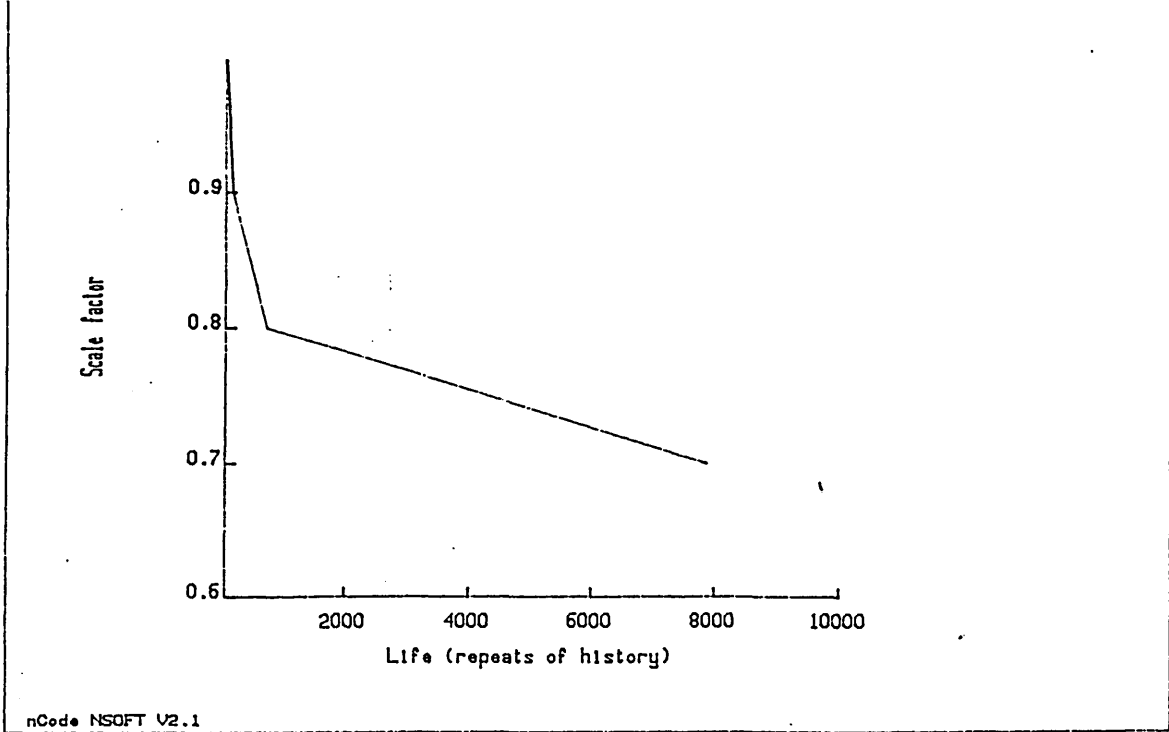
Table 6.1 Results of Analysis.

FACTOR	FATIGUE LIFE (REPEATS OF HISTORY)
0.7	7866
0.8	715
0.9	157
1.0	58

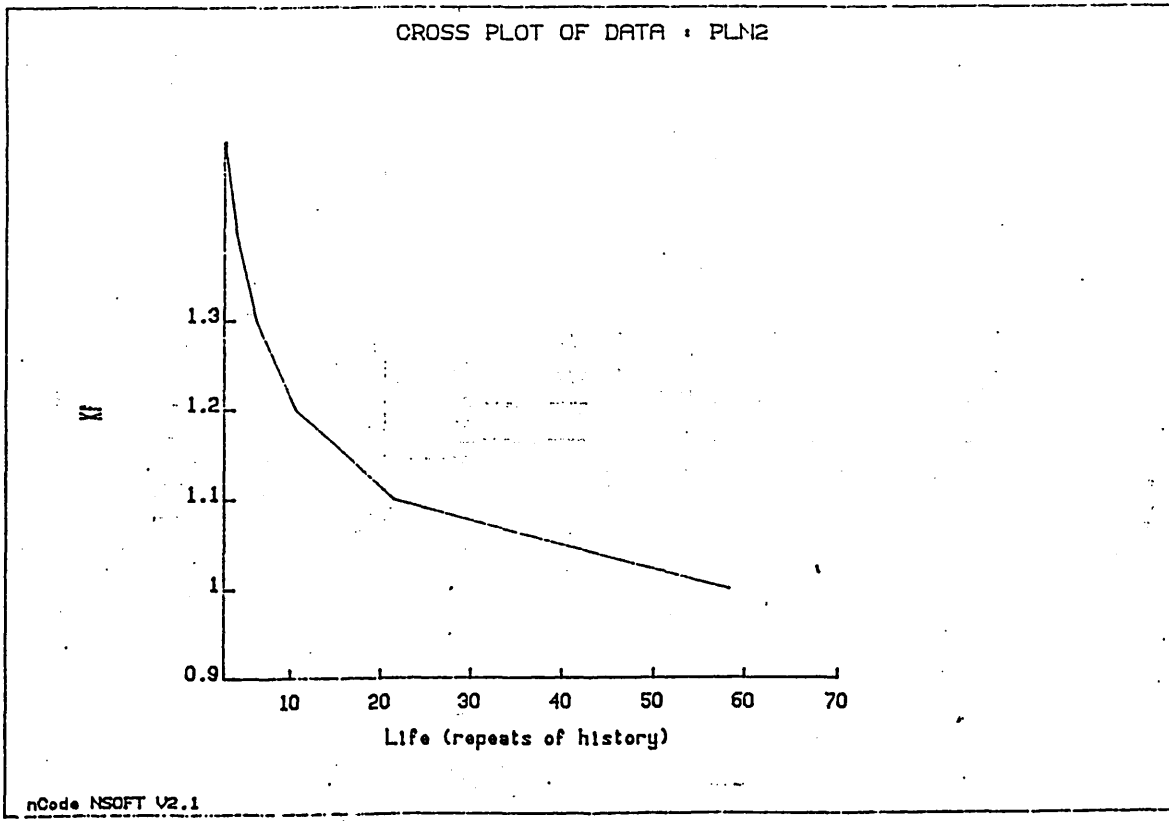
Table 6.2 Strain Factor versus
Life Analysis.

FACTOR	FATIGUE LIFE (REPEATS OF HISTORY)
1	58
1.1	21
1.2	11
1.3	62
1.4	4
1.5	2.8

Table 6.3 Stress Concentration Factor K_f Versus Life Analysis.



a) Strain Factor Versus Fatigue Life.



b) Stress Concentration Factor, K_f Versus Fatigue Life.

Fig. 6.2. Fatigue Life Assessment.

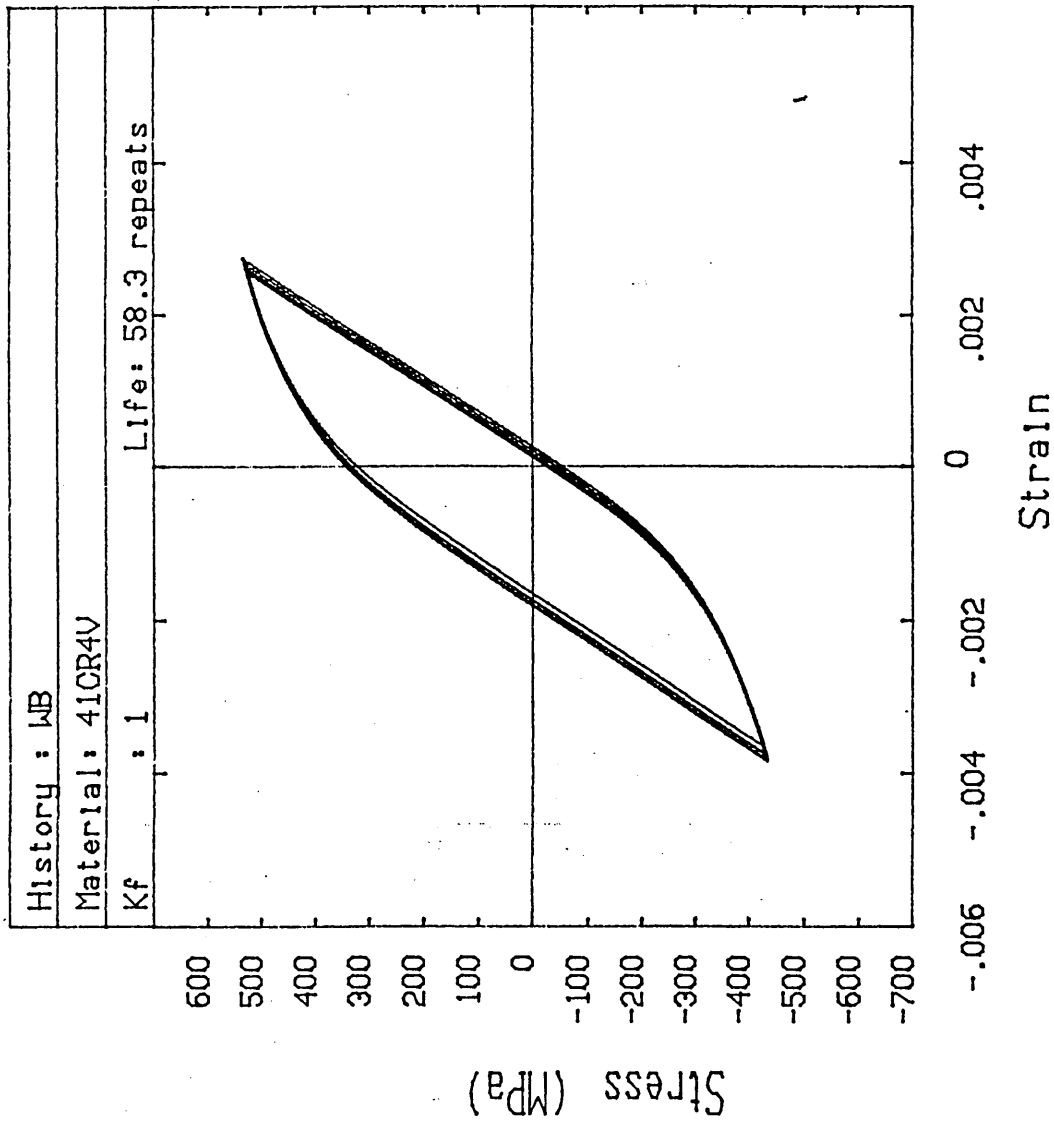


Fig. 6.3 Hysteresis Loops.

nCode NSOFT V2.1

CYCLE DISTRIBUTION FOR HISTORY : WB

Maximum tower height : 49

Units : Local Strain

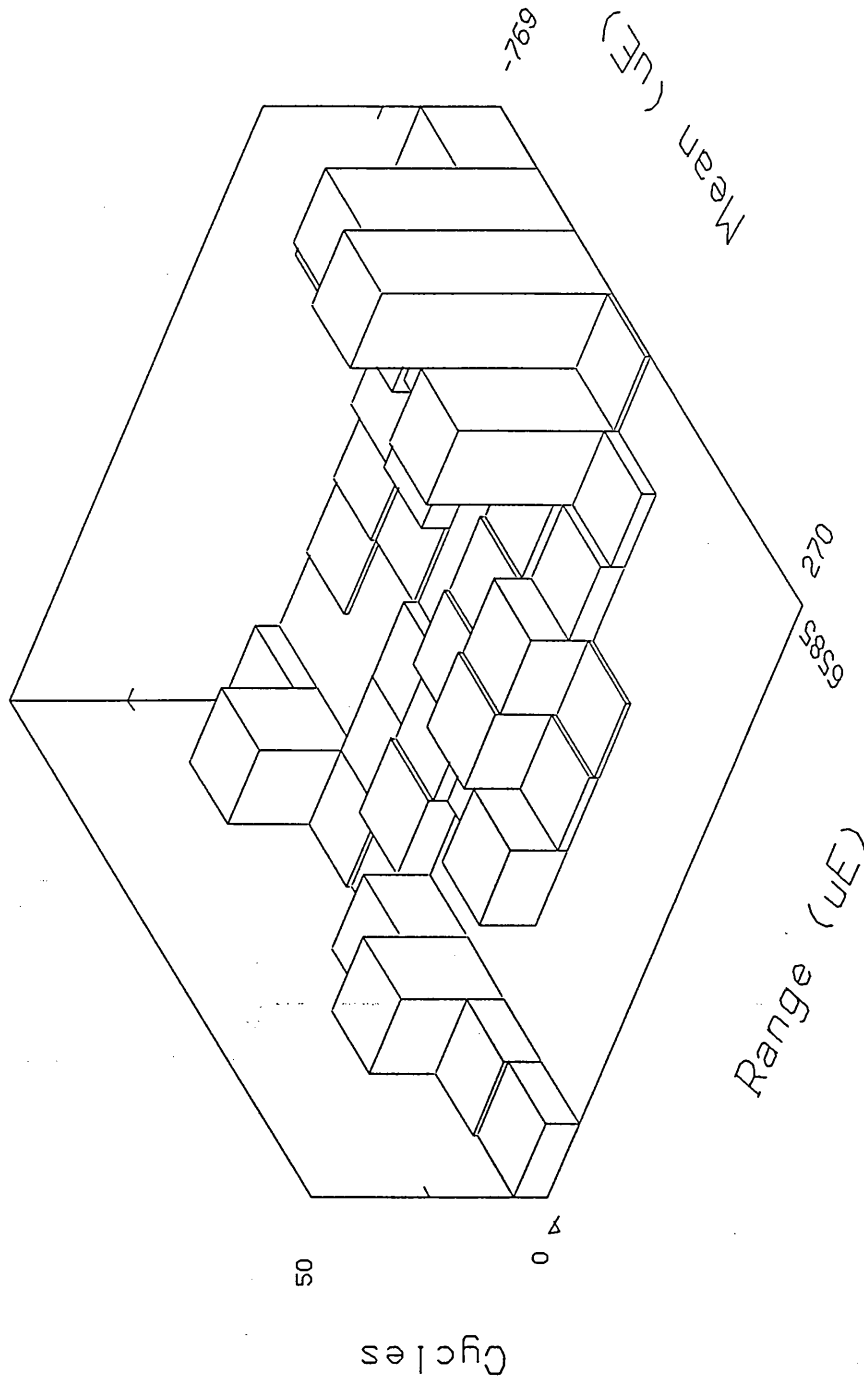


Fig. 6.4 Cycle Distribution For Washboard History.

DAMAGE DISTRIBUTION FOR HISTORY : DAMAGE

Maximum tower height : 34.8664

Units : Local Strain

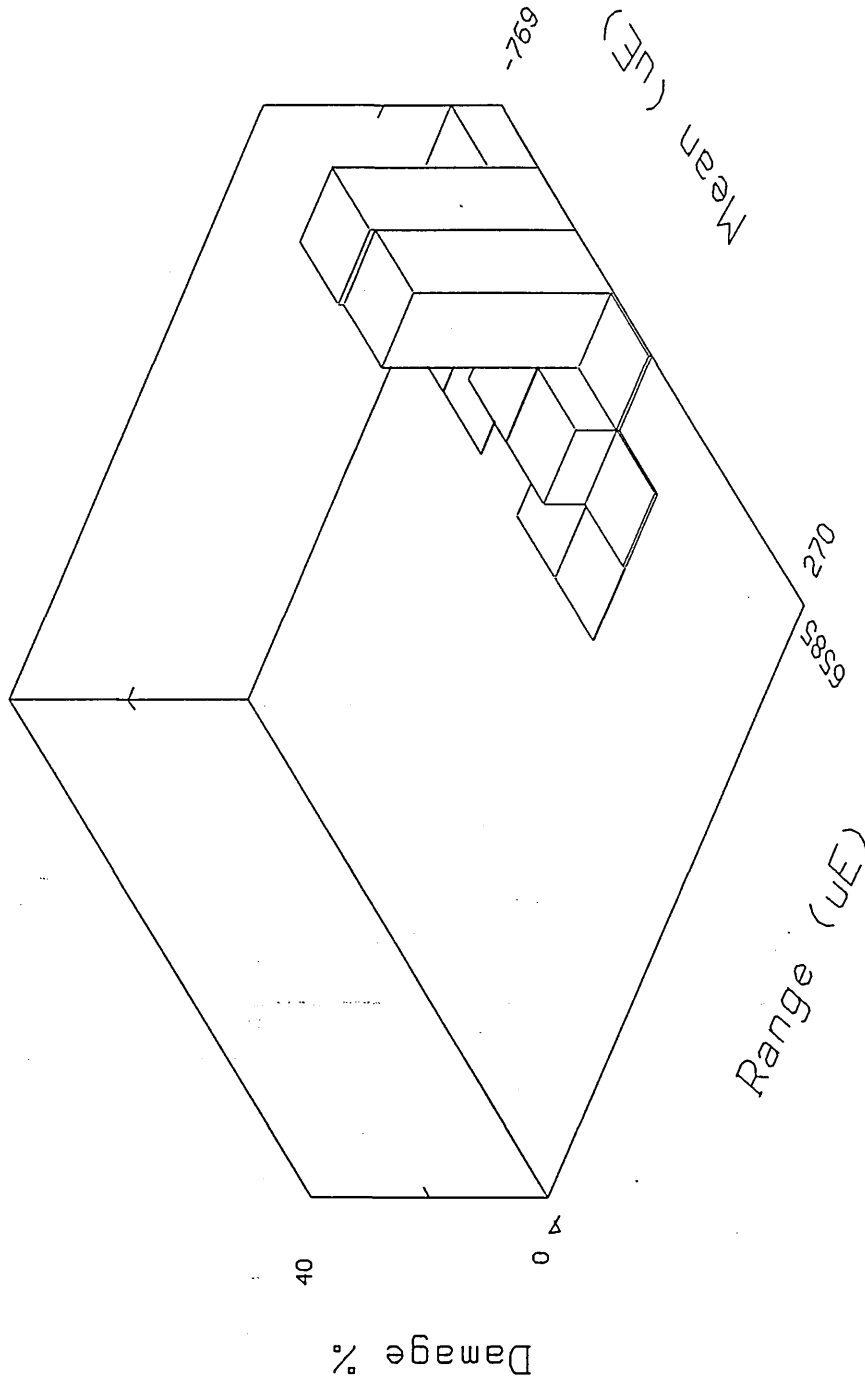


Fig. 6.5 Damage Distribution For Washboard History.

FATIMAS LOAD-TIME SERVICE HISTORY									
LOAD kN	F. E. + NEUBER				F. E. + ENERGY				
	Max Princ. Stress	Tresca	Von Mises	Max Princ. Strain	Max Princ. Stress	Tresca	Von Mises	Princ. Strain	
20	36861	2.69×10^5	4.4×10^5	9.27×10^4	2.82×10^5	5.35×10^6	5.35×10^6	7.52×10^5	
25	4337	2874	5688	2604	4337	10430	13733	8471	
30	157	245	308	231	595	867	920	715	
35	40	58	63	54	140	208	231	202	
40	17	23	31	22	63	91	90	80	

Table 6.4 FATIMAS Predicted Fatigue Lives For The Steering Arm
Number Of Blocks To Failure Of The Service History

FATIMAS LOAD-TIME SERVICE HISTORY									
LOAD kN	F.E. + NEUBER					F.E. + ENERGY			
	Maximum Princ. Stress	Tresca	Von Mises	Max Princ. Strain	Max Princ. Stress	Tresca	Von Mises	Princ. Strain	
20	1.63x10 ⁷	1.18x10 ⁸	1.9x10 ⁸	4.1x10 ⁷	1.2x10 ⁸	2.4x10 ⁹	2.4x10 ⁹	3.3x10 ⁸	
25	1.9x10 ⁶	1.3x10 ⁶	2.5x10 ⁶	1.1x10 ⁶	1.9x10 ⁶	4.6x10 ⁶	6.1x10 ⁶	3.7x10 ⁶	
30	6.9x10 ⁴	1.08x10 ⁵	1.30x10 ⁵	1.02x10 ⁵	2.6x10 ⁵	3.8x10 ⁵	4.1x10 ⁵	3.2x10 ⁵	
35	1.7x10 ⁴	2.56x10 ⁴	2.78x10 ⁴	2.4x10 ⁴	6.2x10 ⁴	9.2x10 ⁴	1.0x10 ⁴	8.9x10 ⁴	
40	7.5x10 ³	1.01x10 ⁴	1.37x10 ⁴	9.7x10 ³	2.8x10 ⁴	4.0x10 ⁴	4.1x10 ⁴	3.5x10 ⁴	

Table 6.5 FATIMAS Predicted Fatigue Lives For The Steering Arm
Number Of Cycles To Failure Of The Service History.

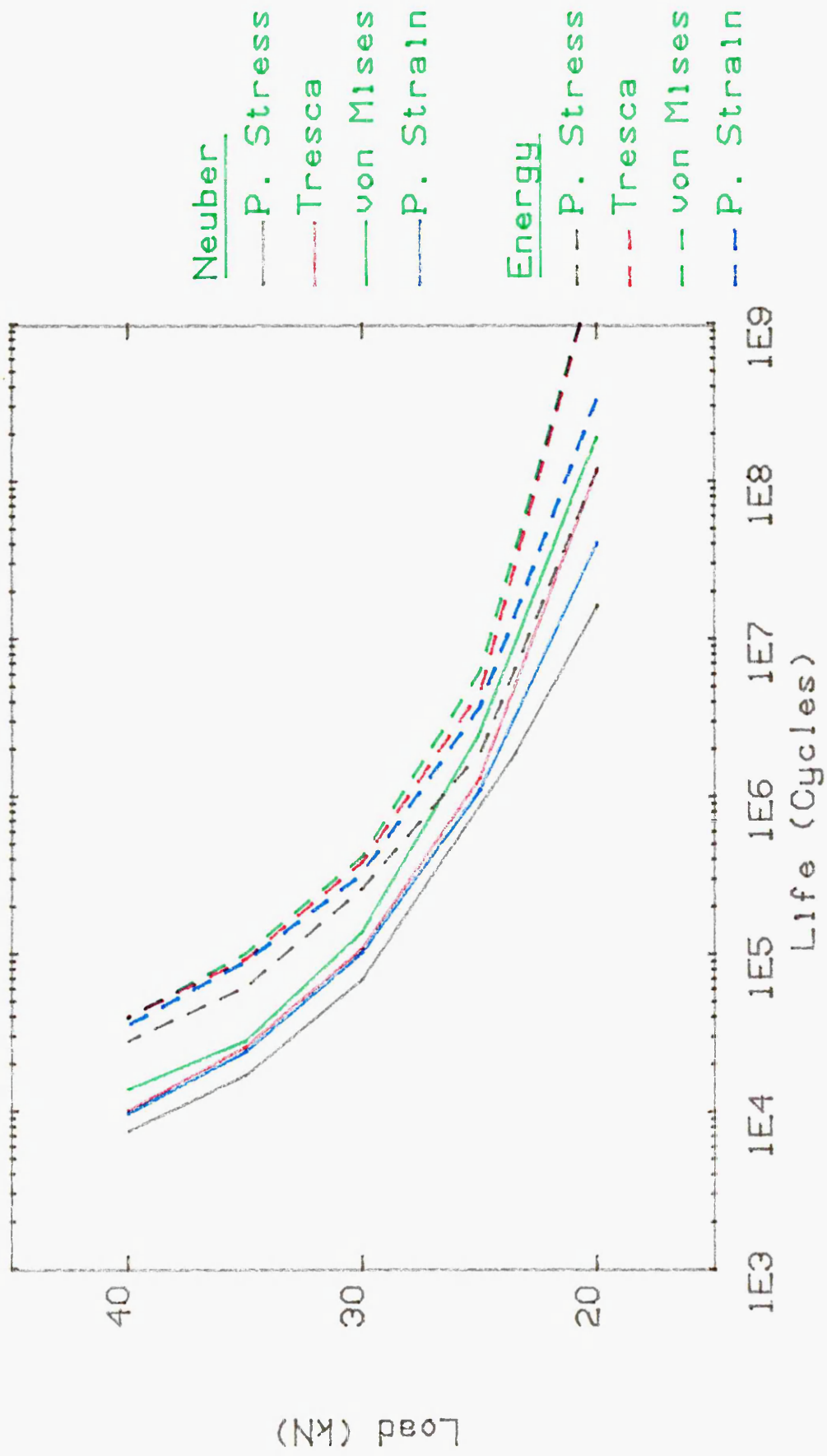


Fig. 6.6 Load Versus Life Comparison Of The FE Predicted Fatigue Lives.

FATIMAS LOAD-TIME SERVICE HISTORY										
FATIMAS		F.E. + NEUBER				F.E. + ENERGY				
LOAD kN	STRAIN TIME SERVICE HISTORY	Max Princ. Stress	Tresca	Von Mises	Max Princ. Strain	Max Princ. Stress	Tresca	Von Mises	Princ. Strain	
33	58	63	101	125	91	231	338	360	308	
29.8	158	157	266	360	231	595	867	9020	715	
26.5	720	499	1060	1629	867	2049	4337	5688	3343	
23.3	7866	3343	7764	13733	5688	13733	36861	5.26x10 ⁴	26197	

Table 6.6 FATIMAS Predicted Fatigue Lives For The Steering Arm. Number Of Blocks To Failure Of The Service History.

FATIMAS		FATIMAS LOAD-TIME SERVICE HISTORY									
LOAD kN	STRAIN TIME SERVICE HISTORY	F. E. + NEUBER				F. E. + ENERGY					
		Max Princ. Stress	Tresca	Von Mises	Max Princ. Strain	Max Princ. Stress	Tresca	Von Mises	Princ. Strain		
33	2.56×10^4	2.7×10^4	4.5×10^4	5.5×10^4	4.0×10^4	1.02×10^5	1.49×10^5	1.6×10^5	1.36×10^5		
29.8	6.98×10^4	6.9×10^4	1.2×10^5	1.6×10^5	1.02×10^5	2.6×10^5	3.8×10^5	3.98×10^5	3.2×10^5		
26.5	3.2×10^5	2.2×10^5	4.7×10^5	7.2×10^5	3.8×10^5	9.05×10^5	1.9×10^6	2.5×10^6	1.5×10^6		
23.3	3.47×10^6	1.5×10^6	3.4×10^6	6.07×10^6	2.5×10^6	6.07×10^6	1.6×10^7	2.3×10^7	1.15×10^7		

Table 6.7 FATIMAS Predicted Fatigue Lives For The Steering Arm Number Of Cycles
To Failure Of The Service History.

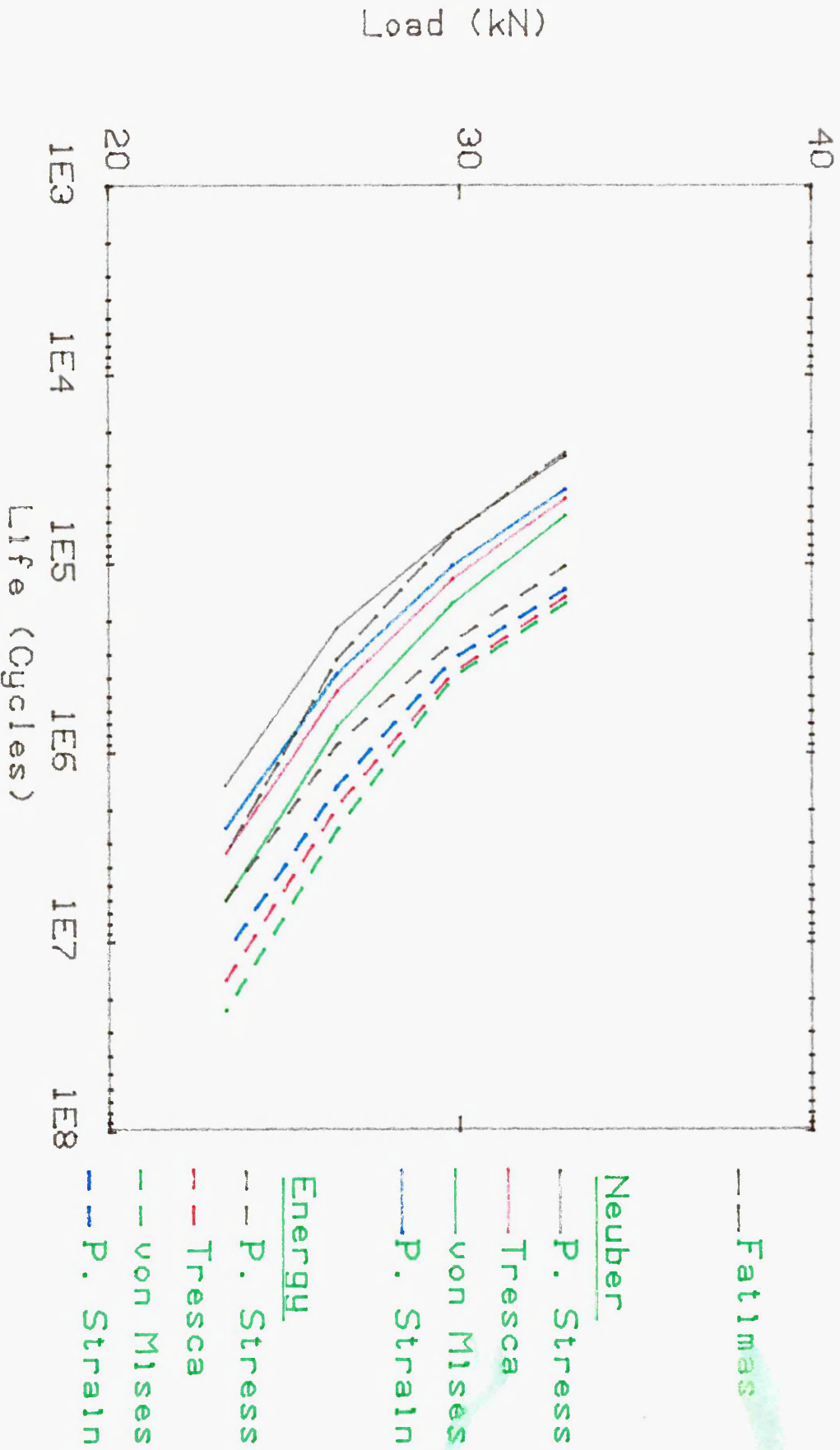


Fig. 6.7 Load Versus Life Comparison Of The FATIMAS Measured History, And FE Predicted Fatigue.

CHAPTER 7

FATIGUE TESTING

7.1 Introduction

To verify the results obtained from the computerised fatigue life predictions, a number of experimental tests were performed.

Testing of the steering arm was undertaken to determine the fatigue life of the component under "realistic" variable amplitude load histories. The number of cycles to failure obtained from the above test was compared with computerised results obtained from using FATIMAS software. Failure of the component was defined as when a visible crack of approximately 3 mm was observed.

7.2 Test Equipment

Scanning Electron Microscope: A Philips S.E.M was used for examination of the fracture surface. The S.E.M provided a qualitative examination of surfaces, and magnifications of X80,000 were possible, maintaining an excellent depth of focus.

7.3 Fatigue Testing

The Dartec 9500 computer controlled multiaxial testing machine described in section 5.2, was used for fatigue life evaluation of the steering arm.

The strain history data file WB.DAT, shown in figure 7.1, was converted to a load history suitable for the Dartec

profile generator file WB.PG, shown in figure 7.2, using the 'Load' program. The measured strain values were used to produce a load/strain calibration curve, shown in figures 5.4. Ideally the component should be cyclically stabilised prior to strain gauge measurement. However, this was not possible. This problem was overcome by imposing a 10% reduction on the 36.5 kN load value obtained from the measured monotonic load/strain calibration curve for the maximum strain value of 2734 Micro-strain obtained from the strain based service history. The 33 kN load value was used to scale the strain based history to a load history for experimental fatigue life evaluation.

The WB.PG file was loaded and the actuator was set to run at a frequency of 2 Hertz.

It was required to modify the machine in order to apply the load in a way which resembled or simulated the actual service conditions. This was achieved by the attachment to either end of the actuator of a swivel joint as shown in figure 5.1. These units provided +/-45 degrees of freedom in one direction and +/-5 degrees of freedom in the other, which represented the actual transmission of force from the steering rod to the steering arm.

7.3.1 Crack Detection Methods

Several methods were considered for measuring crack initiation, a brief operational procedure for each system is detailed below:-

a) **Crack Propagation Gauges:**

These gauges were used for indicating the rate of crack propagation in the specimens, through micro-measurement of the cracks. The gauge consisted of a number of resistor strands connected in parallel. When bonded to a structure, progression of the surface crack through the gauge pattern caused successive open-circuiting of the strands, resulting in an increase in total resistance. This produced stepped increases with successive open circuiting which was recorded on a chart recorder. To facilitate the use of crack propagation gauges the surface of the specimen was polished, which itself affects the fatigue life of a component. It is equally important to have some knowledge of the point where the crack initiates and this limits the application of such gauges in 'real' components [78].

b) **Direct Current Potential Difference Crack Monitoring System:**

In this d.c. method a large direct current was applied along the length of the specimen and the potential drop due to the growing fatigue crack, monitored. However, due to the high current density requirements of the method it can only be used for monitoring the growth of long cracks. Long current leads are necessary with this method causing difficulties with small specimens. There were further problems with vibrations which reduced the maximum frequency at which the fatigue tests could be carried out. Another disadvantage was the need to electrically insulate

the specimen from the testing machine. This limited the maximum load to which the specimen was subjected due to early failure of the insulating material [75].

c) **Alternating Current Potential Difference Crack Monitoring System:**

In this method a constant a.c. current was applied along the length of a specimen and the potential difference due to the growing fatigue crack was monitored. The a.c. method had been developed to overcome the above mentioned problems. The method utilises a relatively low current density and is suitable for all test piece geometries. A major advantage of the method is that it can be used at elevated temperatures and in hostile environments. However, the technique is relatively expensive to use. The major disadvantage of the system is the need to electrically insulate the component from the testing machine [76, 77].

d) **Dye Penetrant Method:**

The dye penetrant method consists of a three stage process using a cleaner, penetrant and a developer. In the cleaning stage the cleaner is used to clean the surface to be inspected, and then the penetrant is applied. This is left for at least 15 minutes until the penetration is completed. The excess penetrant is removed from the surface by the cleaner. In the last stage a thin film of developer is applied and left for at least 10 minutes prior to inspection for any defects. The disadvantage of

this method is that the crack length can not be accurately measured. However, the dye penetrant method was found to be the most acceptable method of crack detection and hence it was used [78].

7.3.2 Fatigue Crack Initiation Tests

Fatigue testing of the steering arm under variable amplitude loading to crack initiation was performed. A total of five components were tested at four different load levels. Two components were tested using the load calibrated measured strain-time service history for a 33 kN load. The steering arm failed at 84 and 97 blocks of the load history, or 37128 and 42874 cycles.

In order to verify the experimental result before subsequent tests were conducted, a comparison was made between experimental and FATIMAS measured strain-time service history predicted fatigue life results. FATIMAS predicted Fatigue life of 58 (25636 cycles) blocks of the strain history was obtained. These results showed close agreement with the experimental results. Hence, the accuracy of data conversion was confirmed.

In order to assess the fatigue life of the steering arm at lower load increments the load calibrated service history was reduced by 10% over three successive tests until the load was 70% of the initial value. Therefore, the measured strain history was scaled over the three remaining experimental tests. Thus, maximum load increments of 29.6, 26.5, and 23.3 kN were applied. The

results of the experimental tests and FATIMAS predictions are listed in tables 7.1 and 7.2 and shown in figures 7.3 and 7.4.

7.4 Visual Examination Of The Fracture Surface

Figure 7.5 shows the fracture surface of the component after testing to failure under a maximum 33 kN load. An examination of the fracture surface showed three distinct regions.

- a) An area surrounding the initiation point marked, in which subsequent slow crack propagation occurred, reaching a point half way through the thickness. Overall, this area appeared to be flat.

This was due to repeated impact of the two surfaces under alternating loads. The radial marks at the corners of the top surface were caused by the progression of the crack into these areas.

- b) The core of the component shows evidence of more ductile failure, which was confirmed by Scanning Electron Microscope (SEM), shown in figures 7.9 to 7.11. The ductile fracture zone started at a crack length of approximately 60% of the component thickness.
- c) A final band of catastrophic crack propagation consistent with over-load at a crack length of approximately 75% of the total component thickness.

7.5 Fractography Investigation

The complete fracture surface, shown in figure 7.5 was then examined using a scanning electron microscope.

- a) Figure 7.6 shows the surface immediately surrounding the initiation point. This surface was microscopically flat with evidence of scuffing possibly due to repeated impact of the two crack surfaces during the first part of the test.

The fatigue crack evidently originated at the change in thickness, at which point the maximum stress concentration occurred as identified by finite element analysis, and shown in figure 4.7.

Figure 7.7 is typical of the slow crack propagation region. The surface contains shell marks perpendicular to the applied stress and were characteristic of slow fatigue crack growth.

Figure 7.8 shows the transition area between slow growth fatigue and ductile shear fracture. Secondary cracks on this surface are intergranular.

- b) Figures 7.9 to 7.11 show an area of ductile shear fracture. There were mixed fracture modes in this area and ductile dimpling, typical of ductile fracture was clearly visible. Also visible were areas where intergranular fracture had occurred. The spherical beads in the cavity roots are non-metallic inclusions of manganese sulphide, as can be seen from

the spectra of inclusion, shown in figure 3.6, which serve to initiate ductile failure.

- c) Figures 7.12 to 7.14 show the area of final brittle fracture. Two modes of fracture are clearly visible. The intergranular fracture mode predominates, but large regions of cleavage also were present.

7.6 Microstructure

As described in sections 3.4 and 3.5 the component was austenised at 1200°C and oil quenched after forging. This treatment resulted in a 50% bainitic/martensitic microstructure, with the proportion of martensite being greater at the component surface.

Tempering was carried out at 600°C by the manufacturer. However, cooling conditions after tempering are not known, but it is thought likely that air cooling was used. This would have resulted in slow progress through the critical 450°C region and caused temper embrittlement [79, 80]. The presence of extensive intergranular cracking in the central and final crack zone would support this view.

7.7 Discussion

The predicted fatigue lives obtained using FATIMAS for the measured strain-time history and FATIMAS for load calibrated strain-time histories were compared with load controlled experimental results.

Of the five components, two were tested using the load calibrated strain history. The steering arm failed at 84

(37128) and 97 (42874 cycles) blocks of the load history, respectively. The FATIMAS measured strain-time history based fatigue life was 58 (25636 cycles) blocks of the washboard signal. Thus, the experimental results were higher by factors of 1.4 and 1.6 (29% and 39%) respectively, as shown in figures 7.3 and 7.4. During the durability assessment of the prototype truck on proving grounds, the failure of the steering arm occurred after 120 circuits; this is quite close to both the FATIMAS strain history results of 58 repeats and prototype experimental results of 84 and 97 repeats of the washboard signal which suggests that only the washboard surface has caused the damage.

The strain history was reduced by 10% over the remaining three experimental tests to assess the effect on fatigue life of adjusting the magnitude of the washboard history. These were then converted to a load history for experimental fatigue life assessments. Experimental fatigue lives of 230 (101660 cycles), 874 (386308 cycles), and 4635 blocks (2075546 cycles) were obtained for load values of 29.8, 26.5, and 23.3 kN respectively, which compare well with FATIMAS experimental strain-time history predicted results of 158 (69836 cycles), 720 (318240 cycles), and 7866 (347672 cycles) blocks of the strain histories.

For calibration loads of 29.8 and 26.5 kN the experimental results were higher by factors of 1.54 (34%) and 1.2 (17.6%) when compared to the FATIMAS results. For a

calibration load of 23.3 kN the FATIMAS result was higher than the experimental result by a factor of 1.7 (41%) as shown in figure 7.4.

Figure 7.4 displays a plot of the predicted fatigue lives based on cyclic load/strain calibrated strain-time history and FATIMAS measured strain service history versus the experimental data. Also shown is the 100% correlation line and factor of 3 scatter band. The predictions based on Neuber's method and the energy density approach and FATIMAS strain-time service history results show good correlation with the experimental results with 66% of the points falling within a factor 3 scatter.

The FATIMAS strain-time service history predicted fatigue lives fall below the 100% correlation line for load increments of 33 (2734 micro-strain), 29.8 (2461 micro-strain) and 26.5 (2187 micro-strain) kN, showing that the predictions are conservative when compared to the experimental results. For a 23.3 kN the predicted fatigue lives are non-conservative and above the correlation line.

The above results confirm the previously derived conclusion that Neuber's rule underestimates the fatigue life of the component below the material yield point, thereafter, overestimates the life. The predicted fatigue lives based on the energy density method were found to be non-conservative and above the 100% correlation line in all cases. The predictions based on Tresca, von Mises and maximum principal strain load-time

service history calibrated washboard signal were found to be above and outside the scatter band, showing that the above equivalent methods grossly overestimated the fatigue life of the steering arm,. The predictions based on maximum principal strain also have been overestimated but not to the same extent.

The fatigue life predictions of Neuber load-time service histories were found to be in close agreement with both the FATIMAS strain-time and experimental results. The predictions based on maximum principal stress method were found to be the most conservative. Closest agreement is achieved with both Tresca and maximum principal strain methods.

DISPLAY OF SIGNAL : WB

Full file data :

13705 points.

370.4 pts/sec

Max = 2734

Min = -3846

Mean = -367.8

S.D. = 1559

Displayed :

13705 points.

from pt 1

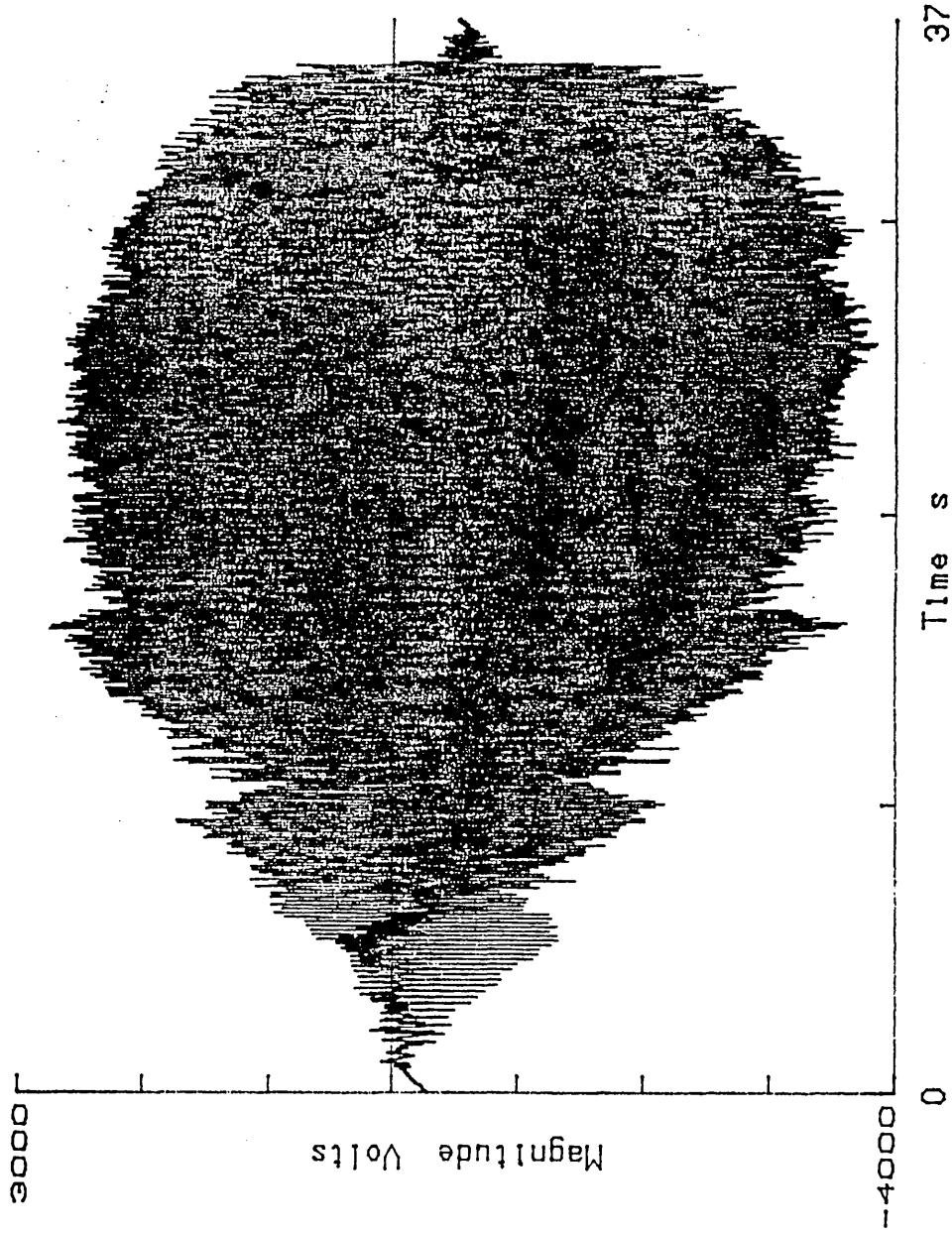


Fig. 7.1 Washboard Strain-Time Service History.

nCode NSOFT

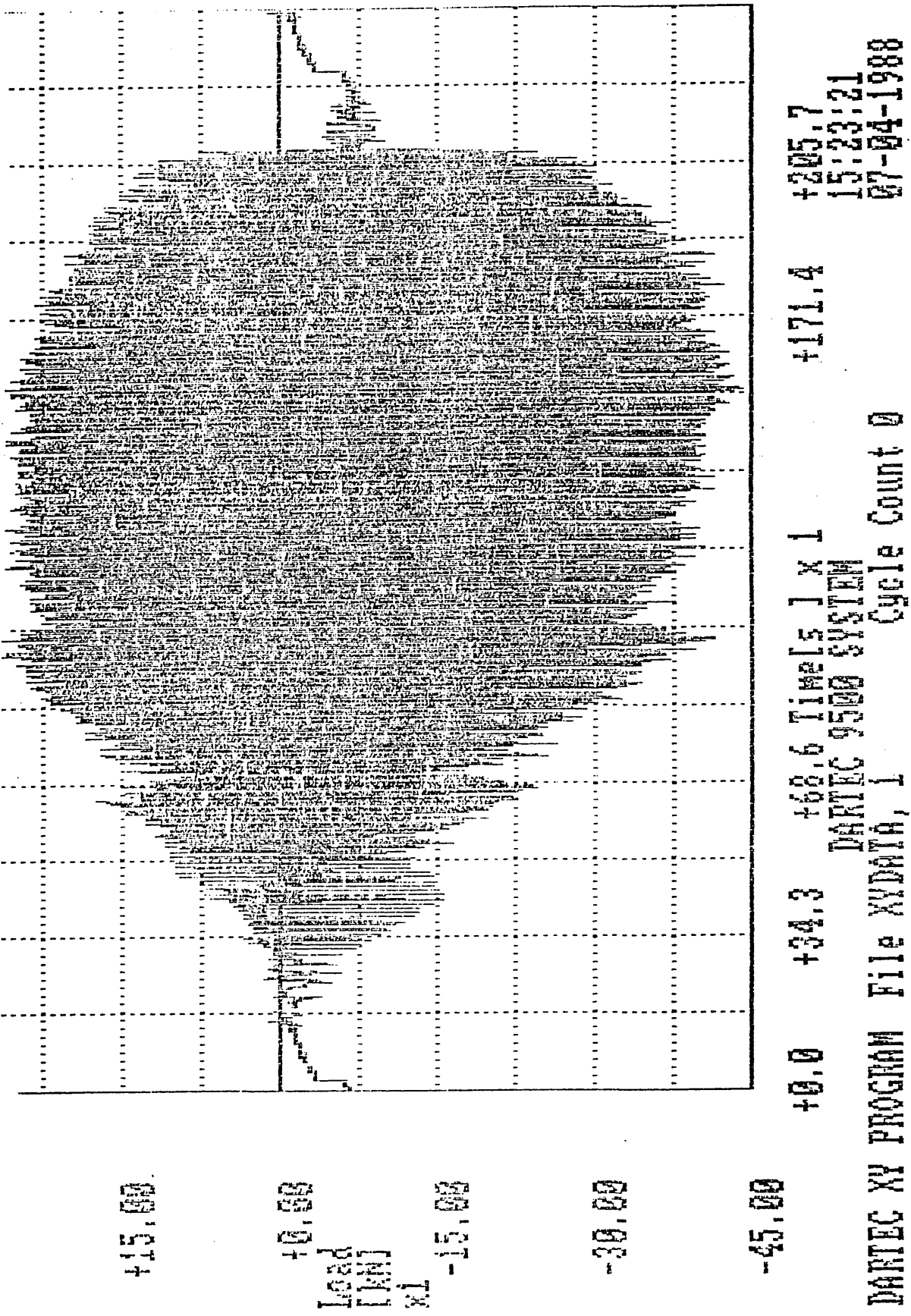


Fig. 7.2 Washboard Load-Time Service History.

		FATIMAS LOAD-TIME SERVICE HISTORY												
EXPERI-MENTAL	FATIMAS	F.E. + NEUBER				F.E. + ENERGY				STRAIN TIME SERVICE HISTORY	Max Princ. Stress	Tresca	Von Mises	Princ. Strain
		LOAD SERVICE HISTORY	Max Princ. Stress	Tresca	Von Mises	Max Princ. Strain	Max Princ. Stress	Tresca	Von Mises					
		84 / 97	58	63	101	125	91	231	338	360	308			
		230	158	157	266	360	231	595	867	9020	715			
		26.5	720	499	1060	1629	867	2049	4337	5688	3343			
		23.3	7866	3343	7764	13733	5688	13733	36861	5.26x10 ⁴	26197			

Table 7.1 The Experimental and Predicted Fatigue Lives to Failure of the Steering Arm: (Number blocks of the Washboard)

		FATIMAS LOAD-TIME SERVICE HISTORY												
EXPERI-MENTAL		FATIMAS		F.E. + NEUBER					F.E. + ENERGY					
LOAD SERVICE HISTORY	LOAD SERVICE HISTORY	STRAIN SERVICE HISTORY	Max Princ. Stress	Tresca	Von Mises	Max Princ. Strain	Max Princ. Stress	Tresca	Von Mises	Princ. Strain	Max Princ. Stress	Tresca	Von Mises	Princ. Strain
33	3.7×10^4 / 4.3×10^4	2.56×10^4	2.7×10^4	4.5×10^4	5.5×10^4	4.0×10^4	1.02×10^5	1.49×10^5	1.6×10^5	1.36×10^5	1.02×10^5	1.49×10^5	1.6×10^5	1.36×10^5
29.6	1.02×10^5	6.98×10^4	6.9×10^4	1.2×10^5	1.6×10^5	1.02×10^5	2.6×10^5	3.8×10^5	3.98×10^5	3.2×10^5	2.6×10^5	3.8×10^5	3.98×10^5	3.2×10^5
26.5	3.86×10^5	3.2×10^5	2.2×10^5	4.7×10^5	7.2×10^5	3.8×10^5	9.05×10^5	1.9×10^6	2.5×10^6	1.5×10^6	9.05×10^5	1.9×10^6	2.5×10^6	1.5×10^6
23.3	2.1×10^6	3.47×10^6	1.5×10^6	3.4×10^6	6.07×10^6	2.5×10^6	6.07×10^6	1.6×10^7	2.3×10^7	1.15×10^7	6.07×10^6	1.6×10^7	2.3×10^7	1.15×10^7

Table 7.2 The Experimental and Predicted Fatigue Lives to Failure of the Steering Arm: (Number of cycles of the washboard signal)

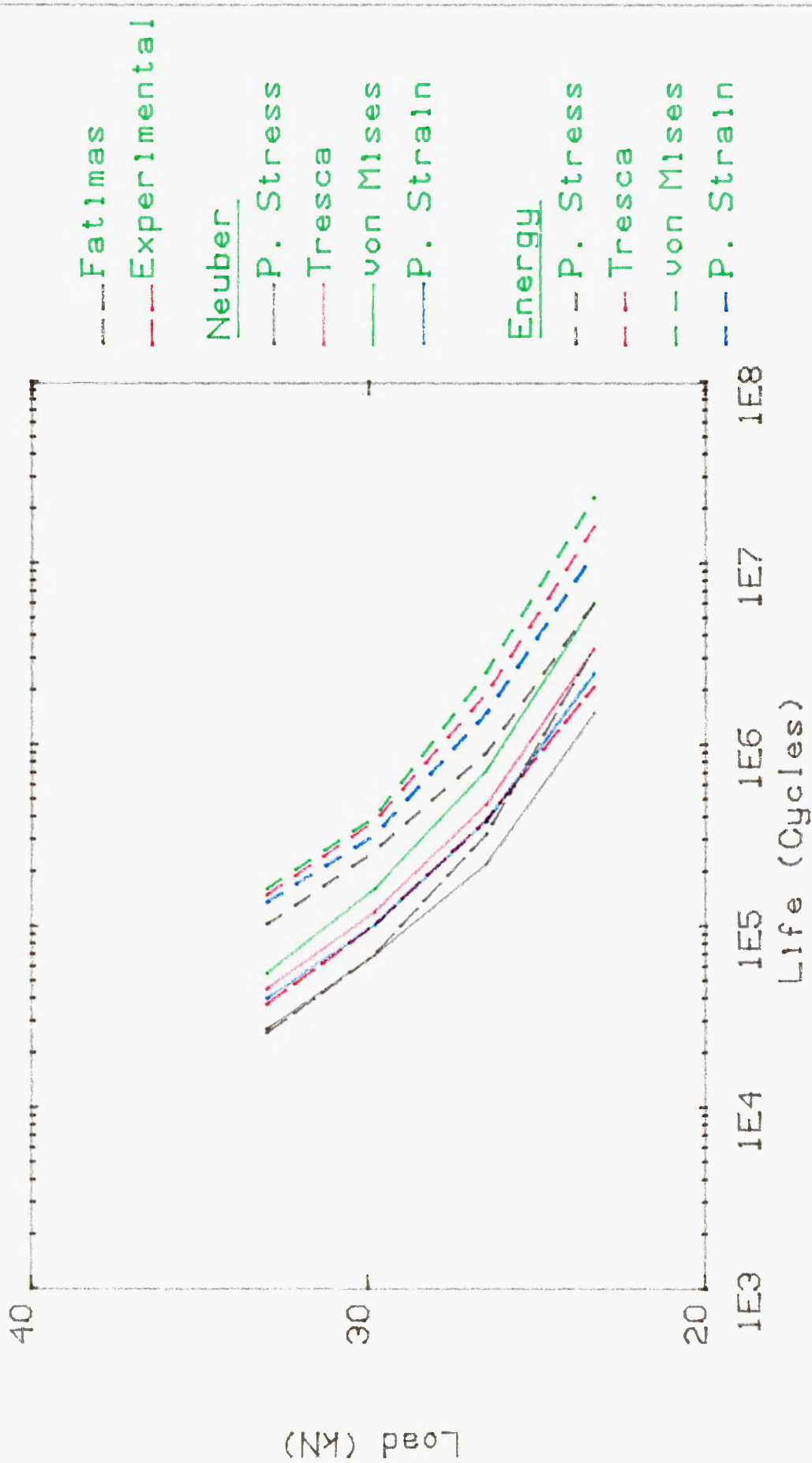


Fig. 7.3 Load Versus Life Comparison Of The Experimental And FATIMAS Predicted Fatigue Lives.

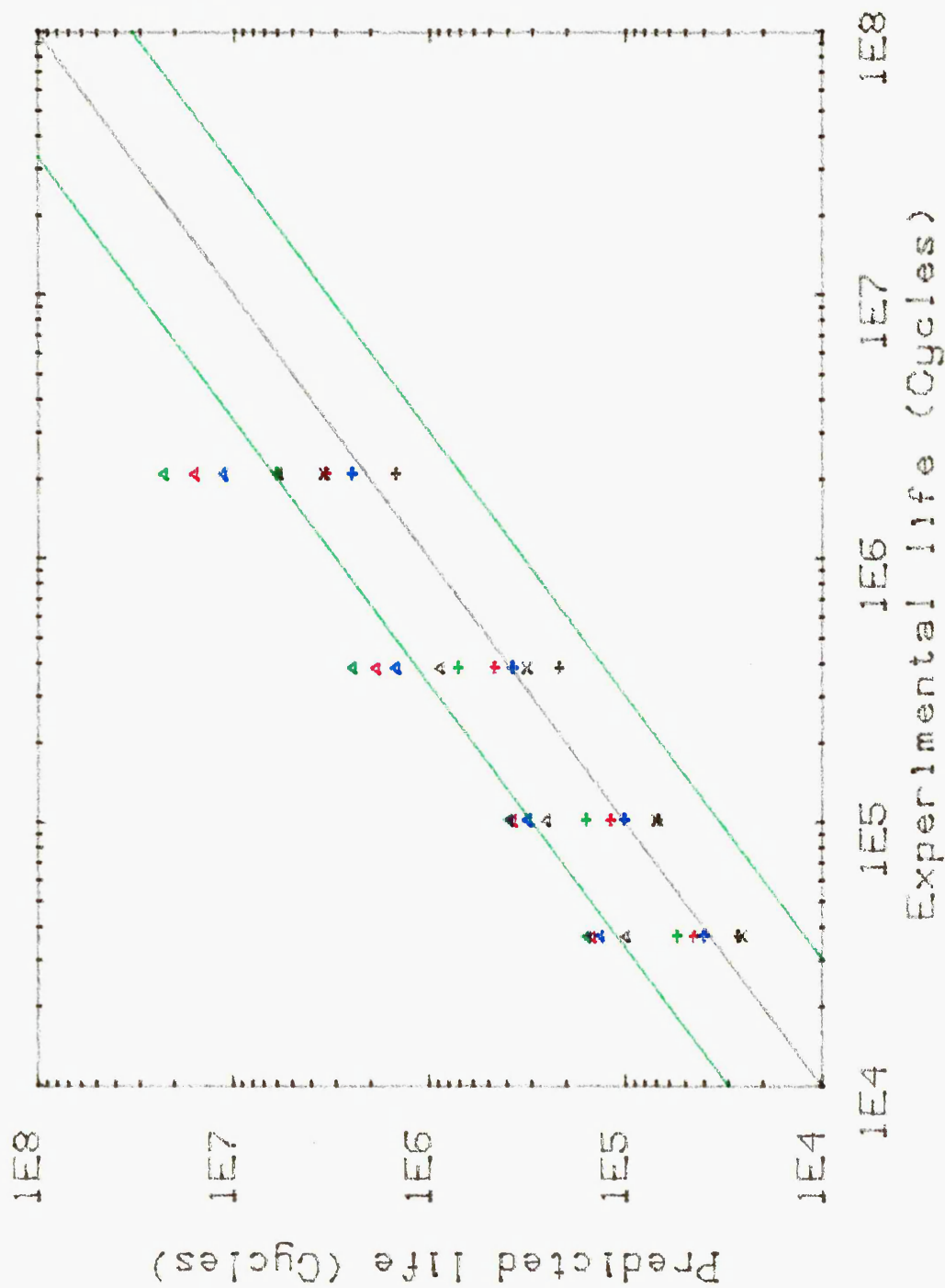


Fig. 7.4 Comparison Of Experimental And FATIMAS Predicted Fatigue Lives

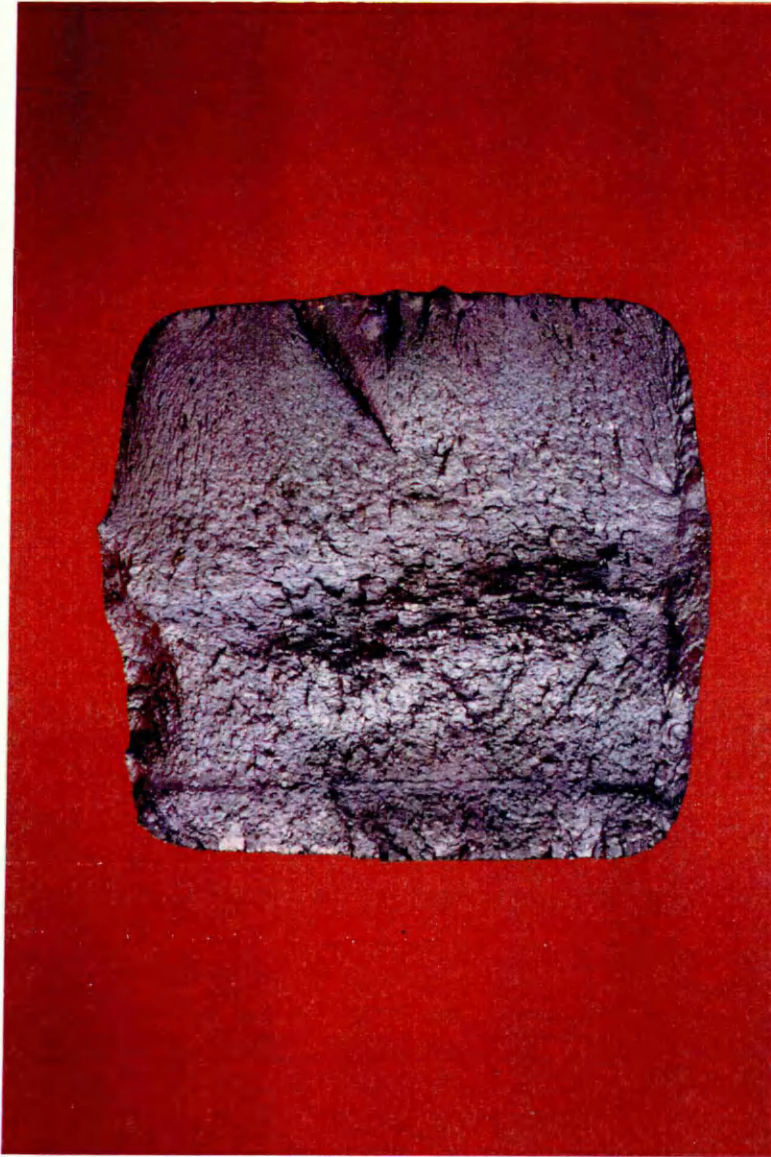


Fig. 7.5 The Fracture Surface Of The Component (x1.5)

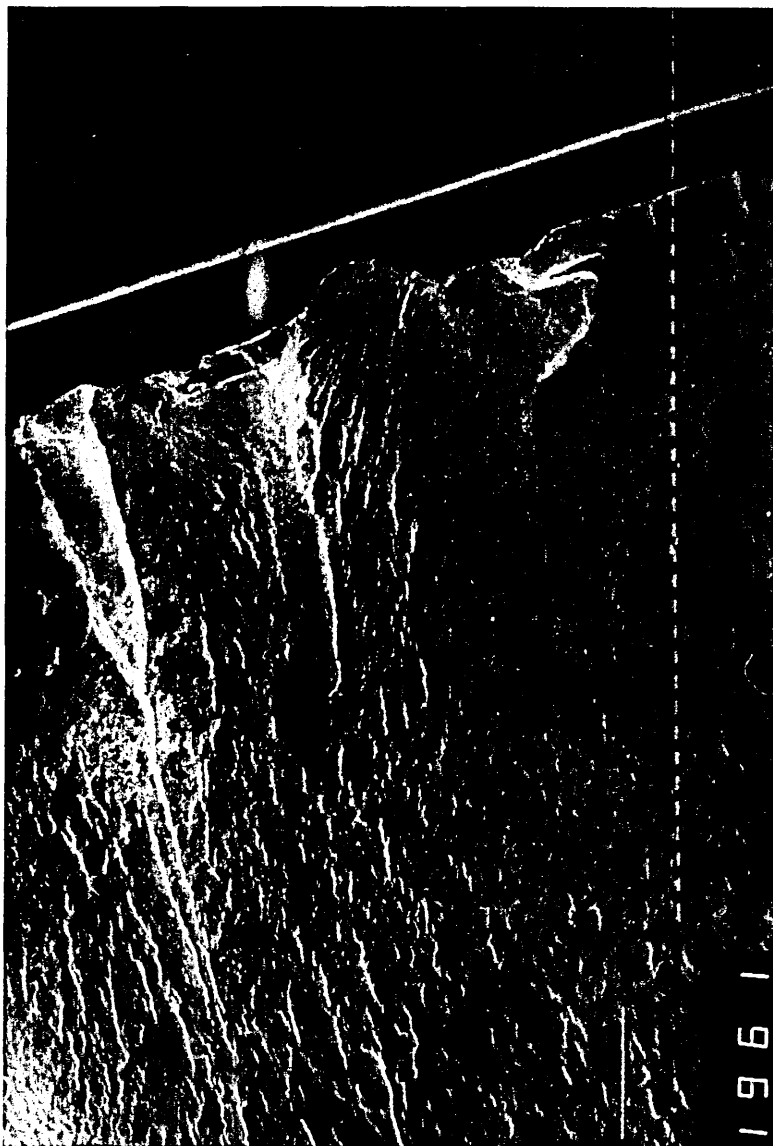


Fig. 7.6 The Surface Immediately Surrounding Initiation Point. This surface is macroscopically flat with evidence of scuffing due to repeated impact of the two crack surfaces (x30).



Fig. 7.7. Crack propagation region. The surface contains shell marks perpendicular to the applied stress (x1000).

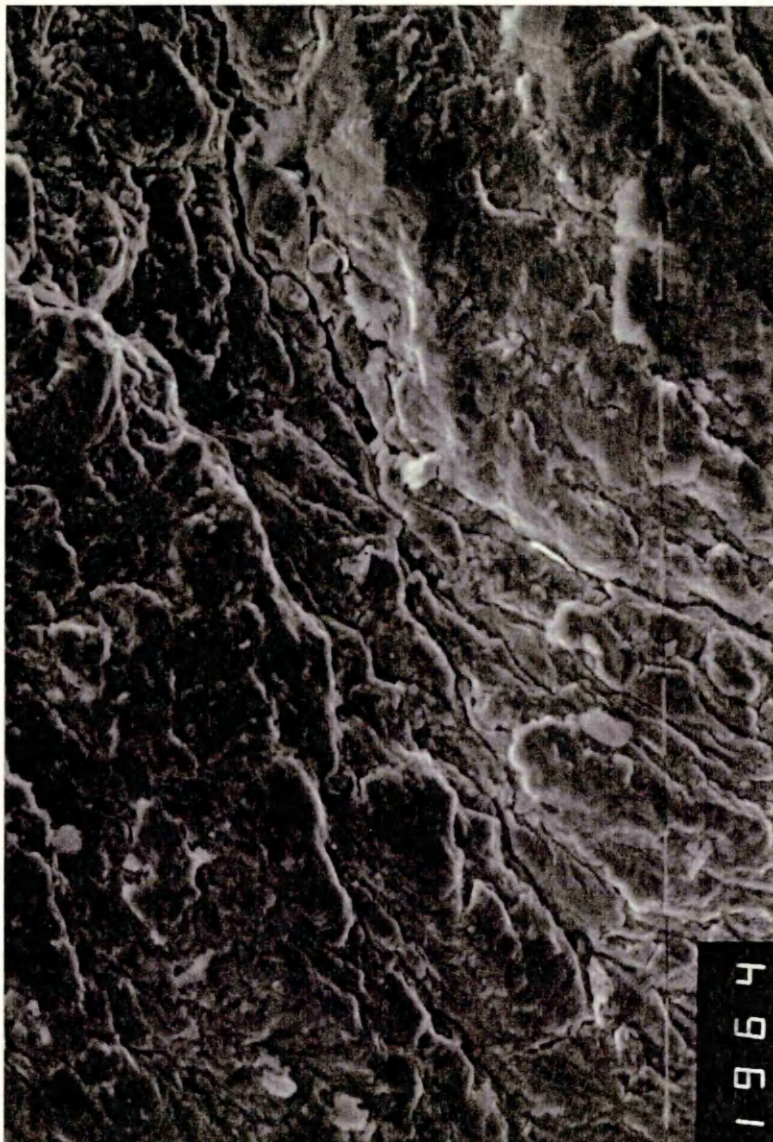


Fig. 7.8 Showing the transition area between slow crack growth fatigue and ductile shear failure (x1100).



Figure 7.9 Showing an area of ductile shear failure. The spherical beads in the cavity roots are non-metallic inclusions of manganese (x5000).



Fig. 7.10 An Area of Ductile Fracture. Mixed Fracture Modes are clearly visible, ductile dimpling, typical of ductile fracture and inter-granular fracture (x2000).

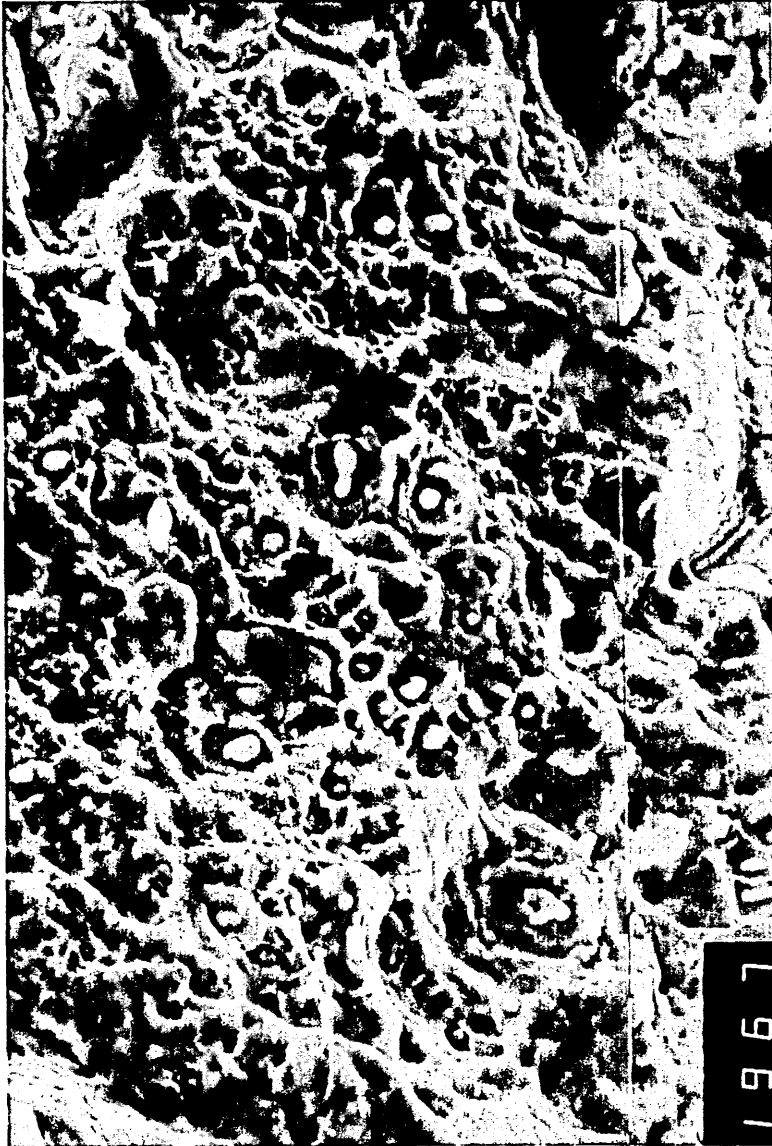


Fig. 7.11 An area of ductile fracture, showing non-metallic inclusions of manganese sulphide, which serve to indicate ductile failure (x2100).



Fig. 7.12 Final brittle fracture. Two modes of fracture are visible. The intergranular fracture mode predominates, but there exists large regions of cleavage (x5000).

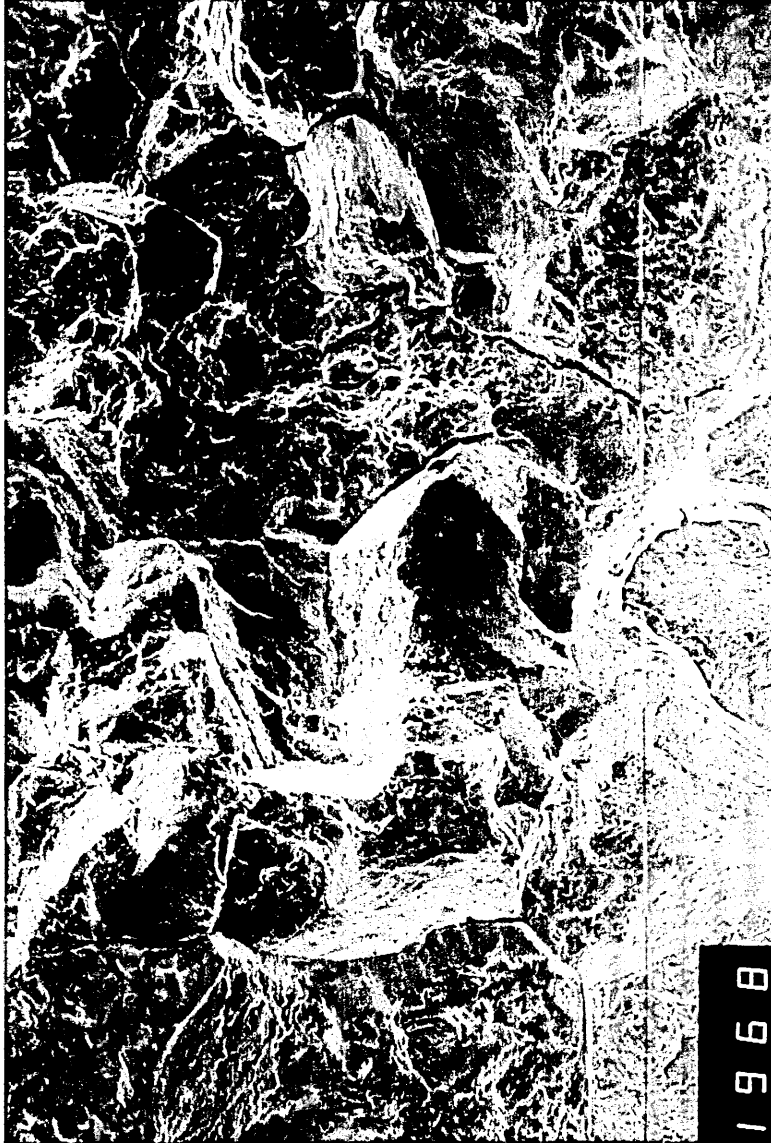


Fig. 7.13 Brittle fracture. Showing intergranular and cleavage fracture (x150).

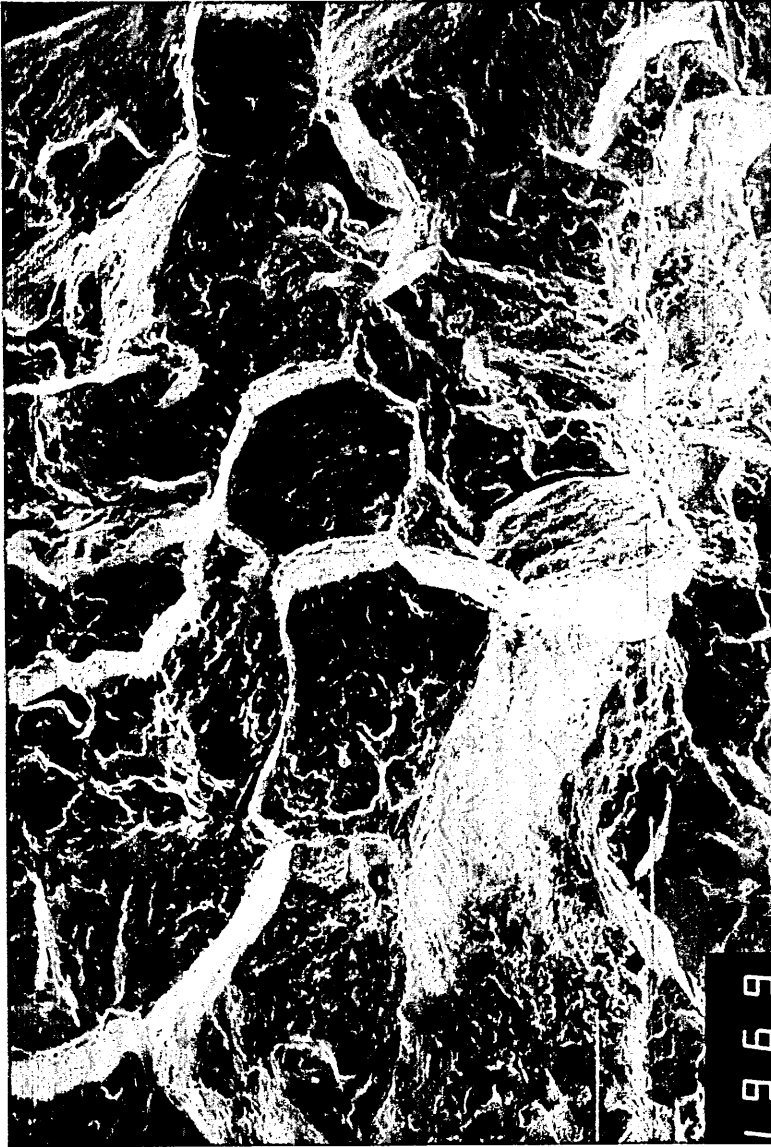


Fig. 7.14 Brittle fracture region. Final catastrophic failure (x150).

CHAPTER 8

INTEGRATED FE AND FATIGUE COMPUTATIONS

8.1 New Software Structure

As a result of this investigation an integrated CAD software package is being developed by nCode International Limited in conjunction with PAFEC, by which durability of engineering components can be predicted in the conceptual design stage. The purpose written PAFEC/FATIMAS suite is called FALCON and was used to predict the fatigue life of the steering arm through a range of service histories using the elastic finite element stress data. The FALCON package requires a load-time service history which was provided for the steering arm as outlined in section 4.5. The FALCON package uses the elastic finite element equivalent stresses to convert the load-time service history to a strain service history, using Neuber's method. This is then used in conjunction with the cyclic stress/strain curve to develop a local elastic/plastic stress-time history which is used for fatigue life prediction. This takes account of the non-linear, load-strain relationship which was not included in the work described in section 6. The FALCON package uses the following equivalent methods; principal stress, Tresca, von Mises, and σ_{xx} . These are used in conjunction with the cyclic stress/strain data, Neuber's equation and rainflow counting for fatigue life prediction.

The flow chart of figure 8.1 shows the relationship between FALCON and the FEA system.

The procedure adopted in applying the FALCON package to fatigue life prediction of the steering arm component is as follows:-

- 1) Actual loading conditions experienced by the component during service are simulated on the F.E. model.
- 2) Elastic finite element analysis is carried out.
- 3) The cyclic properties of the material are entered.
- 4) The washboard load history is entered.
- 5) The critical location is identified and the surface finish strength reduction factor was entered.
- 6) Fatigue life prediction is carried out.
- 7) PIGS is used to display the results. The actual damage at each node surrounding the critical location was displayed. The life maps for 33 kN load increments are shown in figures 8.2 to 8.5.

8.2 Steering Arm Fatigue Predictions

Fatigue life predictions of 80 blocks (3.5E4 cycles), 85 blocks (3.7E4 cycles), 113 (4.9E4 cycles) and 147 (6.5E4 cycles) of the load-time service history were obtained for maximum principal stress, σ_{xx} , Tresca and von Mises, respectively for load value of 33 kN in the load history signal.

The predicted fatigue lives obtained using FATIMAS for measured strain-time history and FATIMAS for FE load calibrated measured strain-time histories were compared with load-time service history results obtained using the FALCON package. The results are listed in tables 8.1 and 8.2 and shown in figure 8.6.

The FATIMAS package used with measured strain-time history gave a predicted fatigue life of 58 blocks ($2.6E4$ cycles). Fatigue life predictions of 63 blocks ($2.8E4$ cycles), 101 blocks ($4.5E4$ cycles), 125 blocks ($5.5E4$ cycles) and 91 blocks ($4.0E4$ cycles) of strain history derived from Neuber's method were obtained for maximum principal stress, Tresca, von Mises and maximum principal strain respectively under the 33 kN load. For the same load, predictions of 231 blocks ($1.0E5$ cycles), 338 blocks ($1.5E5$ cycles), 360 blocks ($1.6E5$ cycles) and 308 blocks ($1.4E5$ cycles) of the signal were obtained using the energy density approach, load calibrated strain-time history. The FALCON package predicted fatigue lives of 80 blocks ($3.5E4$ cycles), 85 blocks ($3.7E4$ cycles), 113 blocks ($4.9E4$ cycles) and 147 blocks ($6.5E4$ cycles) of washboard load-time service history. As mentioned earlier, experimental tests gave lives of 84 and 97 blocks respectively. These results are summarised in Table 8.1 and 8.2.

The FATIMAS fatigue life predictions based on the measured strain-time service history are in close agreement with those obtained using the FALCON package. However, all of the predictions based on Neuber's equation were lower and all

based on the energy density approach were higher than the FALCON results.

The FATIMAS strain-time history predicted fatigue lives and the FALCON results are compared with the experimental data in figure 8.6 on which the 100% correlation line and factor of 3 scatter bands are shown. The predictions show a good correlation with experimental fatigue life data for a crack length of approximately 3mm. All data falls within a factor 3 scatter band when plotted. The FATIMAS fatigue life predictions with both the strain-time service history and F.E. and Neuber's load calibrated washboard signal are in close agreement with those obtained using the FALCON package. All data is within a factor 3 of scatter. However, all of the life predictions based on the energy density approach are non-conservative and much higher than the FALCON results. Best correlation was achieved using both the maximum principal strain and Tresca with Neuber's load-time histories.

8.3 Discussion

The reason for any lack of correlation between FALCON results and those obtained using Neuber's method are due to the following assumption:

Approximate linear extrapolation (single point calibration) was used for calibration of the measured washboard strain-time service history for fatigue life predictions. Thus, this increased the accuracy of the fatigue life predictions obtained using Neuber's method and decreases the correlation between the FALCON results and those obtained using the energy density approach.

8.4 Conclusions

The elastic/plastic strain values obtained using F.E. calculated equivalent stresses and both Neuber's equation and the energy density approach have been used successfully to convert a load history to a strain history suitable for fatigue life analysis. A comparison of these results with the experimental data reveals that the load/strain fatigue life predictions as seen in figures 6.6 and 6.7 give good agreement, with 66% of the points falling within a factor of 3 scatter band. With the FATIMAS measured strain-time history and FATIMAS load-time service history with Neuber fatigue life predictions, all of the points are within a factor 3 scatter band. The results confirm the accuracy of the procedures employed to obtain the elastic/plastic strains from finite element results using both the energy density and Neuber's rule. These specific relationships have been used to adjust the known measured washboard strain-time history for fatigue life assessment. The flow chart shows the steps taken to achieve the results, see figure 8.7.

The FATIMAS package relies upon measured service history which is not available at the design stage (as shown in figure 8.7, (route 1)). However, the F.E. integrated technique can be used with a load history in the early design stage to assess the integrity and durability of engineering components at a CAD workstation. This enables the engineer to design a component and apply finite element analysis to stress the component using the

available nominal load history. The stress data can then be used to obtain elastic/plastic strains in conjunction with either Neuber's or the energy method using a range of load increments. This can then be used to create a service history which can be input into the FATIMAS software to assess the durability of the component, as shown in figure 8.7, (route 3).

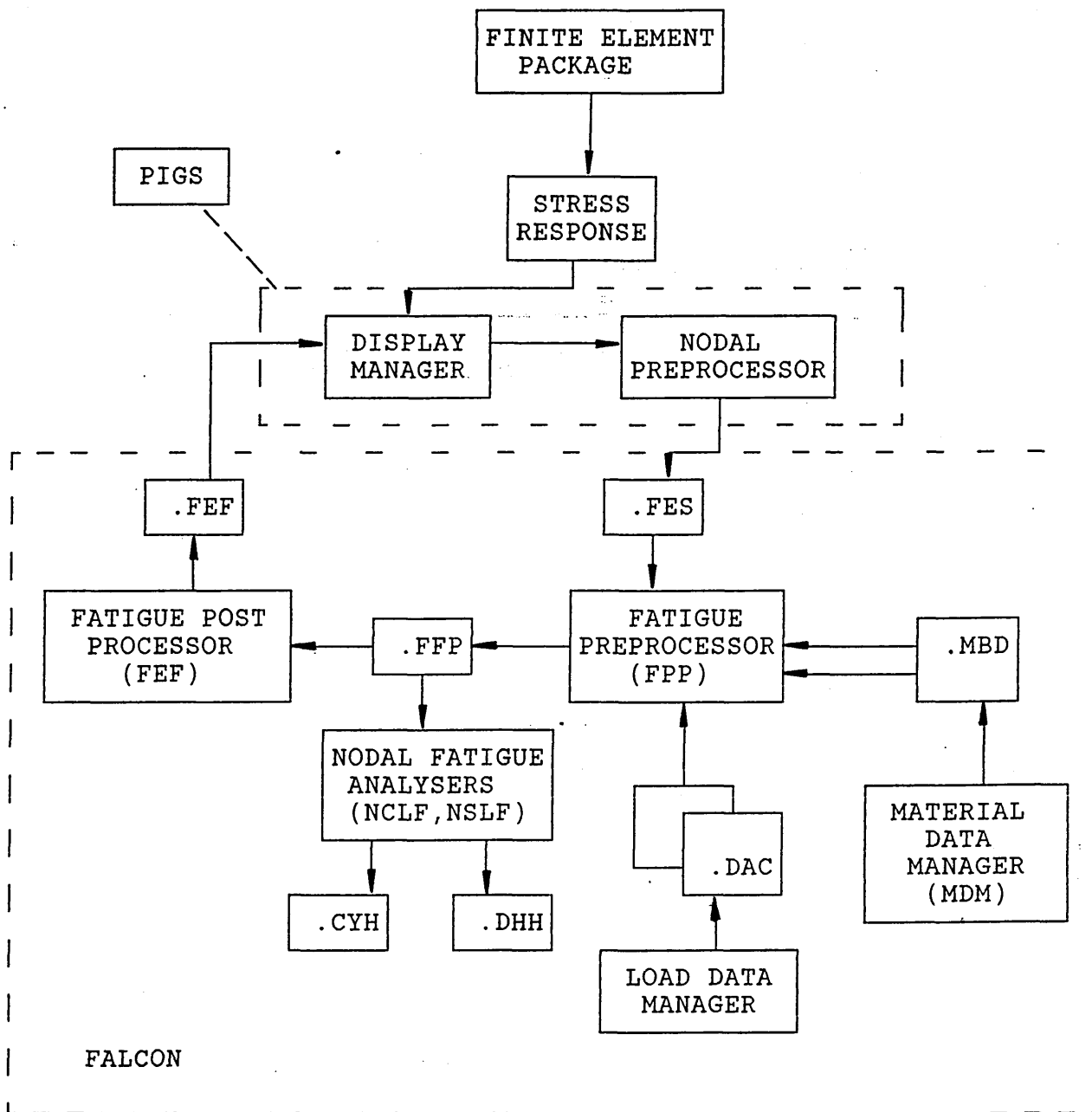


Fig. 8.1 AN OVERVIEW OF THE FALCON STRUCTURE.

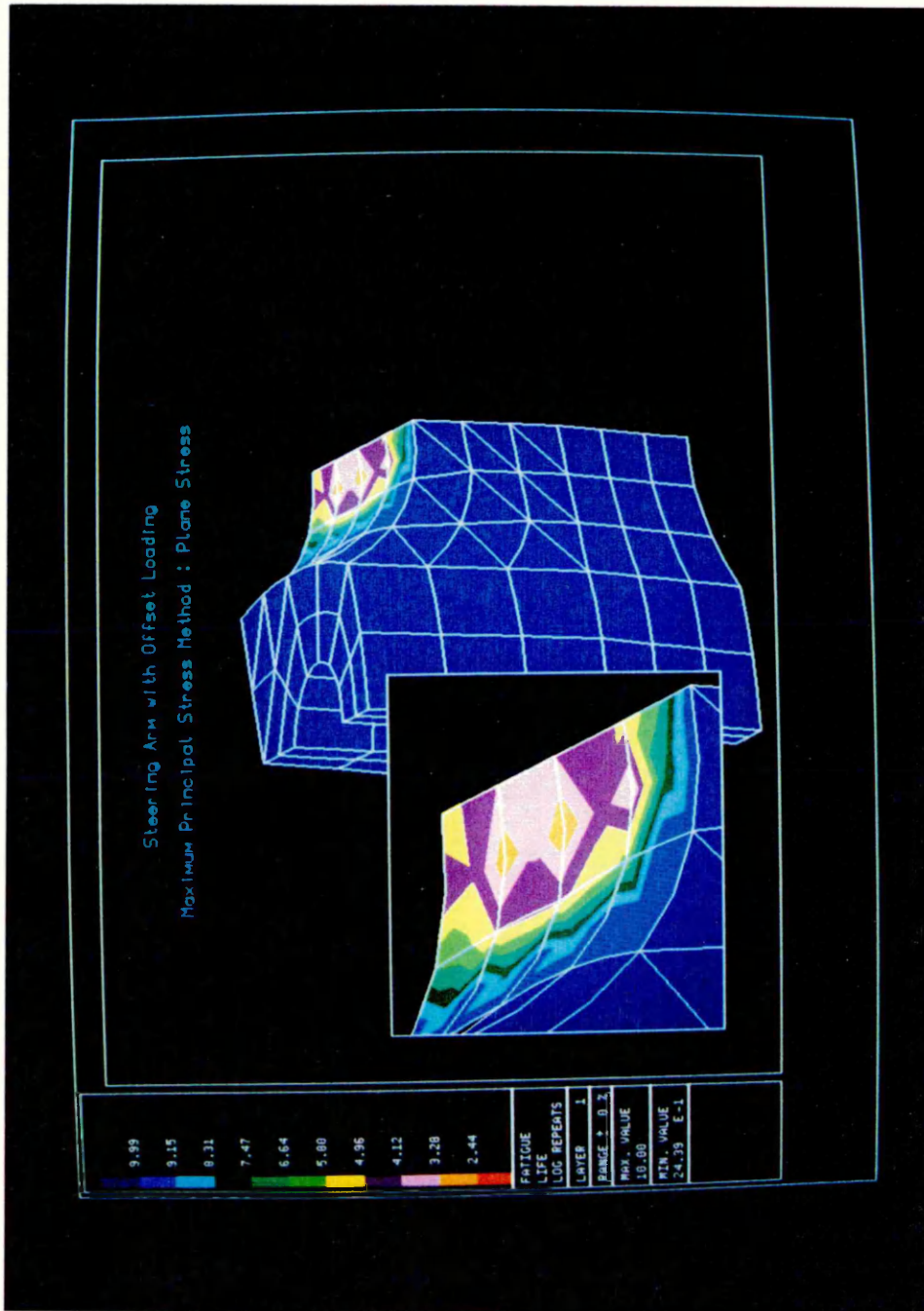


Fig. 8.2 Fatigue Life Contours for the Steering Arm (Maximum Principal Stress method).

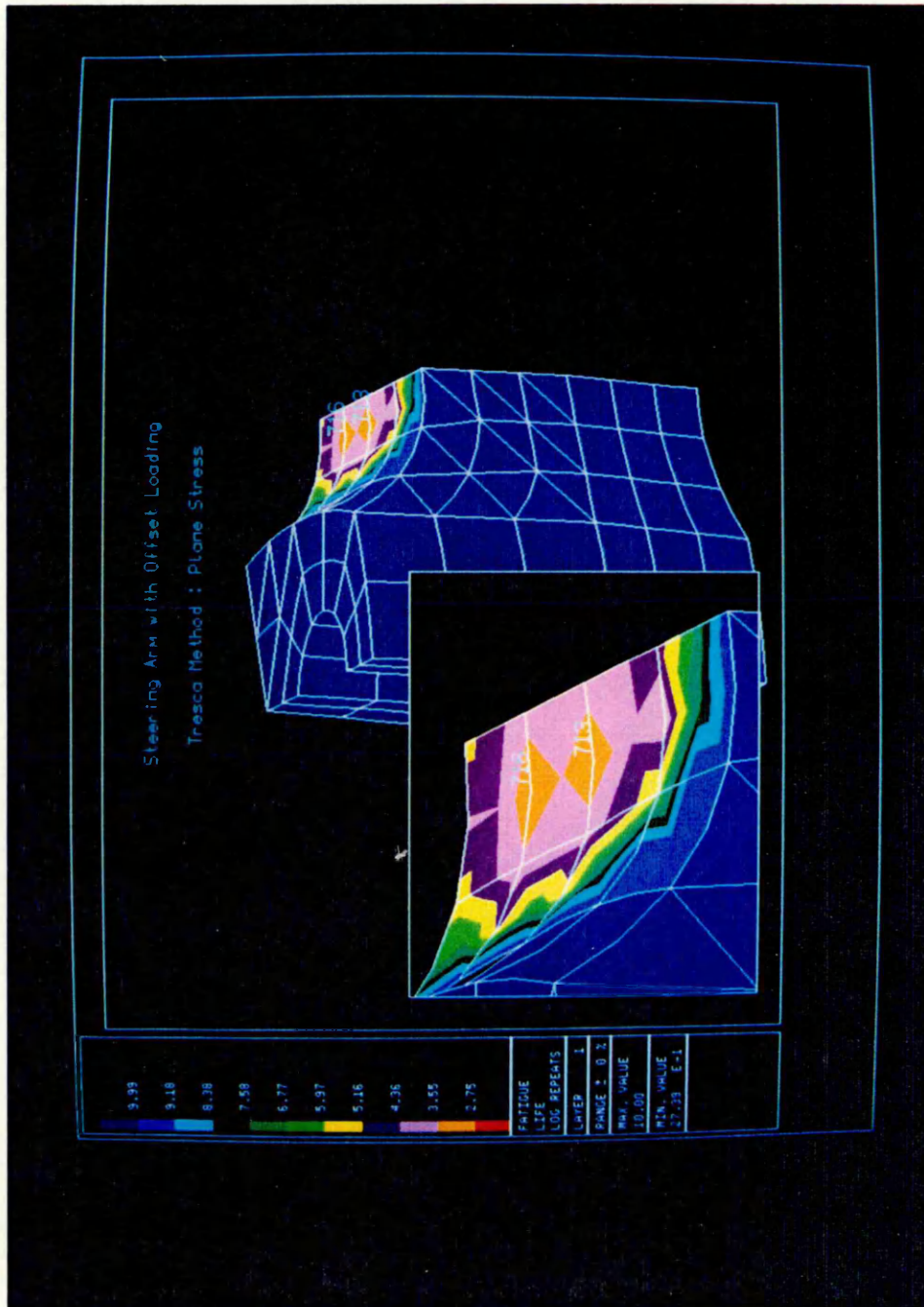


Fig. 8.3 Fatigue Life Contours for the Steering Arm (Tresca's Method).

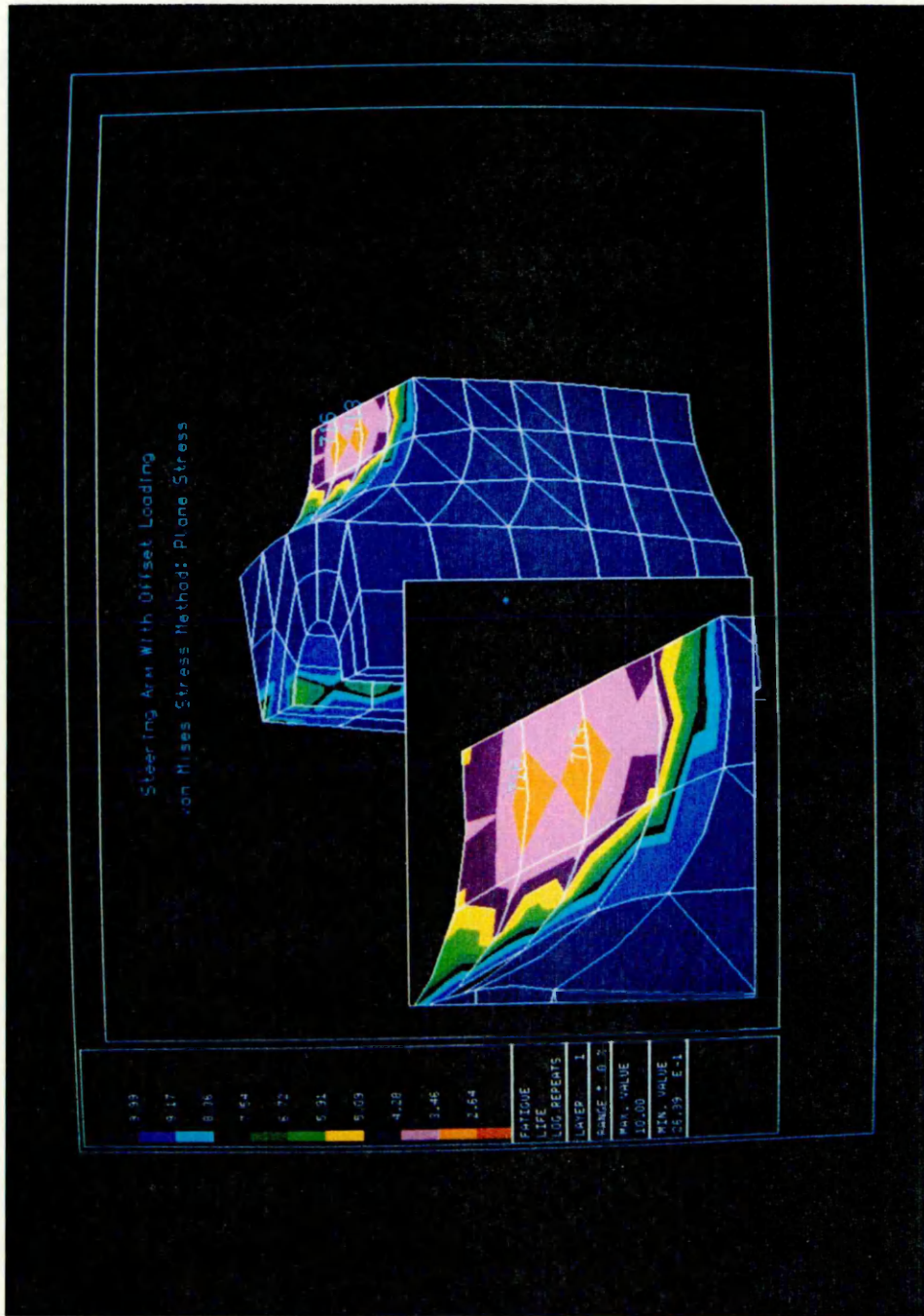


Fig. 8.4 Fatigue Life Contours for the Steering Arm (von Mises' method).

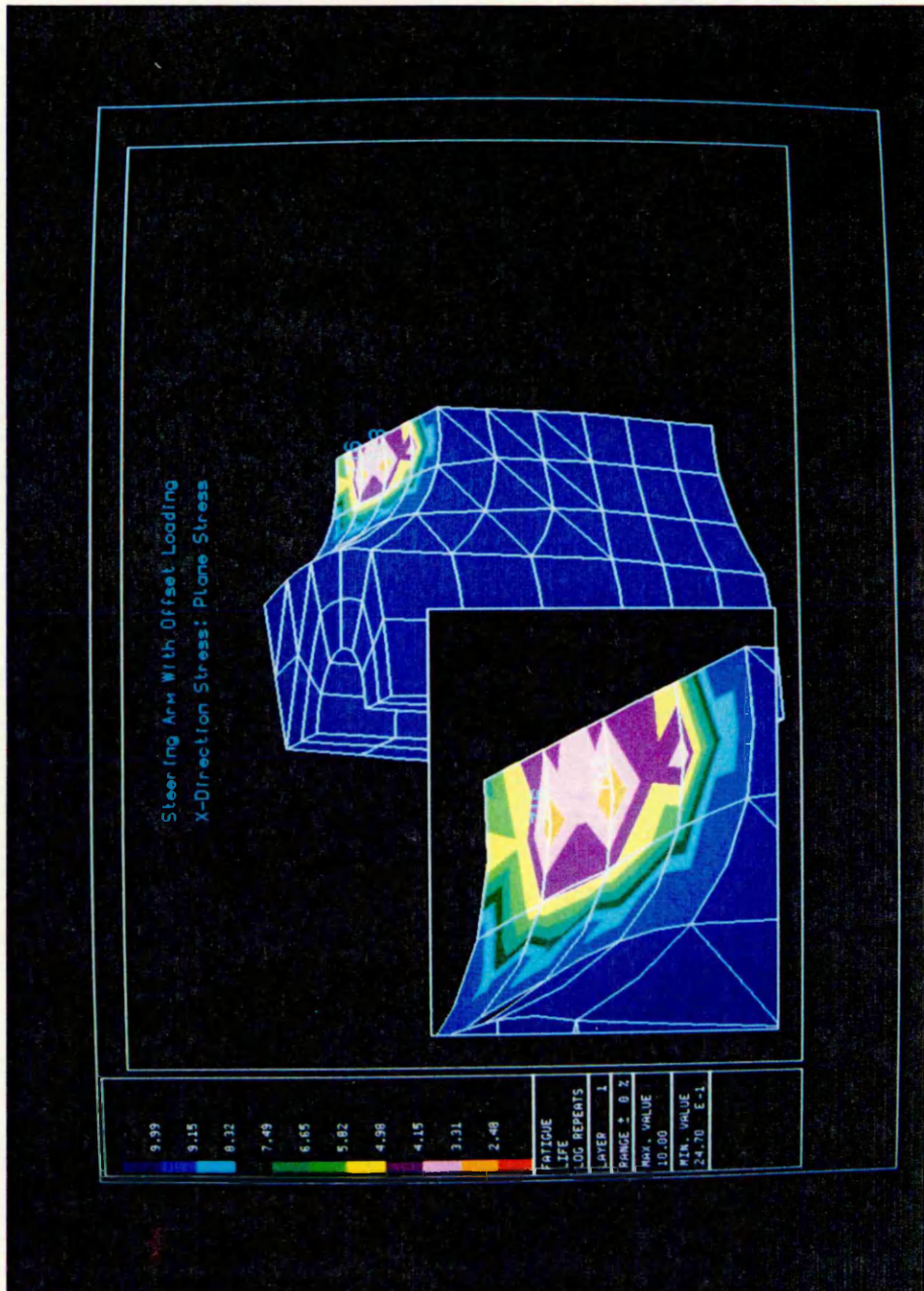


Fig. 8.5 Fatigue Life Contours for the Steering Arm (σ_{xx} method).

LOAD KN	EXPERIMENTAL SERVICE HISTORY	FATIMAS LOAD-TIME SERVICE HISTORY										FALCON LOAD-TIME SERVICE HISTORY			
		FATIMAS STRAIN TIME SERVICE HISTORY		F.E. + NEUBER				F.E. + ENERGY				Maximum Princ. Stress	Tresca	Von Mises	60x
		LOAD HISTORY	TIME	Max Princ. Stress	Tresca	Von Mises	Max Princ. Strain	Max Princ. Stress	Tresca	Von Mises	Princ. Strain				
33	84 / 97	58	63	101	125	91	231	338	360	308	80	113	147	85	
29.6	230	158	157	266	360	231	595	867	9020	715					
26.5	874	720	499	1060	1629	867	2049	4337	5688	3343					
23.3	4635	7866	3343	7764	13733	5688	13733	36861	5.26x10 ⁴	26197					

Table 8.1 The Experimental and Predicted Fatigue Lives using both FATIMAS and FALCON package (Number of blocks to failure of the Steering Arm)

EXPERI-MENTAL	FATIMAS		FATIMAS LOAD-TIME SERVICE HISTORY										FALCON LOAD-TIME SERVICE HISTORY			
	LOAD SERVICE HISTORY KN	STRAIN TIME SERVICE HISTORY	F.E. + NEUBER					F.E. + ENERGY					Maximum Princ. Stress	Tresca	von Mises	6xx
			Max Princ. Stress	Tresca	Von Mises	Max Princ. Stress	Max Princ. Strain	Tresca	Von Mises	Max Princ. Strain	Tresca	Von Mises				
33	3.7×10^4 / 4.3×10^4	2.56×10^4	2.7×10^4	4.5×10^4	5.5×10^4	4.0×10^4	1.02×10^5	1.49×10^5	1.6×10^5	1.6×10^5	1.36×10^5	3.5×10^4	4.99×10^4	6.5×10^4	3.7×10^4	
29.8	1.02×10^5	6.98×10^4	6.9×10^4	1.2×10^5	1.6×10^5	1.02×10^5	2.6×10^5	3.8×10^5	3.98×10^5	3.2×10^5						
26.5	3.86×10^5	3.2×10^5	2.2×10^5	4.7×10^5	7.2×10^5	3.8×10^5	9.05×10^5	1.9×10^6	2.5×10^6	1.5×10^6						
23.3	2.1×10^6	3.47×10^6	1.5×10^6	3.4×10^6	6.07×10^6	2.5×10^6	6.07×10^6	1.6×10^7	2.3×10^7	1.15×10^7						

Table 8.2 The Experimental and Predicted Fatigue Lives using both FATIMAS and FALCON package. (Number of blocks to failure of the steering arm).

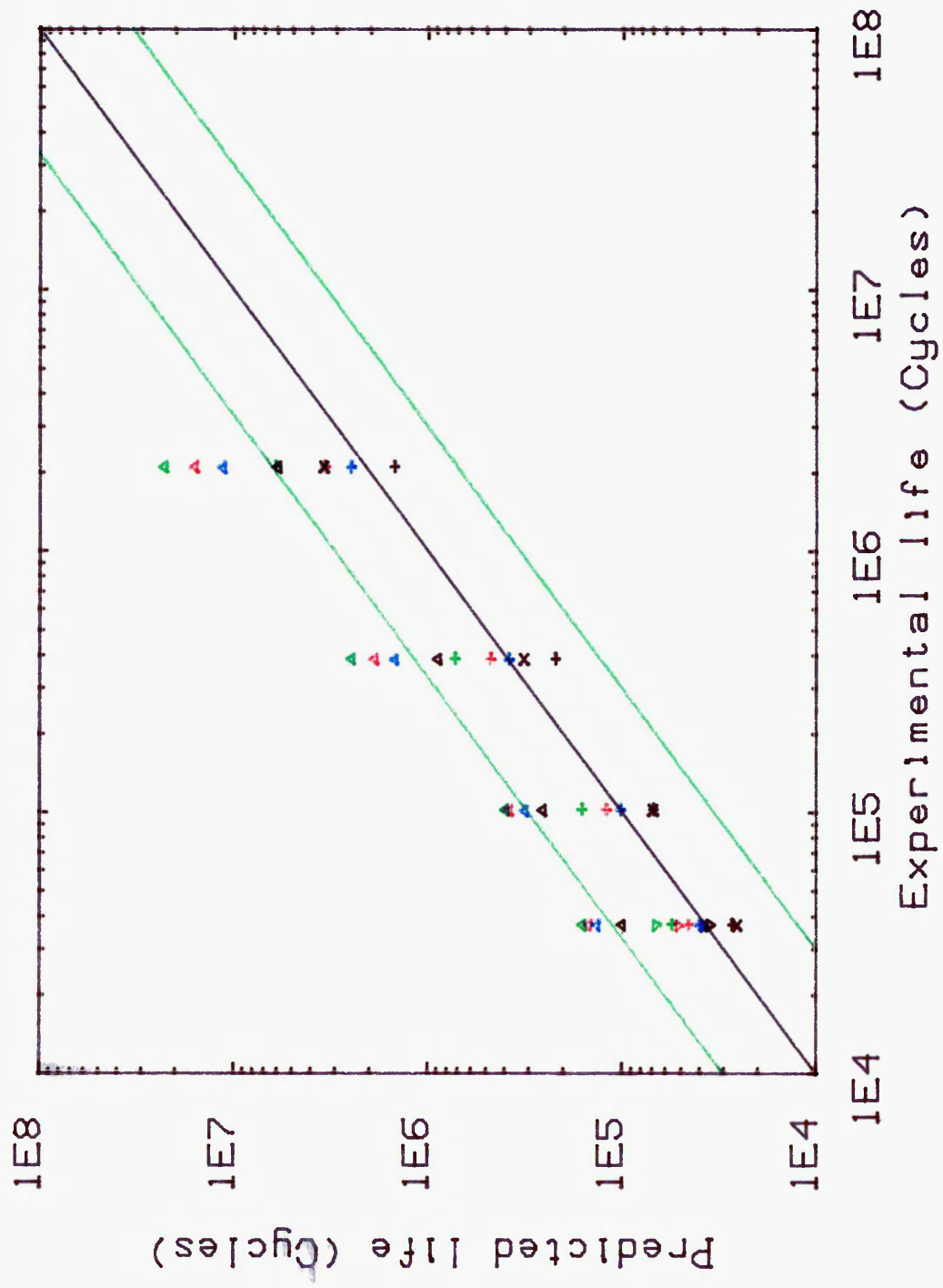


Fig. 8.6 Comparison Of The Experimental, FALCON And FATIMAS Predicted Fatigue Lives.

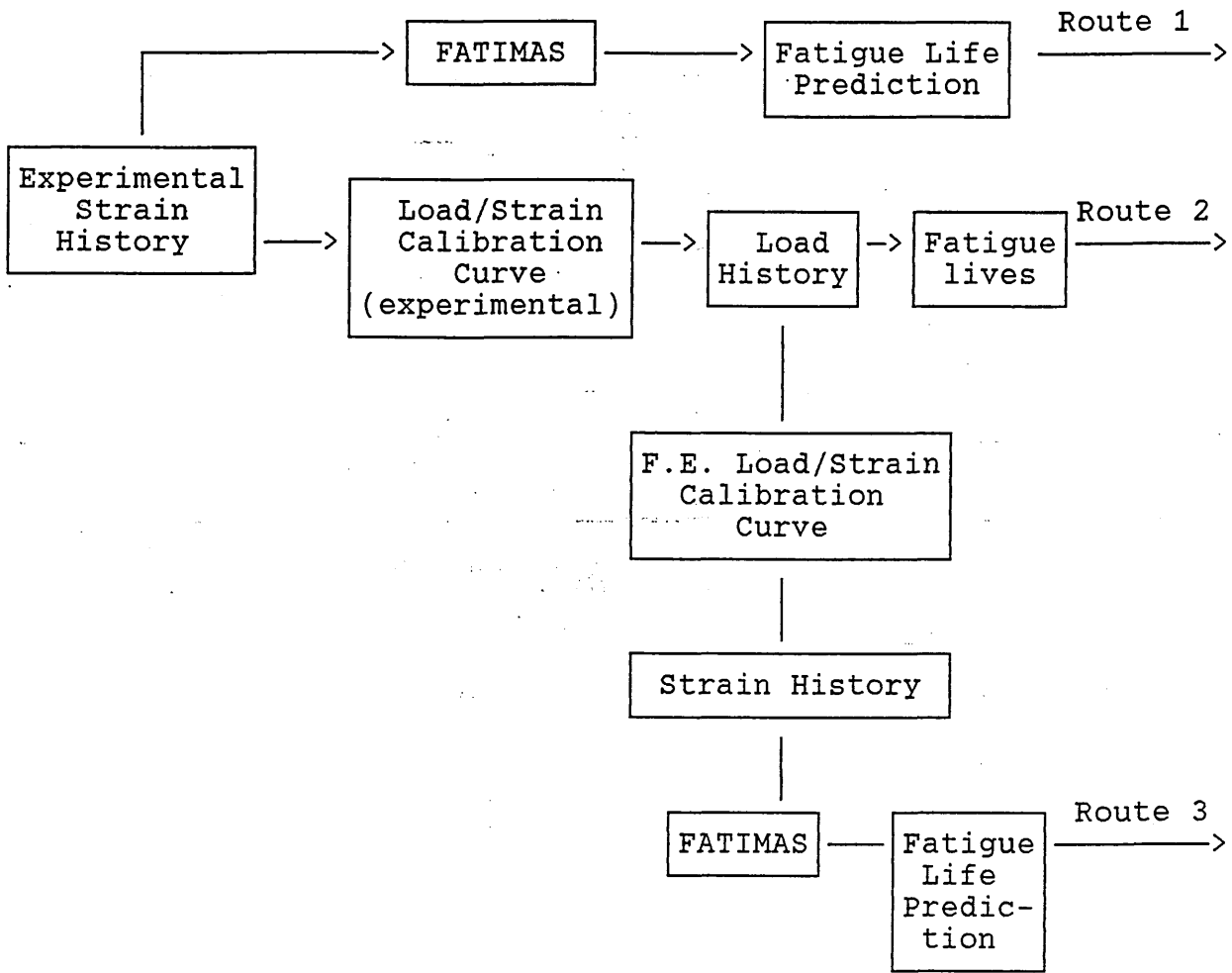


Fig. 8.7 The Flow Chart showing an overview of the routes taken to assess the fatigue life of the steering arm.

CHAPTER 9

DISCUSSION

9.1 Introduction

The principal objective of the present work has been to identify the data requirements for the development of computer software to estimate the fatigue life of engineering components at the conceptual design stage. In particular, the programme has investigated ways of supplying appropriate data to existing computer packages which use the critical-location method of fatigue life assessment and pseudo-experimental data in the form of component strain histories. Typical of these types of software is the software suite FATIMAS, which hitherto have tended to be used as development rather than design tools.

Finite element methods give stress fields which have been useful in component design, however, fatigue life prediction can be a reality if the finite element stress field can be translated into local strain histories for input into fatigue life prediction software. Several alternative ways of achieving this objective have been investigated by using a real engineering component, namely a steering arm.

A three dimensional model of the steering arm was created and used to select the relevant surface boundary coordinates needed for the development of a finite element mesh. A three dimensional elastic finite element analysis of the steering arm was performed employing quadratic

isoparametric solid elements in order to identify the fatigue critical locations. The local elastic/plastic strains required for fatigue life estimation of the component were then calculated. Both the energy density and Neuber's method were used to predict strains necessary for incorporation into the critical location method.

To provide experimental comparison with the theoretical analysis a number of strain gauges were installed around the critical location of an experimental component identified by the finite element analysis. Measured static strain values were obtained for load increments of 10 kN up to a 70 kN load and compared to the calculated elastic/plastic strains obtained using the above techniques, as shown in figure 5.4. An arbitrary 10% reduction in the measured strains was imposed to account for cycle-dependent softening of the component material. This was then used to plot an applied load/local strain calibration curve for conversion of the service strain history to a service load history suitable for fatigue testing of the steering arm.

Load control fatigue tests were performed on the steering arm using a Dartec computer controlled multi-axial servo-hydraulic fatigue testing machine with automated test control and data acquisition systems. A total of five components were tested to crack initiation. The experimental results were compared to computer based fatigue life predictions obtained using the FATIMAS software package.

The main objective of this section is to discuss the experimental and theoretical results. It is divided into two sections, computer based modelling and analysis, and theoretical and experimental fatigue life assessment.

9.2 Computer Based modelling and analysis

The elastic finite element results were compared with the measured strains in the elastic region. For a 20 kN load the F.E. calculated maximum principal strain at the highest stressed node (node 12) was 9% higher than the measured strain, listed in tables 4.2 and 5.2. Given the approximate nature of the finite element and the measured strains, also the simplifications in geometry, this can be considered to be a satisfactory correlation.

Since local strains are used for fatigue damage evaluation, the first requirement for fatigue life estimation is to develop a technique for calculation of the plastic strain field. Current computer programs predict local strains from nominal stresses and strains using Neuber's method for both elastic and plastic conditions. Hence, it is important to compare the estimated and measured strains for a range of load increments which provide both elastic and plastic local strains.

The multiaxial elastic F.E. calculated stresses around the critical location were reduced to equivalent stresses using maximum principal stress, von Mises, Tresca and maximum principal strain methods, listed in tables 4.1 to

4.3. The maximum values found were then used in conjunction with both Neuber's rule and the energy density approach as well as the monotonic uniaxial stress/strain curve to estimate the elastic/plastic strains. These were then compared to the measured strains in both elastic and plastic ranges, listed in tables 5.2, and 5.3 and shown in figure 5.4.

Figure 5.5 displays the graphical representation of the same data, which shows that the estimated strains fall above the 100% correlation line using both methods. Both Neuber and the energy density calculations correlate well with the measured results throughout the elastic and plastic regions. Maximum differences of 15.5% was observed in the elastic range (10 kN load), and 20% was observed in the plastic region (70 kN load).

The experimental results confirm that Neuber's equation gives less accurate predictions than the energy density method when plastic yielding occurs. From the above discussion it is clear that the accuracy of the described methods appear to be dependent upon the extent of propagation of the plastic zone at the notch tip [37, 63]. It can be concluded that both Neuber's rule and the energy density method can be used to estimate the elastic/plastic stress/strain values for any loading conditions, ahead of a notch if appropriate elastic stress field and the material stress/strain curves are known. While Neuber analysis is found to give a lower accuracy than the energy method, it is significant that all the predictions

are conservative when compared to the energy density method in the elastic and plastic region.

Having proved that the above techniques can be applied successfully to obtain the monotonic notch root elastic/plastic strains, attempts were made to estimate the cycle dependent elastic/plastic strain values. Table 4.5 lists the estimated strains and figure 4.10 displays the cyclic notch root load/strain calibration data. Good correlation exist between the measured and estimated strains based on both monotonic and cyclic stress/strain curves in the elastic region. However, estimated strains in the plastic region are grossly overestimated when compared with the experimental and those obtained on the basis of the monotonic stress/strain curves. This can be explained with reference to figure 4.8 which shows that the onset of cyclic yielding for the component material occurs at approximately 20 kN load. Consequently, at this load the component material experienced some plastic deformation. The above results show that both Neuber's rule and the energy density method overestimate the local strains above the yield point. As the load increases the degree of correlation decreases, which indicates that the accuracy of the results are dependent upon the extent of the plastic deformation at the notch root. This confirms the previous conclusion that Neuber's method grossly overestimates the plastic strain in the plastic region when compared to those obtained using the energy density method. The F.E. calculated stresses have been reduced to a single equivalent stress using maximum principal

stress, von Mises, Tresca, and maximum principal strain methods. Both Neuber's rule and the energy density approach were used in conjunction with both monotonic and cyclic stress/strain curves to estimate the local elastic/plastic strains. Applied load/local strain curves are shown in figures 4.9 and 4.10. These are described by the following relationship between local strain, ϵ , and applied load, P:

$$\epsilon = \frac{p}{C_1} + \left(\frac{p}{C_2}\right)^{1/d} \quad - \quad 9.1$$

Where C_1 , C_2 , and d are constants.

Constants C_1 , C_2 and d can be determined for the relationship by using linear regression analysis. Previously the development of the applied load/local strain curves has not been possible at the pre-prototype design stage. However, it is now possible to employ elastic F.E. analysis to identify the most critical location within a component for detailed investigation. Applied load/local strain curves are then developed and used to create a load service history or to modify the existing measured strain-time history. Further more the described technique avoids the time consuming and error-prone calculation of stress concentration factor, K_f .

9.3 Theoretical And Experimental Life Evaluation

In this section the results of life calculations for the steering arm are presented and discussed. The life prediction procedure based on a critical location approach as embodied in the FATIMAS software package was employed with cyclic stress/strain data, geometric information and the measured strain history to predict the fatigue life of the component.

The experimental fatigue lives obtained from load controlled tests carried out by converting the known washboard strain-time history to a load history were compared to FATIMAS predictions using the original washboard strain signal and those obtained using the developed load history with elastic FE equivalent methods and both the energy density and Neuber's methods to predict a strain history which was used in FATIMAS to give fatigue life. The results are listed in tables 7.1 and 7.2 and shown in figures 7.3 and 7.4.

The predictions show a good correlation with experimental data with 66% of the points falling within a factor of 3 scatter band. The predicted lives based on FATIMAS experimental strain-time history, FATIMAS load calibrated strain history and FALCON load-time service history are within a factor 3 scatter band when compared to the experimental lives. The following reasons are associated with the lack of correlation between the FALCON load-time service history and those obtained using the FATIMAS load calibrated strain-time history and the experimental results.

Single point calibrations were used for conversion of the strain-time history to a load-time history. Consequently, linear extrapolation was used instead of more sophisticated calibration method based on equation 9.1. Therefore, lower load reversals have been applied than the actual load reversals, which has lead to fatigue life predictions and experimental results which are overestimated.

The FATIMAS strain based and FATIMAS load/local strain calibrated based results, appear to give conservative fatigue life estimates at short lives around $10E4$ cycles, and non-conservative estimates at long lives around $10E6$ cycles. Figure 7.3 shows a plot of load factor versus number of cycles to failure of the component which support this view [69, 83].

The fatigue lives based on Neuber's rule are more conservative than both the FALCON results and those based on the energy approach. Therefore these results are more acceptable as a design tool.

Of the four methods (maximum principal stress, Tresca, von Mises and maximum principal strain), applied to predict the fatigue lives of the steering arm, the predictions based on Neuber's rule and both Tresca and maximum principal strain were found to be most suitable for life

evaluation above the yield point of the component material. The fatigue life results based on Neuber's rule and the maximum principal stress theory were found to be overestimated. This technique is often used in life evaluation of brittle materials [64]. The lives based on the energy density approach and equivalent methods were found to be conservative and furthest away from the experimental results in both the elastic and plastic region.

Despite the aforementioned limitations, the local stress/strain approach has been proved to be an effective method of fatigue life estimation and its present use in the early stages of design/development has proved an effective industrial tool.

The degree of correlation suggests that the local stress/strain method can be used successfully to predict the fatigue life of engineering components under constant and variable load histories. To date this has required extensive historical data on strain histories for components similar to the one being designed or the building and in service measurement of prototypes. However, it is now possible to create a suitable load history for a specific engineering component using the finite element analysis, equivalent stress reductions and Neuber's method to predict fatigue lives of engineering components without recourse to prototype building.

CHAPTER 10

10. CONCLUSIONS AND SUGGESTIONS FOR FUTURE WORK

10.1 Computer Based Analysis

In the present investigations, two techniques have been employed for estimation of local elastic/plastic strain components required for input to the fatigue life assessment package, FATIMAS.

- a) The energy density approach.
- b) Neuber's rule.

The multiaxial elastic F.E. calculated stress components at the critical location were reduced to a single parameter using the maximum principal stress, von Mises', Tresca, and maximum principal strain methods. These were used in conjunction with both the monotonic and cyclic stress/strain curves and both (a) and (b) to develop a number of applied load/local strain calibration curves which can be used to create a variable load-strain service history.

In all cases the difference between the monotonic measured and the F.E. produced local strains were found to be less than 20% for all the cases considered. It can be considered that a good correlation exists between the measured and estimated strains despite the following inaccuracies arising from applying the F.E. package and affixing strain gauges.

- i) Loading and restraint of the component lacks precision.
- ii) The complexity of the component geometry necessitates the employment of approximations in defining the finite element skeleton.
- iii) Homogeneous material properties are assumed for the steering arm medium.
- iv) Difficulties arising from positioning the strain gauges coincident with defined F.E. nodal positions.
- v) Difficulties arising from positioning the strain gauges coincident with the direction of the principal plane.

The techniques employed for estimation of the monotonic local strains were used for calculation of the local strains under cyclic loading conditions. As a result a number of cyclic applied load/local strain calibration curves were developed.

The FATIMAS strain based history and FATIMAS load based history predicted and FALCON fatigue lives were compared with experimental results. It can be observed that 66% of the points were within a factor of 3 scatter band, respectively.

Although fatigue lives based on Neuber's estimated strains are conservative when compared to those based on the energy density method, a designer has increased confidence when using a technique that underestimates fatigue lives.

As a result of this investigation an integrated CAD software package has been developed by nCode International Limited and PAFEC by which durability of engineering components can be predicted in the conceptual design stage. At the time of publication the FEA/FATIMAS package was in ^{the} development stage, however, a number of life maps for the steering arm have been produced in order to demonstrate the capabilities of the package.

10.2 Practical Applicability Of The Technique

Consideration of the computerised and experimental results suggest that the technique developed is suitable for quantitatively predicting the fatigue life of engineering components in the early design stage to an acceptable levels of accuracy. To put these achievements in perspective, a consideration of the practical applicability of the aforementioned techniques are discussed.

Implementation of such a technique would depend upon the availability of:-

- i) Knowledge of the cyclic stress/strain properties of the component material.
- ii) Knowledge of the strength reduction factor, K_t .
- iii) Detailed knowledge of the service loading to which the component will be subjected.

Ideally, a strength reduction factor, K_t , equal to unity may be used. The finite element analysis determines the

highest stress within the component at a node within the defined mesh, however, it is very unlikely that the node coincides with the point of maximum stress within the structure. Furthermore the effects of surface finish are not considered within the analysis. Surface irregularities may act as a catalyst for localised stress concentration which may exceed the maximum predicted stress. Consequently, a strength reduction factor, K_f , greater than unity should be used.

The above technique can be used to predict the stress/strain behaviour at the critical location if knowledge of the nominal load history is known, from which a constant or variable service history may be produced. Fatigue life predictions based on the critical location approach can be made for any combination of material and component geometry using a stipulated load history. Geometry, material and load history changes necessitated through redesign can be readily executed with confidence. The technique can also be used to reduce the weight of existing components while retaining the desired stiffness and service durability.

10.4 Scope For Future Work

In its present form, the critical location approach is only capable of accurately estimating the fatigue life of engineering components to crack initiation, (defined as when a crack length of approximately 3 mm is observed within a component). This may be good enough for the ground vehicle industry and indeed it has been successfully used in the estimation of fatigue life. However, in situations where most of a component's life is spent in crack propagation, or for structures in which defects are present at the beginning of service, the propagation life is the total fatigue life. Consequently, crack initiation analysis becomes irrelevant. Therefore, further research is required to enhance the software to model crack growth.

The use of polymeric materials in ^{the} ground vehicle industry is becoming increasingly popular. The weight reduction, corrosion resistance and ease of manufacture offers greater design flexibility than those associated with conventional materials. The use of plastic materials in vehicle exterior and under the bonnet parts are well established, and it is estimated that the consumption of plastic materials will increase from 10% to about 20% of a car's weight within next 10 years [85, 86]. In spite of such rapid expansion, the fatigue behaviour of the polymeric materials is not as advanced as that of metals. It is in this area that validation of ^{the} critical location approach must be investigated. This can be achieved by

further research to obtain the cyclic properties of engineering plastics and then application of the data in the testing and evaluation of actual components.

The degree of biaxiality at the highest stressed node in the steering arm was found to be 9% which is relatively low. Further investigation would be rewarding by analysing components with higher orders of biaxiality to assess the capabilities of the FALCON package.

REFERENCES

1. GROTE, P. E., FASH, J. W.,
"Integration Of Structural Dynamics Testing And Durability Analysis,"
Sound And Vibration, Vol. 21, no.4, April 1987.
2. FASH, W., LUND, R. A.,
"Enhancing The Design Development Cycle Through Computer Integrated Engineering For Durability," SAE paper no. 871942
Presented At SAE Passenger Car Meeting And Exposition,
Dearborn, Michigan, October 19-22, 1987.
3. SHERRATT, F., EATON, D.,
"Fatigue Life Estimation By Local Stress/Strain Methods,"
Journal Of The Society Of Environmental Engineers, September
1983, PP. 28-36.
4. SHERRATT, F.,
"Fatigue Life Estimation Using Simple Fracture Mechanics,"
Journal Of The Society Of Environmental Engineers, March
1983, PP. 23-27.
5. SHERRATT, F.,
"Fatigue Life Estimation: A Review Of Traditional Methods,"
Journal Of The Society Of Environmental Engineers, December
1982, PP. 23-30.
6. TAN, S.T., and YUEN, M.M.F.,
"Integrating Solid Modelling With Finite Element Analysis,"
Computer Aided Engineering Journal August 1986.
7. CLARKE, R. B.,
"Making Finite Element Analysis Available To Design At The
Concept Stage,"
Proc Instn Mech Engrs, 1988, Vol 202, no. B2.
8. MARPLES, D.L.,
"The Decisions Of Engineering Design,"
Journal Of The Institute Of Engineering Design, 1960.
9. LATHAM, R. L., TERRY, G. J., TAYLOR, H. K.,
"The Problem Analysis By Logical Approach System,"
Work Study And Management, Feb 1968.
10. CROSS, N.,
"Engineering Design Methods"
Wiley And Sons Ltd, 1989.
11. FRENCH, M. J.,
"Conceptual Design For Engineers"
Design Council, London, 1985.

12. PUGH, S., SMITH, D. G.,
"Dumper Truck Design Highlights Industrial/Academic Co-
operation"
Design Engineering, PP. 27-29, August 1974.
13. PUGH, S., SMITH, D.G.,
"CAD In The Context Of Engineering Design: The Designers
View Point"
Proceeding Of 2nd International Conference - Computers In
Engineering And Building Design, PP. 193-198, CAD 76.
14. "WOHLER'S Experiments On The Strength Of Metals"
Engineering, August 23, 1967, P. 160.
15. GERBER, W.,
" Bestimmung Der Zulossigne In Eisen Konstruktionen,"
Zeitschrift Des Bayerischen, Ver6, 1874, P. 101.
16. GOODMAN, J.,
"Mechanics Applied To Engineering"
Longmans, Green And Company, London, 1899.
17. BASQUIN, O. H.,
"The Exponential Law Of Endurance Tests,"
In Proceeding, American Society For Testing And Materials,
no. 10, 1910, PP. 625-630.
18. STANTON, T. E., And BAIRSTOW, L.,
"The Resistance Of Materials To impact,"
In Proceedings, Institute Of Mechanical Engineers (London),
Parts 3/4, 1908, PP. 889-919.
19. BAIRSTOW, L.,
"The Elastic Limits Of Iron And Steel Under Cyclic
Variations Of Stress"
Philosophical Transaction (A), Vol 210, 1909-1910, PP. 35-
55.
20. GOUGH, H. J.,
"The Fatigue Of Metals"
Scott, Greenwood And Son, London 1924.
21. HAIGH, B. P.,
"The Relative Safety Of Mild And High-Tensile Alloy Steels
Under Alternating And Pulsating Stresses"
Proc, Ins Automob Eng, Vol24, 1929/1930, P. 320.
22. ALMEN, J. O., BOERGEHOLD, A. C.,
"Rear Axle Gears: Factors Which Influence Their Life"
In Proceedings, American Society For Testing And Materials,
Vol 35, Part 2, 1935, PP. 99-146.
23. ALMEN J. O., BLACK, P. H.,
"Residual Stresses And Fatigue In Metals"
McGraw-Hill Book Co, New York, 1963.

24. NEUBER, H.,
 "Theory Of Stress Concentration For Shear Strained Prismatic Bodies With Arbitrary Non-Linear Stress/Strain Law,"
 Transactions Of The American Society Of Mechanical Engineers, Series E, Vol 28, Dec 1961, PP. 544-550.
25. MINER, M. A.,
 "Cumulative Damage In Fatigue"
 Trans, ASME, J. Appl. Mech, Vol 67, Sept 1945, P. 159.
26. PALMGREN, A.,
 "Die Lebensdauer Von Kugellagern"
 ADVL 68, 1924, P. 339.
27. GASSNER, E.,
 "Betriebsfestigkeit, Eine Bemessungsgrundlage Fur Konstruktionsteile Mit Statistisch Wechselnden Betriebsbeanspruchungen Konstruktion, Vol 6, no. 3, 1954, PP. 97-104.
28. IRWIN, G. R.,
 "Analysis Of Stresses And Strain Near The End OF a Crack Traversing A Plate"
 Trans, ASME, J. Appl. Mech, Vol 24, 1957, P. 361.
29. COFFIN, L. F.,
 "A Study Of The Effect Of Cyclic Thermal Stresses On Ductile Metals"
 Transaction Of The American Society For Testing And Material, Vol 76, 1954, PP. 931-950.
30. MANSON, S. S.,
 "Behaviour Of Material Under Conditions Of Thermal Stress,"
 Heat Transfer Symposium, University Of Michigan Engineering Research Institute, 1953, PP. 9-75.
31. WATSON, P., HILL, S. J.,
 "Fatigue Assessment Of Ground Vehicle Components"
 Design Of Fatigue And Fracture Resistant Structure, ASTM STP 761, P. R. Abelkis and C. M. Hudson, Eds, American Society For Testing and Materials, 1982, PP. 5-27.
32. FATIMAS USER MANUAL,
 "Program Developed By nCode International Limited, SHEFFIELD, For Fatigue Life Estimation By Local Stress/Strain Method".
33. MEDUSA, A Prime Product For Two And Three Dimensional Solid Modelling.
34. PAFEC 75, Theory And Result Manual, "Program For Automatic Finite Element Calculation, Pafec Limited, NOTTINGHAM".
35. PAFEC 75, Data Preparation Manual, "PAFEC Limited, NOTTINGHAM".

36. FEES, Training Manual, "FEES Limited, CAMBRIDGE".
37. GLINKA G.,
"Energy Density Approach To Calculation Of Inelastic Strain/Stress Near Notches And Cracks"
Engineering Fracture Mechanics, Vol. 22, no. 3, PP. 485-508, 1985.
38. TOPPER, T. H., WETZEL, R. M., MORROW, J.,
"Neuber's Rule Applied To Fatigue Of Notched Specimens,"
Journal Of Materials, JMLSA, Vol 4, no. 1, March 1969, PP. 200-209.
39. SANDOR, B. I.,
"Fundamentals Of Cyclic Stress And Strain"
The University Of Wisconsin Press, 1972.
40. COWBURN, D., DABELL, B. J.,
"Design Optimization Of Front Axle Beams"
C111/85, IMechE 1985.
41. TUCKER, L., BUSSA, S.,
"The SAE Cumulative Fatigue Damage Test Program"
paper no. 750038, SAE Automotive Engineering Congress And Exposition, Detroit, MI, February 24-28, 1975.
42. BROWN, M. W., MILLER, K. J.,
"A Theory For Fatigue Under Multi-axial Stress/Strain Conditions,"
Proceeding, Institution Of Mechanical Engineering, Vol. 187, PP. 745-755, 1973.
43. STADNICK, S. J., MORROW, J.,
"Techniques For Smooth Specimen Simulation Of The Fatigue Behaviour Of Notch Members"
Testing For Prediction Of Material Performance In Structures And Components, ASTM STP 515, American Society For Testing And Materials, 1972, PP. 229-252.
44. ENDO, T. and MORROW, J.,
"Cyclic Stress/Strain And Fatigue Behaviour Of Representative Aircraft Metals"
Journal Of Materials, IMLSA, Vol. 4, no. 1, March 1969, PP. 159-175.
45. LANDGRAF, R. W., MORROW, J., and ENDO, T.,
"Determination Of The Cyclic Stress/Strain Curve,"
Journal Of Materials, JMLSA, Vol. 4, no. 1 March 1969, PP. 176-188.
46. BAIRSTOW, L.,
"The Elastic Limits Of Iron And Steel Under Cyclic Variations Of Stress"
Philosophical Transactions Of The Royal Society Of London, Series A, Vol. 210, 1910, PP. 35-55.

47. DUGDALE, D. S.,
"Stress/Strain Cycles Of Large Amplitude"
Journal Of The Mechanics And Physics Of Solids, Vol. 7, no. 2, 1959, PP. 135-142.
48. OSGOOD, C. C.,
"Fatigue Design"
International Series On The Strength And Fracture Of Materials And Structures, Second Edition, Pergamon Press, 1982.
49. MORROW, J.,
"Fatigue Properties Of Metals"
Paper Submitted To Fatigue Design Committee Of Society Of Automotive Engineers Iron And Steel Technical Committee Division 4, April 1964.
50. SMITH, K. N., WATSON, and TOPPER, T. H.,
"A Stress/Strain Function For The Fatigue Of Metals,"
Journal Of Materials, JMLSA, Vol. 4. Dec. 1970, PP. 767-778.
51. TOPPER, T. H., SANDOR, B.I., and MORROW, J.,
"Cumulative Fatigue Damage Under Cyclic Strain Control,"
Journal Of Materials, Vol 4, no. 1, March 1969, PP. 189-199.
52. ENDO, T., MITSUNAGA, K., TAKAHASHI, K., KOBAYASHI, K., MATSUISHI, M.,
"Rain Flow Method, The Proposal And The Application"
Memoir Kyushu Inst. Tech., Engg., no. 28, 33 (1974) In Japanese.
53. DEVLUKIA, J., DAVIES, J.,
"Fatigue Analysis Of Vehicle Structural Components Under Biaxial Loading"
C104/85, IMechE 1985.
54. FASH, J. W., SOCIE, D. F., and Mc DOWELL, D. L.,
"Fatigue Life Estimates For A Simple Notched Component Under Biaxial Loading"
Multi-axial Fatigue, ASTM STP 853, K. J. Miller and M. W. Brown, Eds., American Society For Testing And materials, Philadelphia, 1985, PP. 497-513.
55. BENHAM, P. P., WARNOCK, F. V.,
"Mechanics Of Solids And Structures"
A Pitman International Text, Pitman Publishing, PP. 357-370, 1976.
56. HEARN, E. J.,
"Mechanics Of Materials"
An Introduction To the Mechanics Of Elastic And Plastic Deformation Of Solids And Structural Components, Second Edition, Pergamon press, PP. 401-429, 1985.

57. GARUD, Y.S.,
"Multiaxial Fatigue: A Survey Of The State Of The Art"
Journal Of Testing And Evaluation, JTEVA, Vol 9, No 3, May
1981, PP. 165-178.
58. DOWLING, N. E., BROSE, W. R.,
"Notched Member Fatigue Life Predictions By The Local Strain
Approach"
Fatigue Under Complex Loading Analyses And Experiments, SAE,
Vol 6, PP. 55-84.
59. HOFFMANN, M., SEEGER, T.,
"A Generalized Method For Estimating Multi-axial
Elastic/Plastic Notch Stresses And Strains Part 1: Theory,"
Journal Of Engineering Materials And Technology, Vol. 107,
PP. 250-254, October 1985.
60. HOFFMANN, M., SEEGER, T.,
"A Generalized Method For Estimating Multi-axial
Elastic/Plastic Notch Stresses And Strains Part 2:
Application And General Discussion"
Journal Of Engineering Materials And Technology, Vol. 107,
PP. 255-260, October 1985.
61. WETZEL, R. M.,
"Fatigue Under Complex Loading"
Advances In Engineering, Vol. 6, Society Of Automotive
Engineers, Warrendale, Pa. 1979.
62. MOLSKI, K., GLINKA, G.,
"A Method Of Elastic/Plastic Stress And Strain Calculation
At A Notch Root"
Materials Science And Engineering, Vol. 50, PP. 93-100,
1981.
63. GLINKA, G., OTT, W., NOWACK, H.,
"Elastoplastic Plane Strain Analysis Of Stresses And Strains
At the Notch Root"
Journal Of Engineering Materials And Technology, Vol. 110,
PP. 195-204, July 1988.
64. FATEMI, A., SOCIE, D. F.,
"A Critical Plane Approach To Multi-axial Fatigue Damage
Including Out-Of-Phase Loading"
Fatigue Fract Engng Mater Struct, Vol.11, no. 3, PP. 149-
165, 1988.
65. MILLER, K. J.,
"Fatigue Under Complex Stress"
Metal Science, August/September 1977.
66. McDIARMID, D. L.,
"Designing For High-Cycle Biaxial Fatigue Using Surface
Strain Records"
Multi-axial Fatigue, ASTM STP 853, K. J. Miller and M. W.
Brown, Eds. American Society For Testing and Materials,
Philadelphia, PP. 431-439, 1985.

67. McDIARMID, D. L.,
"Crack Systems In Multi-axial Fatigue"
Advances In Fracture Research, Proceeding Of The 7th
International Conference On Fracture (ICF7), Houston, Texas,
20-24 March 1989.
68. McDIARMID, D. L.,
"Fatigue Behaviour Under Out-Of-Phase Bending And Torsion,"
Journal Of The Royal Aeronautical Society, March 1981.
69. FINLEY, W. N., Transaction, American Society Of Mechanical
Engineers, Vol 79, 1957, P 1337.
70. ALBERT, W. A. J.,
"Uber Treibseile am Harz," Archiv Fur Mineralogie,
Geognosie, Bergbau Und Hutterkunde, Vol 10, 1838, PP. 215-
234.
71. ANDREWS, T.,
"The Effect Of Strain On Railway Axels And The Minimum
Flexion Resistance Point In Axels"
Transactions Of The Society Of Engineers, Nov 1895, PP. 181-
234.
72. LANDGRAF, R. W.,
"The Resistance Of Metals To Cyclic Deformation,"
Achievements Of High Fatigue Resistance In Metals And
Alloys, ASTM STP 467, American Society For Testing And
Materials, 1970, PP. 3-36.
73. ROLLASON, E. C.,
"Metallurgy For Engineers"
Fourth Edition, Edward Arnold Publishing Company, PP. 175-
211.
74. VAN VLACK, L. H.,
"Materials Science For Engineers"
Fourth Edition, Addison-Wesley Publishing Company, PP. 373-
415.
75. HALLIDAY, M. D., and BEEVERS, C. J.,
"The d.c. Electrical Potential Method For Crack Length
Measurement," Engineering Materials Advisory Services Ltd,
The Chameleon Press Ltd, London, 1980, PP. 85-113.
76. WEI, R. P., and BRAZILL, R. L.,
"An a.c. Potential System For Crack Length Measurement,"
Engineering Materials Advisory Services Ltd, The Chameleon
Press Ltd, London, 1980, PP. 190-202.
77. WATT, K. R.,
"A Consideration Of An a.c. Potential Drop Method For Crack
Length Measurement"
Engineering Materials Advisory Services Ltd, The Chameleon
Press Ltd, London 1980, PP. 202-222.

78. RICHARS, C.E.,
"Some Guidelines To The Selection Of Techniques,"
Engineering Materials Advisory Services Ltd, The Chameleon
Press Ltd, London, 1980, P. 461.
79. WOODFINE, B.C.,
"Temper-Brittleness: A Critical Review Of The Literature,"
Journal Of The Iron And Steel Institute, March 1953.
80. WOODFINE, B. C.,
"Some Aspects Of Temper-Brittleness"
Journal Of The Iron And Steel Institute. March 1953.
81. LEWIS, D. J.,
"Taking The Stress Out Of Stress Analysis:Using Finite
Element Method"
CEGB Research, April 1985.
82. GOLDTHORPE, M. R.,
"The Finite Element Method Applied To Elastic Stress
Analysis"
Department Of Mech Eng, University Of Sheffield.
83. TUCKER, L. E., CODDINGTON, R. C., CROSHECK, J. E.,
"Finite Element Based Life Prediction For Product
Evaluation"
Society Of Automotive Engineers, 1979, Pa 790856.
84. MUSIOL, C., DRAPER, J., SYKES, N., MORTON, K.,
"Advances In Computer Aided Design Against Fatigue"
C234/81 IMechE, 1981.
85. RIGBY, R. B.,
"Thermoplastics Automotive Applications"
Engineering Plastics - Shaping the Future, Conf., Dec 1986,
PP. 6-24.
86. LOFTHOUSE, M. G.,
"Plastic - 2000 AD"
Engineering Plastics - Shaping the Future, Conf., Dec 1986,
PP. 1-5.
87. Collins Concise English Dictionary of The English Language
Collins: London and Glasgow